



'KAPPA (κ): PHYSICAL UNDERSTANDING AND ESTIMATION APPROACHES TARGETED TO APPLICATIONS

AUTHORS			REVIEW			APPROVAL		
NOM	DATE	VISA	NOM	DATE	VISA	NOM	DATE	VISA
O.J. KTENIDOU (ISTerre)			Ph. RENAULT (Swissnuclear)			P. Traversa		
			F. Scherbaum (Potsdam University)			G. Senfaute		

EDF Project 'Seismic Ground Motion Assessment' (SIGMA)
Contract no. 3000-5910108964

Deliverable 2

'Kappa (κ): Physical understanding and estimation approaches targeted to applications'

Olga-Joan Ktenidou

4 May 2014

EXECUTIVE SUMMARY

This report presents the research conducted under Contract no. 3000-5910108964 and is submitted to EDF as Deliverable 2 under Article 3: 'Reunions - rapports'. The report consists of six chapters, including an introduction to the topic and scope of research; a series of chapters that describe the work conducted within this contract and address the main research questions, referring to publications; a concluding section with recommendations and future perspectives; and an annex with a list of publications dating from the beginning of the contract.

Chapter 1 makes an introduction to the topic of high-frequency attenuation (κ , or κ), its importance to seismic hazard for critical facilities, and the main questions surrounding it today.

Chapter 2 covers the state of the art on the topic of κ . It focuses on the approaches used, classifies them into a taxonomy targeted to applications, and also discusses correlations with V_{s30} .

Chapter 3 includes work that furthers the understanding of the physical background of κ . New Zealand near-field data from Christchurch are used to investigate effects of sensor orientation, instrument and data frequency constraints, and excitation level. Greek data from a local network (Euroseistest) are used to investigate the consistency between different measurement approaches, find correlations of κ_0 with various site characterization parameters, and to introduce a possible physical model of κ_0 that includes asymptotic regional values and scattering.

Chapter 4 focuses on κ estimation for low-seismicity areas. Swiss data from hard rock stations are used to test the uncertainty in κ estimates, by testing sensitivity to various data selection criteria and to the trade-off with Q . Data from the US Transportable Array in Southern Arizona are used to illustrate the particular difficulties of measuring κ from low-magnitude, bandlimited data, and how these may be addressed.

Chapter 5 focuses on major databases and how these are being prepared today for the computation of κ . We use the examples of the NGA-West2 and NGA-East and discuss the pre-processing necessary to produce the spectra and then the scanning of the datasets to identify records for which specific κ measurement approaches can be used.

Chapter 6 summarises the work and offers some recommendations for the measurement of κ , and describes topics that need further research.

The Annex contains a list of publications.

TABLE OF CONTENTS

EXECUTIVE SUMMARY	3
1. INTRODUCTION	5
2. STATE OF THE ART	6
3. IMPROVING OUR UNDERSTANDING OF THE PHYSICS OF KAPPA.....	8
3.1 κ_0 in Christchurch: directional dependencies, nonlinearity, and magnitude considerations.....	8
3.2 κ_0 in Euroseistest: possible physical basis for regional dependency and the effect of scattering.....	10
4. MEASURING KAPPA FOR LOW-SEISMICITY REGIONS.....	12
4.1 κ_0 estimates for hard rock SED stations in Switzerland using a high-frequency approach	12
4.2 Measuring κ in Arizona from the Transportable Array	14
5. PREPARING A MAJOR DATABASE FOR MEASURING KAPPA.....	16
5.1 Selecting data and measuring κ for the NGA-West project	16
5.2 Selecting data and measuring κ for the NGA-East project	18
6. CONCLUDING REMARKS AND FUTURE PERSPECTIVES.....	21
ANNEX: SUMMARY OF PUBLICATION ACTIVITY DURING THE CONTRACT	23

1. INTRODUCTION

One of the global challenges that geoscientists and engineers are faced with today is risk mitigation pertaining to seismic hazard. The Fukushima Dai-ichi accident made it clear that we must reassess the way seismic risk is addressed for critical infrastructure. The current regulatory paradigm is shifting towards a risk-informed one, where safety is defined with respect to an acceptably low risk level. In a probabilistic framework risk is estimated based on hazard (seismic loading), fragility, and exposure of people and property. In this context, this requires estimating not only the mean risk but also its range, and thus quantifying uncertainties becomes critical. For seismic risk, the uncertainty lies mostly in the hazard, and more specifically in the ground motion model. For typical sites, uncertainty in the hazard using standard (ergodic) methods leads to a range of about 100 in risk, while uncertainty in the fragility leads to a range of about 10 in the risk. So the way to get the greatest uncertainty reduction in seismic risk is to reduce uncertainty in ground motion estimation, which is primarily done with ground motion prediction equations (GMPEs). When using global GMPEs, the largest uncertainty in ground motion models lies not in the region-specific source properties, but in the site-specific site effects and site/region-specific path effects. So site response, including the rock site properties, is a key issue. Though we have interpreted phenomena linked to classic (low-frequency) site response and constrained its estimation, ground response in the high frequency range is still an open scientific question, as it was up to now considered unimportant. Recently, however, classic low-frequency site proxies (such as near-surface velocity V_{s30}) have proven inadequate in describing rock motion in its entire frequency range, and complementary high-frequency proxies were sought. This is very important for infrastructures that are built on rock and are sensitive to high frequencies, e.g. concrete dams and nuclear facilities. The new proxy established for this purpose is the high-frequency attenuation factor kappa (κ). κ is critical to hazard applications. The frequencies it controls (above 10-20 Hz) are important to the seismic response of safety-related equipment in nuclear facilities. However, it is still not completely understood. For instance, in 2013, the PEGASOS Refinement Project concluded that the risk for Swiss facilities is driven by uncertainty in κ . κ is elusive as to its physical origin and components, and difficult to constrain because of the numerous ways there are to measure it. This makes it not only interesting but also necessary to address its estimation, physical meaning, and variability.

Existing κ values in academic and grey literature exhibit large scatter, even following its classic definition. So we begin from a state-of-the-art review of all existing approaches for κ estimation, grouping those that are more internally consistent and more suited to specific applications (Chapter 2). We then focus on specific datasets and use some of these approaches to better understand certain aspects of the the physics underlying kappa. We use the Euroseistest set to propose a physical model including possible regional values and the contribution of damping and scattering (Chapter 3a). We also use the Christchurch dataset to investigate the sensitivity of κ to component orientation and excitation level (Chapter 3b). When dealing with very large global databases, before κ calculation, it is important to account for certain physical considerations as well as data constraints, in determining which approach to use and choosing appropriate subsets of data where these can be applied. Such procedures are ongoing in NGA-West (Chapter 4). Finally, κ_0 is very important for characterizing hard rock in stable continental regions, but in such regions it is also more difficult to constrain, since events are fewer and have small magnitudes. This is rendered more difficult yet if networks have limited bandwidth. We investigate how such obstacles may be overcome (Chapter 5).

2. STATE OF THE ART

When it comes to κ_0 , the debate as to its interpretation is still on as to whether kappa is due to site, path, and/or source effects. But more importantly, even in applications where kappa is used to represent site effects (such as ground motion simulations and GMPE adjustments from host to target regions), it is measured using a variety of approaches: on the high-frequency part of the acceleration Fourier spectrum, on the low-frequency part of the displacement spectrum, on the site transfer function, from fittings to the acceleration response spectrum, from broadband inversions, or using the inverse random vibration theory to derive GMPE-response-spectrum-compatible Fourier spectra. We suggest that in order to reduce the ambiguities, kappa should always be given a notation consistent with the approach used to measure it. We group these approaches into families according to basic features, such as the range of frequencies over which κ_0 is computed and the trade-off with path effects, and suggest that certain families of measurement approaches may be more compatible with certain applications. We then discuss the alternative option for estimating κ_0 when site-specific records are not available, based on empirical correlations with V_{s30} . We collect previously published correlations and demonstrate the scatter observed across different studies. Finally, we make suggestions as to how κ_0 estimation can be made in a more consistent way with the applications that use it, and how existing correlations can be made more consistent to improve both the inference of κ_0 in the absence of site-specific data and the physical understanding of κ_0 .

This chapter reports the work shown in publication J1 and its earlier versions: L1, L2, A2 (see Annex).

Taxonomy of κ : A Review of Definitions and Estimation Approaches Targeted to Applications

by Olga-Joan Ktenidou, Fabrice Cotton, Norman A. Abrahamson, and John G. Anderson

INTRODUCTION

In a way perhaps not dissimilar to stress drop (Atkinson and Beresnev, 1997), the high-frequency attenuation parameter κ (kappa), introduced by Anderson and Hough (1984), is one of the most used yet least understood or agreed-upon parameters in engineering seismology. It describes the deviation at high frequencies between observed Fourier amplitude spectra calculated from seismograms and an ω^{-2} source model, such as the Brune (1970) model. Almost 30 years after its introduction, κ is used by seismologists and engineers alike and constitutes an important input parameter for several applications. Perhaps because of its importance, it is estimated, physically explained, and used in many different ways. This note aims to illustrate the multiple approaches to its estimation, and to suggest that, in order to reduce ambiguities, the parameter should always be given a notation consistent with its measurement and application to help avoid inconsistencies in its application of κ scaling to ground-motion models.

Hanks (1982) observed that above a given frequency the acceleration spectrum decays sharply. He termed this frequency f_{\max} (e.g., Fig. 1a) and attributed it mainly to local site conditions. Soon after, Anderson and Hough (1984) introduced an alternative parameter to model this decay, which is the one most commonly used today: κ . They measured κ directly from the high-frequency part of the acceleration Fourier amplitude spectrum of a record. Above a certain frequency (which they named f_c but we will call here f_1), the overall shape of the spectrum generally decays exponentially with frequency; the decay constant is most easily measured by finding a linear approximation to the spectrum plotted in log-linear space. The slope of the linear approximation is $-\pi\kappa$ (e.g., Fig. 1b). In this note we use the notation κ_r for individual observations of κ , for example, the κ value corresponding to the slope of a particular record; this record may be at any epicentral distance $R_e \geq 0$. Anderson and Hough (1984) also observed that κ_r at individual stations increases with distance and concluded that it includes components related both to the local geology of the top few km of crust beneath the station and to the regional structure. They then suggested that the site component of κ (denoted κ_0) could be computed by extrapolating the κ_r values

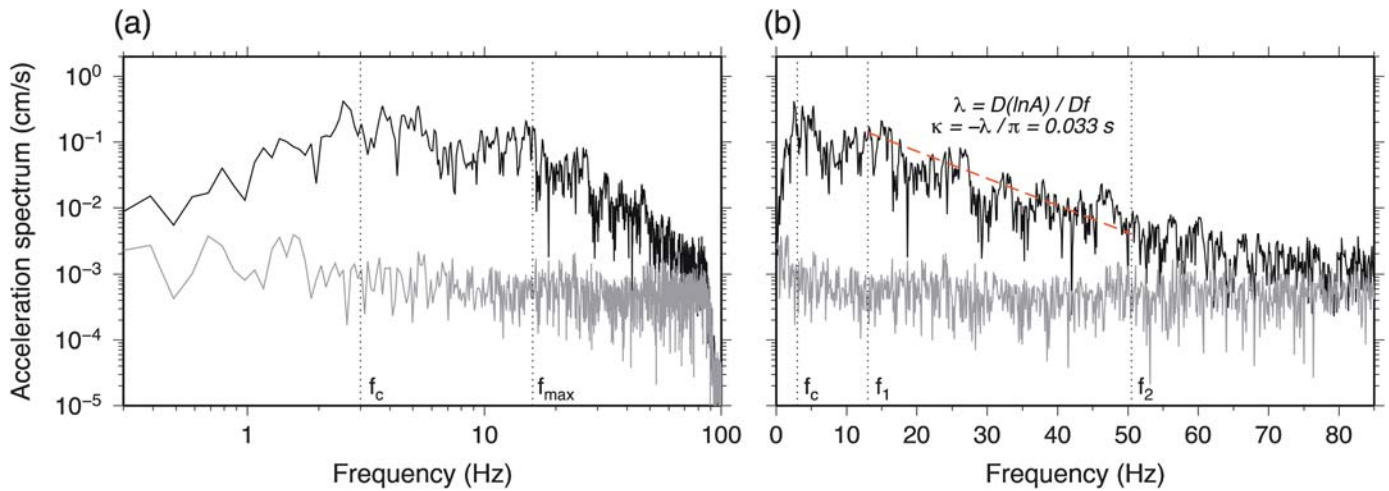
to zero epicentral distance, thus correcting for the regional effect of anelastic Q .

In this note, we discuss the use of κ_0 in various engineering seismology applications today and why interest in this parameter has been revived. We briefly discuss its possible physical interpretations, and detail the known approaches to estimate κ_0 from seismic records. We group these approaches into families according to basic features, such as the range of frequencies over which κ_0 is computed and the trade-off with path effects. We then discuss the alternative option for estimating κ_0 when site-specific records are not available, based on empirical correlations with V_{s30} . We collect previously published correlations and demonstrate the scatter observed across different studies. Finally, we make suggestions as to how κ_0 estimation can be made in a more consistent way with the applications that use it, and how existing correlations can be made more consistent to improve both the inference of κ_0 in the absence of site-specific data and the physical understanding of κ_0 .

κ : A MULTITUDE OF APPLICATIONS, PHYSICAL INTERPRETATIONS, AND MEASUREMENT METHODS

Importance of κ_0 and Fields of Application

Over the last decades, κ has been used in different applications. In source studies, removing the attenuation term is fundamental in order to study self-similarity of the source spectrum; this can be done by inverting for the theoretical Q , using empirical Green's functions (EGFs) or multiple EGFs to remove path and site effects, measuring spectral parameters from the coda, or using κ_r to correct for high-frequency attenuation (e.g., Irikura, 1986; Abercrombie, 1995; Mayeda and Walter, 1996; Hough, 1997; Lancieri *et al.*, 2012). In the generation of synthetic ground motion using point-source or finite-fault stochastic or hybrid simulation approaches, κ_0 is applied as a low-pass filter to constrain high frequencies, affecting peak ground motion and spectral shape (Boore, 1986; Beresnev and Atkinson, 1997; Boore, 2003; Graves and Pitarka, 2010). Even in physics-based simulations using theoretical Green's functions (TGFs; e.g., Zeng *et al.*, 1994; Graves, 1996; Halldorsson and Papageorgiou,



▲ **Figure 1.** (a) Definition of f_{\max} as the onset of the crashing of the S-wave spectrum (solid black line), plotted on a log–log scale. Also shown are the corner frequency and the noise spectrum (solid gray line). (b) Definition of $\kappa_{r,AS}$ as the slope of the spectrum in the frequency range (f_1 – f_2) in log–linear space.

2005; Mai *et al.*, 2010; Schmedes *et al.*, 2010; Foster *et al.*, 2012), imposing such a constraint is necessary to achieve realistic results at high frequencies. The amount of the κ correction in such approaches depends on how Q is incorporated in the TGFs. In the creation and calibration of ground-motion prediction equations (GMPEs) based on stochastic simulations, near-surface attenuation is implicitly considered through a set of κ_0 values considered applicable to the region (e.g., Toro *et al.*, 1997).

Recently, the use of κ in the engineering seismology community has been revived. On the one hand, the need has arisen to adjust GMPEs from host to target regions, often from active regions with soft rock to less active regions with hard rock (Delavaud *et al.*, 2012) with approaches such as the hybrid empirical method of Campbell (2003, 2004). The scaling from soft to hard rock is made considering the differences in V_{S30} and κ_0 to account for both site amplification that is dominant at lower frequencies, and site attenuation that dominates high frequencies (Cotton *et al.*, 2006; Van Houtte *et al.*, 2011). Moreover, in probabilistic seismic hazard assessment (PSHA) for critical facilities, it is common to conduct site-specific site response analyses. This requires adjusting GMPEs, even within the same region, to bedrock level and then computing site response up to the surface. Adjusting the GMPEs to hard-rock conditions requires knowledge of κ_0 . Indeed, the Probabilistic Seismic Hazard Analysis for Swiss Nuclear Power Plant Sites (PEGASOS) Refinement Project (Biro and Renault, 2012) showed that, for hard rock, the V_{S30} and κ_0 corrections can lead to differences up to a factor of 3 in the high-frequency part of the response spectrum. Given the significance of κ_0 , in the past year attempts were also made to explicitly include it in the functional form of GMPEs (Laurendeau *et al.*, 2013), an idea that actually originated as early as Anderson *et al.* (1996).

Physical Interpretations: Source, Path, and Site Components

Since the 1980s, there have been debates as to the origins of κ . The difficulty of mapping κ onto physical parameters was predicted and explained by Hanks (1982) even at the time of introducing f_{\max} , κ 's predecessor, to model what he then called “the crashing spectrum syndrome.” According to him, the catch lies in the fact that it is the absence of signal that is to be interpreted, not its definitive presence. Before the definition of κ or f_{\max} , several observations showed an apparent departure from the scaling law of Aki (1967) for small-magnitude events, that is, the observed source corner frequency, f_c , ceased to increase for decreasing magnitudes. This masking of the expected f_c had been attributed to source-related effects (Bakun *et al.*, 1976), to anelastic and scattering site attenuation (Frankel, 1982), or to both (Archuleta *et al.*, 1982). Then Hanks (1982) and, later on, Anderson (1986) attributed the newly defined f_{\max} to site attenuation. This is the prevalent view today, though some studies have again related it to source properties, such as the width of the ruptured fault zone (Papageorgiou and Aki, 1983; Aki, 1987; Papageorgiou, 1988; Gariel and Campillo, 1989; Papageorgiou, 2003; Tsurugi *et al.*, 2008; Iwakiri and Hoshiya, 2012; Wen and Chen, 2012).

To enable discussion for the origins of κ_r , it is useful to start with a general model encompassing all of the various hypotheses. In equation (1), κ_0 is the site component, κ_s is introduced to represent the source contribution, and $\tilde{\kappa}(R_c)$ follows the notation of Anderson (1991) for a generalized distance dependence on the epicentral distance R_c :

$$\kappa_r = \kappa_0 + \kappa_s + \tilde{\kappa}(R_c). \quad (1)$$

Today, most studies model κ_r as a site and path effect. Datasets with adequate stations and events can also resolve

source contributions, i.e., κ_s (Tsai and Chen, 2000; Purvance and Anderson, 2003; Van Houtte *et al.*, 2011; Kilb *et al.*, 2012). Many of these studies find that κ_s is mostly related to the scatter of κ_r measurements.

In equation (1), the constraint on the distance dependence is that $\tilde{\kappa}(0) = 0$. As expected from studies that find regional variability in Q , there are variable results for the functional form of the distance dependence and importance of this term. The increase of κ_r with distance has been explored in a number of studies. The simplified initial assumption of Anderson and Hough (1984) for linear distance dependence mostly served an illustrative purpose. Notwithstanding, it has proved a reasonable approximation for several datasets (Nava *et al.*, 1999; Douglas *et al.*, 2010; Gentili and Francheschina, 2011; Ktenidou *et al.*, 2013). Other studies find distance dependencies that deviate in different ways from the initial linear assumption (Hough and Anderson, 1988; Hough *et al.*, 1988; Anderson, 1991; Humphrey and Anderson, 1992; Castro *et al.*, 1996; Fernández-Heredia *et al.*, 2012). Some studies have even found negligible distance dependence in some regions out to 80 km (Tsai and Chen, 2000; Purvance and Anderson, 2003).

In summary, then, the literature on studies that have tried to explain the physical processes behind κ is consistent with the model expressed in equation (1), with site conditions having the key role, and source and distance terms having variable importance depending on the region and study. In what follows, we focus on κ_0 , the site parameter of κ_r , which is the most widely accepted point of view.

Measuring κ from Seismic Records: Types of Approaches

People measure κ in different ways. In Table 1, we outline some of the main approaches for estimating κ_0 . Naturally, more examples can be found in the literature, but our aim is to create a relatively small number of approaches, or rather families of approaches, based on certain common features, such as the principle behind the approach, the frequency range over which κ is computed, and how the distance dependence and the trade-off with Q are dealt with.

We make a clear distinction between κ_r and κ_0 . Some of the approaches to measure κ_0 start with individual measurements of κ_r (i.e., observations on individual spectra at some distance r), which must then be combined and extrapolated to zero distance to obtain an estimate of κ_0 for the site. Others yield directly the κ_0 (i.e., the site-specific, zero-distance κ derived from many observations). There are different ways of extrapolating κ_r values to zero distance. A simplified approach is to assume a linear dependence of κ_r with distance and perform a standard linear regression. Considerations of seismic ray theory show that this assumes that Q and the shear velocity are independent of depth. A more general approach is that suggested based on better data by Hough and Anderson (1988) and Anderson (1991), in which the only constraint is that κ_r is a smooth function of distance to be determined by the data, or any nonparametric regression allowing for more realistic

underlying Q structures. We will proceed to describe the main families of approaches for κ estimation.

- *Acceleration Spectrum*: Following the classic definition of Anderson and Hough (1984), κ_r can be directly measured in log-linear space on the high-frequency part of the Fourier acceleration spectrum of the S waves, above f_1 (Fig. 1b). We will refer to this original definition as κ_{r_AS} . Because a component of horizontal wave propagation, affected by Q , is present in these measurements, an extrapolation to zero distance (assuming frequency-independent Q) will lead to the site-specific attenuation component, κ_{0_AS} . This approach can only be used for relatively large event magnitudes, as f_1 must exceed f_c to avoid any trade-off with the source. f_1 is visually picked. It is less than f_{\max} according to Anderson and Hough (1984), whereas Anderson (1986) proposes a more rigorous alternative: f_{95} , at 95% of the spectrum energy. Tsai and Chen (2000) suggest f_1 is similar to the f_{\max} defined by Hanks and McGuire (1981): $f_{\max} = Q\beta/\pi R$ and which can be rewritten as: $f_{\max} = 1/\pi\kappa$ according to Anderson (1986), if Q is independent of frequency.
- *Transfer Function*: A variation of the classic method was proposed by Drouet *et al.* (2010), in which the site-specific κ_0 can be measured directly from the high-frequency part of the site transfer function that has been derived through source-path-site inversions on a set of records from various stations and events. This κ_0 we will call κ_{0_TF} . Here the measurement frequency range is above the resonant peak and any higher mode amplification peaks, and the transfer function is computed using one of the stations as reference, ignoring its site amplification and attenuation. Similarly, Frankel *et al.* (1999) measured κ from surface-to-reference amplification functions relative to an ideal reference site. Motazedian (2006) and Ghofrani *et al.* (2013), on the other hand, applied a similar method to the horizontal-to-vertical spectral ratio, that is, using the vertical component as reference. In those approaches, for a non-zero reference κ , the measured quantity was the difference between horizontal and vertical κ .
- *Source Spectrum*: Another variation of the classic method is the one suggested by Oth *et al.* (2011), who measure κ_r as the high-frequency decay on the Fourier source spectrum, which is actually the Fourier amplitude from the source at depth, recorded at the surface. Their approach first removes the effect of $Q(f)$ to a reference distance of 5 km (where its effect can practically be ignored) and then corrects for the site amplification, without, however, including any high-frequency decay therein. Hence, this decay can be found in the derived source spectra (we name it κ_{r_SS}). κ_{r_SS} corresponds to a virtually zero-distance estimate of κ_0 and no extrapolation is necessary. But because we derive one value per event, we must average all values available at each site to estimate the site's overall κ_{0_SS} . A similar approach is used by Margaritis and Boore (1998), correcting for both site amplification and whole-path attenuation before deriving κ_0 .

Table 1
The Main Families of Approaches Available for Estimating Site-Specific, Zero-Distance κ_0

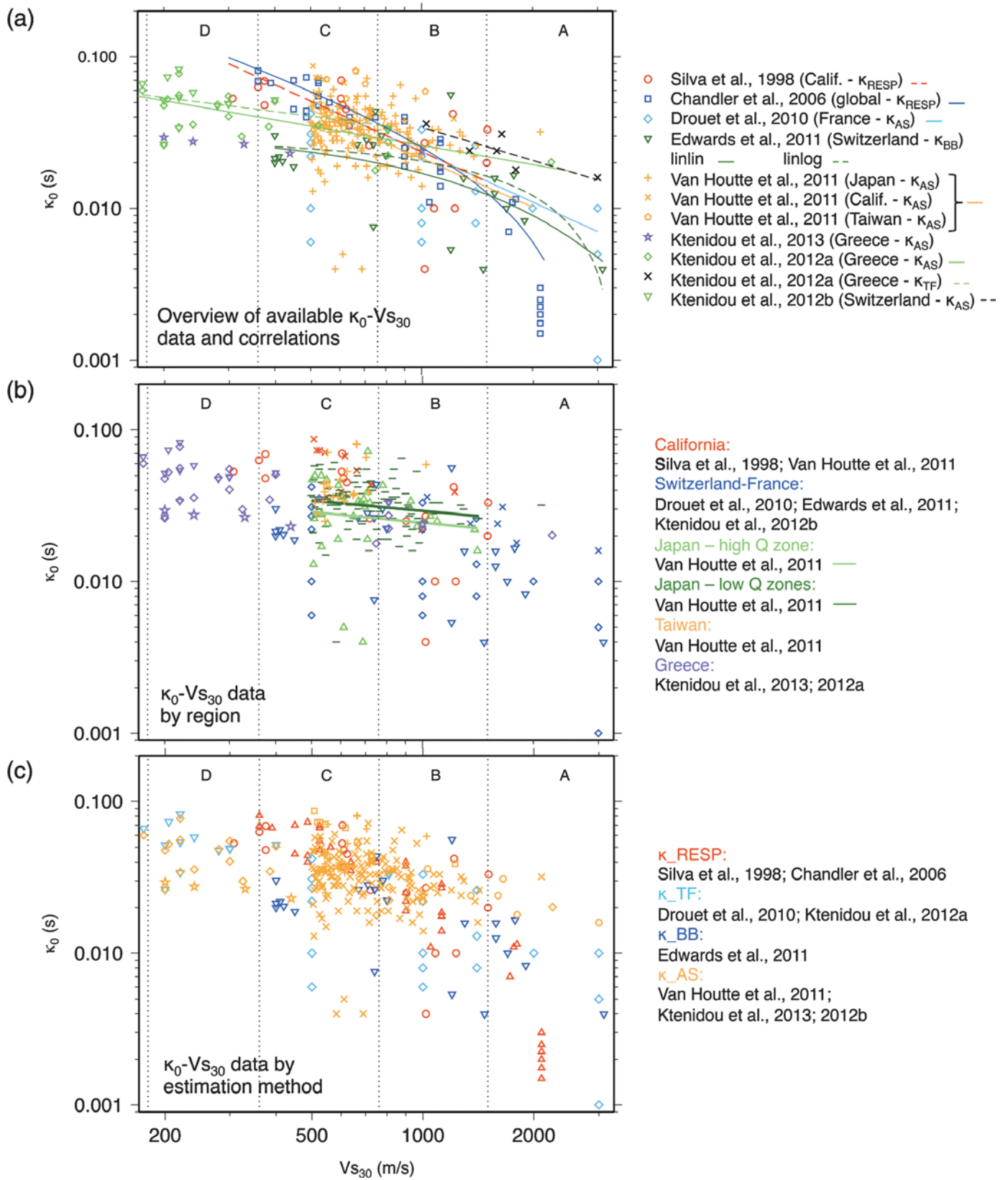
Notation	Principle	Main References	Measurement/ Computation	Freq. Range	Q Effect	Zero-Distance?	Site-Specific?	Possible Uses
κ_{r_AS}	High-frequency decay of the S -wave Fourier spectrum	Anderson and Hough (1984), Hough and Anderson (1988)	Direct measurement on the S -wave Fourier acceleration spectrum above f_c , where it is theoretically flat	High (above f_c)	Present	No	No, extrapolate to $R_e = 0$ for κ_{0_AS}	Host-to-target adjustment of GMPEs
κ_{0_TF}	Analogy to high-frequency decay	Frankel <i>et al.</i> (1999), Drouet <i>et al.</i> (2010)	Direct measurement on the site amplification transfer function	High (above resonant peaks)	Removed	Yes	Yes, ready to use	Host-to-target adjustment of GMPEs
κ_{r_SS}	Analogy to high-frequency decay	Margaris and Boore (1998), Oth <i>et al.</i> (2011)	Direct measurement on the source spectrum (after removal of Q and site amplification effects) and averaging across all spectra recorded at the same site	High (above f_c)	Removed (to 5 km)	Yes	No, average over events for κ_{0_SS}	Host-to-target adjustment of GMPEs
κ_{r_IRVT}	Analogy to high-frequency decay	Al Atik <i>et al.</i> (2014)	Direct measurement on the Fourier spectrum derived from IRVT as compatible with the GMPE response spectrum	High (above f_{peak})	Ignored (use of small R_s in GMPE)	Yes	No, average over $M-R_e$ scenarios for κ_{0_IRVT}	Host-to-target adjustment of GMPEs (host only)
κ_{0_RESP}	Peak and shape of the normalized acceleration response spectrum	Silva and Darragh (1995), Silva <i>et al.</i> (1998)	Fitting of stochastically simulated response spectra (where κ_0 is a model input parameter) coupled with site amplification to observed response spectra	Entire band	Removed	Yes	Yes, ready to use	Stochastic simulations
κ_{r_BB}	Inversion of the entire frequency band of the spectrum	Anderson and Humphrey (1991), Humphrey and Anderson (1992), Silva <i>et al.</i> (1997), Edwards <i>et al.</i> (2011)	Broadband inversion of the entire spectrum for source, path and site terms (usually for moment, f_c and κ_0)	Entire band	Present	No	No, extrapolate to $R_e = 0$ for κ_{0_BB}	Stochastic simulations
κ_{r_DS}	Small magnitudes (strong trade-off with source)	Biasi and Smith (2001)	Direct measurement on low-frequency part of the Fourier displacement spectrum (much below f_c) where it is theoretically flat	Below f_c	Present	No	No, extrapolate to $R_e = 0$ for κ_{0_DS}	Host-to-target adjustment of GMPEs (target only: measure rather than infer from V_{S30})

This table summarizes the notation proposed herein for each approach (or family of approaches), its main principle, the main references, a short description of the approach, the frequency range used, how Q and distance are accounted for, and the possible applications, which, in the opinion of the authors, are most compatible with the approach.

- *Inverse Random Vibration Theory*: The final variation of the original method discussed here does not use actual records, but response spectra produced by GMPEs for short distances. Al Atik *et al.* (2014) use inverse random vibration theory and the technique of Rathje *et al.* (2005) to derive compatible Fourier spectra from a series of response spectra computed through the GMPE formulae for a suite of magnitude and distance scenarios (below 20 km). Then κ_{r_IRVT} can be measured on the high-frequency part of each GMPE-consistent Fourier spectrum, and it is assumed site-specific in as much as the Q effect is considered negligible. However, because one value of κ_{r_IRVT} is derived for each scenario, these values are averaged over all scenarios to estimate a single κ_{0_IRVT} , which may be considered as the GMPE's native or intrinsic κ_0 .
- *Response Spectrum*: In contrast to the classic that relates κ to the decay of the high-frequency part of the Fourier spectrum, another approach relates it to the spectral shape of the normalized response spectrum. Introduced by Silva and Darragh (1995) and later used by Silva *et al.* (1998), this method uses stochastically generated acceleration response spectra (where κ_0 is one of the point-source seismological model input parameters and is applied to the entire frequency range) coupled with the site amplification computed from the site profile. These simulated spectra are then normalized and compared to observed response spectra to compute the input κ (let us denote this one κ_{0_RESP}) that gives the best fit between them. One important difference from all previous approaches is that, here, the entire frequency band is used for the fitting and not only the high-frequency part. In this approach, trade-offs with stress drop are avoided to a degree, as the response spectra are normalized by peak ground acceleration and then stacked (Hiemer *et al.*, 2011).
- *Broadband Inversions*: A large family of approaches which again use the entire frequency band, but are not restricted to short distances, are what we will call here the family of broadband inversions. The essence of these methods is the assumption of a source spectral shape, with the objective of extracting κ_r when the earthquake corner frequency intrudes into the frequency band used for the measurement. These separate the source, path, and site effects in various ways to yield individual values of what we will denote κ_{r_BB} . These are then extrapolated to κ_{0_BB} . One advantage of broadband inversions is that, unlike the classic approach, they are not constrained as much by the event magnitude, meaning they can use more abundant small-magnitude earthquake data. Numerous broadband inversion schemes can be found in literature. Here we will mention only some of the main schemes. Anderson and Humphrey (1991) invert for f_c (or stress drop), spectral level, and κ_r , assuming a smooth spectral shape to partly overcome the trade-off with stress drop. Humphrey and Anderson (1992) perform the broadband inversion after removing the empirical or modeled site response from each spectrum. Based on a method by Scherbaum (1990), Edwards *et al.* (2011) use a simultaneous broadband inversion of the velocity spectrum resolving for f_c , moment, and κ_{r_BB} . Kilb *et al.* (2012) experiment with fixing the stress drop to a reasonable average value to overcome the trade-off and then invert for moment and κ_{r_BB} . Along the same lines, we may also consider the multiple EGF approaches that reduce the trade-off between f_c and κ_{r_BB} (Hough, 1997; Frankel *et al.*, 1999; Hough *et al.*, 1999). Finally, we also mention the approach introduced by Silva *et al.* (1997), which can yield either a site-specific or a site-class-specific κ_0 , depending on the site data available. This is a broadband inversion of the log of the empirical Fourier spectrum, which has been coupled to a smoothed 1D amplification function (derived either from the site profile or the site class); it yields moment and stress drop, and separates κ_0 from the $Q(f)$ model (described by Q_0 and η).
- *Displacement Spectrum*: The classic approach uses relatively large magnitudes in order to measure spectral decay above f_c . Biasi and Smith (2001) proposed an approach that expands the method to very small magnitudes, where data is much more abundant. These authors measure κ_r directly on the Fourier displacement spectrum, keeping much below the (rather high) f_c , rather than on the Fourier acceleration spectrum and keeping above the (rather low) f_c . Rather than using records from earthquakes, say, above M 4, for which f_c is below 10 Hz, and measuring κ_r as the departure of the acceleration spectrum from the horizontal over, say, 10–30 Hz, we can use records from earthquakes with $M < 1$, for which f_c may exceed 70 Hz, and measure κ_r as the departure of the displacement spectrum from the horizontal over potentially the same frequency range. One advantage of this approach (other than the abundance of data) is that the theoretical basis for treating the displacement spectrum at the source as flat below f_c is actually stronger than the basis for treating the acceleration spectrum as flat above it, because the latter depends on the validity of the ω^{-2} assumption. Let us denote individual κ_r values thus measured as κ_{r_DS} , and the extrapolated zero-distance site parameter as κ_{0_DS} (sometimes referred to also as κ_{0_mini}).

Inferring κ_0 from κ_0 - V_{S30} Correlations

The previous section discussed the measurement of κ_0 from data. In practice, when site-specific data is not available (for instance, when adjusting a GMPE to a stable continental region with little seismic activity and instrumentation), κ_0 is often inferred from available site data, namely V_{S30} (Biro and Renault, 2012). For this reason, we now revisit existing κ_0 - V_{S30} correlations and discuss their scatter and applicability. Given that κ_0 is the site component of κ_r , it is reasonable to expect that harder sites will have lower attenuation, and thus κ_0 will decrease as shear-wave velocity increases. Moreover, as V_{S30} is often available, this has led to various investigations of the correlation between κ_0 and V_{S30} values (Fig. 2a). However, the scatter observed in such correlations is large and the correlation of κ_0 with V_{S30} becomes clear only when we compare κ_0 across several site



▲ **Figure 2.** (a) Existing κ_0 - V_{s30} correlations proposed in the literature. (b) Grouping of existing correlation data with region. (c) Grouping of existing correlation data with method. Also shown are the limits of site classes A through E according to the National Earthquake Hazards Reduction Program (NEHRP) (see [BSSC, 2003](#)).

classes, say for a V_{S30} range of 360–1500 m/s (i.e., categories C through A of the National Earthquake Hazards Reduction Program [NEHRP], Building Seismic Safety Council [BSSC], 2003; see Fig. 2a). This large degree of scatter should come as no surprise, for several reasons.

First, V_{S30} is only a proxy for the deeper V_S profile that controls local site amplification. Its adequacy as a proxy for site attenuation, which is tied to the first few km of the profile (Anderson and Hough, 1984; Campbell, 2009), is questionable. From a physical viewpoint, we would also expect other parameters to correlate to κ_0 , possibly tied to the deeper structure. One such example is the depth to bedrock, recently found to correlate to κ_0 to a similar degree as does V_{S30} (Ktenidou et al., 2012).

The second reason is the scatter present in the V_{S30} values themselves, resulting from the method of measuring (or, at worst, inferring) the V_S profile for each site. Moss (2008) and Boore (2006) find differences of 30%–50% in the derived V_{S30} between different methods. For instance, V_S can be measured from invasive methods (such as crosshole and downhole geophysics, P – S suspension logger, cone penetration tests [CPT]) or noninvasive methods (active approaches, such as multichannel analysis of surface waves [MASW], or passive, such as spatial autocorrelation [SPAC] and f – k). Scatter in V_{S30} is a considerable source of uncertainty but lies outside the scope of this note.

The third reason is the heterogeneity in the κ_0 values themselves. Van Houtte et al. (2011) combined all existing correlations starting from the pioneering work of Silva et al. (1998) and up to their own recent analyses to derive global correlations. The data retrieved are heterogeneous in several ways:

1. *Regions*: First, the data come from different regions around the world. It is possible that even for similar sites, quite large regional differences in κ_0 may exist due to regional differences in Q in the shallow crust (Boore and Joyner, 1997). Atkinson (1996) observed this for hard rock sites in eastern and western Canada. Chandler et al. (2006), who used a global dataset to derive their correlations, admit their scatter is partly due to the variability of the underlying crustal Q and V_S profile for similar V_{S30} values.
2. *Methods*: The studies that derived these κ_0 values use a variety of methods: from the classic method of direct measurement on the high-frequency part of Fourier spectra (Douglas et al., 2010; Edwards et al. 2011; Van Houtte et al., 2011), to the measurement on the tail of the site transfer function (Drouet et al., 2010), to the fitting of stochastic point-source simulations to observed response spectra (Silva et al., 1998), to simultaneous broadband inversion of the velocity spectrum (Edwards et al., 2011). Aside from this between-method scatter, one may also consider the possible within-method scatter, due to the different ways users may apply the same method (see e.g., Ktenidou et al., 2013, for an illustration of the strong possible variability within the classic method).
3. *Range of Frequencies*: Considering that the data in the different κ_0 – V_{S30} correlations come from a period of over two decades, we expect instrument type and performance to change from one study to another. Characteristics, such

as the resolution of the analog-to-digital conversion, the sampling rate, the frequency range of flat instrument response, the full scale, and processing tasks such as filtering and resampling, may strongly affect the available range of frequencies in which κ_t is measured. Furthermore, the judgment of the analyst who selects the pertinent frequency range from f_1 to f_2 (Rovelli et al., 1988; Douglas et al., 2010), as well as the possible influence of the corner frequency within that frequency range, all introduce uncertainty into κ_0 estimates. Finally, the frequency range chosen may also bear upon the trade-off of κ_0 with the site amplification transfer function, whether using the classic approach coupled to the transfer function of the 1D soil column (Parolai and Bindi, 2004) or the response spectral approach coupled with the quarter-wavelength amplification of the generic profile (Boore and Joyner, 1997).

No study has compared all different available approaches in terms of κ_0 . Some, however, have compared certain approaches with the classic approach. Edwards et al. (2011) compared the classic method with their broadband inversion, and Ktenidou et al. (2012) compared the classic with the transfer-function approach, both finding similar results, but with considerable scatter. Chandler et al. (2006) compared the classic method to that of response spectral fitting and found the latter approach overpredicted κ_0 values. Biasi and Anderson (2007) found that the displacement-based method gives an upper bound with respect to the classic method. Kilb et al. (2012) found similar though smaller overestimations using the displacement-based method. Ktenidou et al. (2013) found significant variation in κ_0 values when comparing different possible applications of the classic method.

To investigate the effect of the three aforementioned reasons behind the scatter of κ_0 – V_{S30} correlations, we retrieve (κ_0 , V_{S30}) data pairs from the literature and group them according to region and method. To the data collected by Van Houtte et al. (2011), we add recent results from Ktenidou et al. (2012, 2013) and Ktenidou and Van Houtte (2012), some of which use downhole data for the first time in κ_0 – V_{S30} correlations. In Figure 2b, we group κ_0 – V_{S30} data with region. Some separation is suggested between κ_0 values from stable continental (blue points) and active regions (all other colors), though the scatter is large. We then further separate data coming from Japan into two groups, based on the detailed Q values presented in Oth et al. (2011). These authors divided Japan into four polygons with respect to Q structure derived from crustal events (see their figs. 1 and 8 for details). Considering their Q results at high frequencies, where κ is computed, we group these polygons into a high- Q zone (polygon 2, with an average Q ranging from 520 to 900 from 10 to 25 Hz) and a low- Q zone (polygons 1, 3, and 4, with an average Q 350 to 680 from 10 to 25 Hz). We regress for these two zones separately and derive the two mean κ_0 – V_{S30} correlations plotted in the figure as green lines. Indeed, κ_0 is on average 6 ms higher for the low- Q zone (dark green) compared to the lower- Q zone (light green). Though this difference is rather small and lies within the scatter, this suggests the possibility that the

underlying regional Q variation may affect κ_0 for the same V_{S30} . If so, such correlations may need to be used on a regional basis rather than a global one. We then group existing κ_0 - V_{S30} data according to method. In Figure 2c we see that, especially for site classes A and B, that is, soft and hard rocks, some of the lowest κ_0 values are predicted by the response spectrum and broadband approaches (blue, red), and some of the highest values are predicted by the classic approach (orange). It is worth noting that above 1500 m/s the results of the acceleration spectrum (AS) approach are significantly similar for two very different regions: Greece and Switzerland (light green solid line and black dashed line of Fig. 2a). Conversely, for the Swiss data, two different approaches yield significantly different results (dashed black for AS and dark green for BB in Fig. 2a). This is an indication that the approach used may also have introduced a bias into the computation of κ_0 and hence κ_0 - V_{S30} correlations for different approaches may not be directly comparable. Overall, we find effects of both region and method, but at this stage, it is difficult to dissociate them.

We stress once more that the scatter in κ_0 values due to region, method, and frequency range is only partly the reason behind the poor-correlation coefficients in most κ_0 - V_{S30} correlations (usually less than 30%). Another reason, as mentioned above, is the significant uncertainty in the estimation of V_{S30} . Finally, another part of the problem is that κ_0 also relates to other physical parameters, such as, for example, the depth to bedrock, and probably more factors, which have not yet been mapped onto κ_0 . Simply propagating the large scatter in κ_0 into ground-motion models, using the κ correction process given for GMPE adjustments in Al Atik *et al.* (2014), would lead to a standard deviation of the 20 Hz spectral acceleration of 0.9 natural log units just due to κ_0 variability. This greatly exceeds the variability of high-frequency ground motions typically seen in empirical GMPE due to all sources of variability (source, site, and path), indicating that the κ_0 variability is correlated to other factors, which also affect the ground-motion level. Based on the above, reducing the existing inconsistencies arising from computation methods, regions, and ranges of frequencies will not solve the scatter issue, but it is a first step we need to take before we can start to decipher the physical basis of κ_0 and improve our methods of inferring it using more than just V_{S30} . Finally, given the open question of the source component of κ (κ_s of equation 1) and its possible contribution to the scatter, we believe that our suggestions toward consistency may help decipher these components (whether the source affects the scatter in κ or even the median value) and better understand the remaining questions as to the physical interpretation of κ .

TOWARD A MORE CONSISTENT ESTIMATION AND USE OF κ

Suggested Measurement Methods for Given Applications

How should one measure site-specific, zero-distance κ_0 ? Within the scope of the measurement approaches and analyses

suggested within the literature reviewed here, we suggest that certain measurement approaches may be more appropriate to use with certain applications. The general principle is that each measurement method uses a model with implicit assumptions about the effect of κ on the spectrum, and those should be the same, or at least as similar as possible, to the assumptions made in the subsequent applications. We associate the suggested uses with the families of approaches defined in Table 1, taking into account the features of the approaches, such as, for example, the frequency band over which the measurement is performed.

- On the one hand, methods using the entire range of frequencies to compute κ (such as κ_{RESP} and κ_{BB} , that is, the fitting of simulated to observed response spectra and the broadband spectral inversion of Fourier spectra) may be better suited for use in stochastic ground-motion simulations. In such simulations, the κ_0 filter is often applied over the entire frequency band and not only at high frequencies. For instance, in Stochastic Model SIMulation (SMSIM; Boore, 2003), one of the most widely used codes for stochastic simulations, the diminution filter $e^{-\pi\kappa f}$ starts from $f_1 = 0$. In broadband simulations, the entire band is used to invert the Fourier spectrum for source, path, and site effects, whereas in any response spectrum the high frequencies are affected by the full frequency range of oscillators. The computation of κ over the entire spectrum, given its known trade-offs with source parameters at lower frequencies, implies that the inversion results might best be interpreted relative to one another as a set of parameters rather than individually; this is also true for the group of parameters in a seismological model (Scherbaum *et al.*, 2006). Boore *et al.* (1992) made a similar observation, noting that the κ_0 they computed with response spectral fitting for use in simulations might not correspond to the high-frequency classic κ_0 due to the difference in frequency ranges. EGFs may also be used to fix stress drop and avoid trade-offs, again within the notion of interdependence of the model parameters. For TGFs, there is also a trade-off between κ and Q , which depends on how Q is incorporated in the TGFs (frequency-dependent or independent Q).
- On the other hand, methods that derive κ_0 from direct measurements on high frequencies and distinctly separate it from regional attenuation (such as κ_{AS} , κ_{SS} , κ_{IRVT} , and κ_{TF} , i.e., the classic, source-spectrum, inverse random vibration theory, and transfer-function approaches) may tie better with adjustment of GMPEs from a host region (i.e., where the GMPE is well constrained by data) to a target region (i.e., a region where a GMPE is needed but little or no strong-motion data are available to constrain it). We suggest that the κ_{AS} , κ_{TF} , and κ_{SS} approaches may be most suitable for estimating host region κ_0 s (but also target region κ_0 s, if appropriate data are available). In the case of κ_{IRVT} , we suggest it is by definition suitable for host regions, because it pertains to an existing GMPE.
- Finally, in what concerns the target regions in the host-to-target adjustment process, target κ_0 s are, at the moment,

poorly constrained. These regions are often seismically inactive. Hence, the volume and magnitude range of available records does not generally allow use of the classic methods to compute κ_0 . Furthermore, if κ_0 is to be inferred rather than measured, the uncertainty of existing κ_0 - V_{S30} correlations poses a big problem. We suggest that, in the absence of any usable records at the site, κ_0 - V_{S30} correlations may be used, recognizing the large uncertainty in the resulting κ estimate. Correlations based on regional rather than global models should be preferred, for the reasons listed above. But overall, because even regional correlations do not describe κ_0 completely, site-specific measurement of κ_0 rather than inference is strongly recommended. Thus, we suggest that the κ_{DS} approach is well worth investigating further, as it may help make use of very small magnitude events to make site-specific measurements of κ_0 in non-active regions.

To date, no study has undertaken to compare κ_0 values for the same data across all or most of the different measurement methods found in the literature, or examine the effects this may have on its use in existing applications and on the understanding of the underlying physics of κ (though one attempt was made by [Biasi and Anderson, 2007](#)). We believe that such a study could bring to light inconsistencies in the approaches used today and could better demonstrate which κ should be put to which use. Bearing in mind how multifaceted this parameter can be in both its meaning and its estimation, we suggest that when κ values are measured, discussed, and used, they be accompanied by a notation similar to that shown in [Table 1](#). As κ depends on the measurement approach and the underlying models, we believe these notations are needed to better suit the different purposes, as shown in the table.

Suggestions on Instrumentation and Data Processing

To the heterogeneity of the different approaches used, we may also add the possibility of constraints, problems, or errors in the available data or its processing. [Ktenidou et al. \(2013\)](#) show the effect of exceeding the available frequency range either as constrained by the signal-to-noise ratio (this should constrain f_2) or by the corner frequency (this should constrain f_1) in the estimation of κ_0 , but the problem may begin even before this stage. For instance, [Laurendeau et al. \(2013\)](#) point out that, in choosing f_2 for their κ_{AS} estimation, [Van Houtte et al. \(2011\)](#) neglected to account for a low-pass filter present in all KiK-net instruments, which may have affected κ_r . Data should preferably only be used after correcting for instrument response or, at least, checking the maximum usable frequency up to which response is flat. Similar problems may arise due not to the instrument but to the subsequent data processing protocol applied by data suppliers: [Graizer \(2012\)](#) demonstrates that standard procedures of filtering and resampling, which follow, for example, the Caltech protocol, may cause distortion to the Fourier and response spectra, affecting frequencies 6–8 Hz and above. He stresses the need for databases to supply original, unfiltered, un-corrected data in order to preserve high-frequency information in records. The above examples

show that, although technological advances have allowed modern instruments to provide high sampling rates, certain standard practices do not allow us to take full advantage of data at high frequencies. This we believe is partly because we have been using such procedures due to momentum and partly because the interest of the engineering seismology community was focused until recently on lower-frequency response. As early as 1994, [Trifunac \(1994\)](#) pointed out that strong-motion processing tended to stop at 25 Hz, even though it was already technologically possible to extend the limit to 50 Hz. Such an extension would strongly benefit the study of κ . For instance, it would provide the frequency band necessary for the measurement of lower $\kappa_{r,AS}$ values on hard rock, like those coming from small nearby events or in stable regions with high Q . Going to higher frequencies is necessary to better compute very low values of κ_0 , for example, at very hard rock sites, and stable regions, where considerable high-frequency energy is sometimes observed. It has been shown that the ability to measure κ_r for small nearby events depends partly on how far into the high frequencies f_2 can be extended ([Ktenidou et al., 2013](#), fig. 4; [Van Houtte et al., 2013](#)). Today we are more aware of the importance of understanding ground motion at high frequencies, even above 30 or 50 Hz; e.g., [Silva and Darragh \(2012\)](#), and [Laurendeau et al. \(2013\)](#) show the effect of κ at frequencies above 50 Hz. We also have the means to record and acquire data at higher frequencies. However, we need to be aware of pitfalls. For instance, in Japan, for some of the densest and highest-technology networks in the world, sampling rates are of 100 or 200 Hz (K-net and KiK-net, respectively). However, the instruments have a cutoff frequency of 30 Hz ([Aoi et al., 2004](#)), thus significantly limiting the usable band. We propose that future instrumentation initiatives take into account the need to improve knowledge at high frequencies and decide on sampling rates and anti-aliasing filters accordingly. This includes downhole arrays, which will help improve our understanding of hard-rock attenuation. Similarly, we suggest that public databases provide users with the option of direct access to uncorrected, unfiltered data, to avoid the problems outlined by [Graizer \(2012\)](#).

CONCLUSION

In this note, we have made four main suggestions, namely:

- that subscripts should be used when κ_0 is computed from data, so the user knows how the values were estimated,
- that certain families of κ_0 estimation approaches may be more appropriate for certain applications ([Table 1](#)),
- that rendering κ_0 - V_{S30} correlations more consistent in terms of regions and methods may improve the current practice of inferring κ_0 without site-specific data and constitutes a useful step toward deciphering the physical basis of κ_0 , and
- that future instrumentation and signal-processing protocols for open-access databases should take into account the preservation of high-frequency information.

These recommendations notwithstanding, we stress that more research is needed to better comprehend this parameter and the scatter observed in its estimates. ☒

ACKNOWLEDGMENTS

We are thankful for discussions with Philippe Renault and all partners and experts of the PEGASOS Refinement Project, through which the idea for this paper was born. We have also been inspired by Kilb *et al.* (2012), who named certain κ estimation approaches, and comments by Pierre-Yves Bard. The research has been partly funded by the French SIGMA project. We thank Ralph Archuleta, Glenn Biasi, Jim Brune, Art Frankel, Tom Hanks, Maria Lancieri, Aurore Laurendeau, Walt Silva, Chris Van Houtte, and experts of Hanford SSHAC, SWUS SSHAC, Next Generation Attenuation-West 2 (NGA-W2), and SIGMA projects for useful discussions. Warm thanks go to Frank Scherbaum and John Douglas for insightful reviews of what was initially the “Don’t call it kappa!” manuscript. Finally, we thank Dave Boore and the associate editor for thorough reviews that significantly improved the submitted manuscript. Some plots were made using Generic Mapping Tools *v.* 3.4 (www.soest.hawaii.edu/gmt, last accessed March 2013; Wessel and Smith, 1998).

REFERENCES

Abercrombie, R. E. (1995). Earthquake source scaling relationships from -1 to $5 M_L$ using seismograms recorded at 2.5-km depth, *J. Geophys. Res.* **100**, 24,015–24,036.

Aki, K. (1967). Scaling law of seismic spectrum, *J. Geophys. Res.* **72**, 1217–1231.

Aki, K. (1987). Magnitude-frequency relation for small earthquakes: A clue to the origin of f_{\max} of large earthquakes, *J. Geophys. Res.* **92**, 1349–1355.

Al Atik, L., A. Kottke, N. Abrahamson, and J. Hollenback (2014). Kappa correction of ground motion prediction equations using inverse random vibration theory approach, *Bull. Seismol. Soc. Am.* **104**, no. 1, doi: [10.1785/0120120200](https://doi.org/10.1785/0120120200) (in press).

Anderson, J. G. (1986). Implication of attenuation for studies of the earthquake source, in (*Maurice Ewing Series 6*): *Earthquake Source Mechanics*, M. Ewing (Editor), American Geophysical Monograph 37 311–318.

Anderson, J. G. (1991). A preliminary descriptive model for the distance dependence of the spectral decay parameter in southern California, *Bull. Seismol. Soc. Am.* **81**, 2186–2193.

Anderson, J. G., and S. E. Hough (1984). A model for the shape of the Fourier amplitude spectrum of acceleration at high frequencies, *Bull. Seismol. Soc. Am.* **74**, 1969–1993.

Anderson, J. G., and J. R. Humphrey (1991). A least squares method for objective determination of earthquake source parameters, *Seismol. Res. Lett.* **62**, 201–209.

Anderson, J. G., Y. Lee, Y. Zeng, and S. Day (1996). Control of strong motion by the upper 30 meters, *Bull. Seismol. Soc. Am.* **86**, 1749–1759.

Aoi, S., T. Kunugi, and H. Fujiwara (2004). Strong-motion seismograph network operated by NIED: K-NET and KiK-net, *J. Japan Assoc. Earthq. Eng.* **4**, 65–74.

Archuleta, R. J., E. Cranswick, C. Mueller, and P. Spudich (1982). Source parameters of the 1980 Mammoth Lakes, California, earthquake sequence, *J. Geophys. Res.* **87**, 4595–4607.

Atkinson, G. M. (1996). The high-frequency shape of the source spectrum for earthquakes in eastern and western Canada, *Bull. Seismol. Soc. Am.* **86**, 106–112.

Atkinson, G. M., and I. Beresnev (1997). Don’t call it stress drop, *Seismol. Res. Lett.* **63**, 3–4.

Bakun, W. H., C. G. Bufe, and R. M. Stewart (1976). Body wave spectra of central California earthquakes, *Bull. Seismol. Soc. Am.* **66**, 439–459.

Beresnev, I. A., and G. M. Atkinson (1997). Modeling finite-fault radiation from the ω^n spectrum, *Bull. Seismol. Soc. Am.* **87**, 67–84.

Biasi, G. P., and J. G. Anderson (2007). Measurement of the parameter kappa, and reevaluation of kappa for small to moderate earthquakes at seismic stations in the vicinity of Yucca Mountain, Nevada, *Final Technical Report TR-07-007*, Nevada System of Higher Education (NSHE), University of Nevada, Las Vegas (UNLV), 232 pp., doi: [10.2172/920643](https://doi.org/10.2172/920643).

Biasi, G. P., and K. D. Smith (2001). *Site Effects for Seismic Monitoring Stations in the Vicinity of Yucca Mountain, Nevada*, MOL20011204.0045, a report prepared for the US DOE/University and Community College System of Nevada (UCCSN) Cooperative Agreement.

Biro, Y., and P. Renault (2012). Importance and impact of host-to-target conversions for ground motion prediction equations in PSHA, in *Proc. 15th World Conference of Earthquake Engineering*, Lisbon, Portugal, 24–28 September, 10 pp.

Boore, D. M. (1986). Short-period *P*- and *S*-wave radiation from large earthquakes: Implications for spectral scaling relations, *Bull. Seismol. Soc. Am.* **76**, 43–64.

Boore, D. M. (2003). Simulation of ground motion using the stochastic method, *Pure Appl. Geophys.* **160**, 635–676.

Boore, D. M. (2006). Determining subsurface shear wave velocities, *A review 3rd International Symposium on the Effects of Surface Geology on Seismic Motion*, Grenoble, France, 30 August–1 September, Paper No. 103.

Boore, D. M., and W. B. Joyner (1997). Site amplifications for generic rock sites, *Bull. Seismol. Soc. Am.* **87**, 327–341.

Boore, D. M., W. B. Joyner, and L. Wennerberg (1992). Fitting the stochastic omega-squared source model to observed response spectra in western North America: Trade-offs between stress drop and kappa, *Bull. Seismol. Soc. Am.* **82**, 1956–1963.

Brune, J. (1970). Tectonic stress and the spectra of seismic shear waves, *J. Geophys. Res.* **75**, 4997–5009.

Building Seismic Safety Council (BSSC) (2003). The 2003 NEHRP Recommended Provisions for New Buildings and Other Structures, Part 1: Provisions (FEMA 450), <http://bssc.nibs.org> (last accessed January 2013).

Campbell, K. W. (2003). Prediction of strong ground motion using the hybrid empirical method and its use in the development of ground motion (attenuation) relations in eastern North America, *Bull. Seismol. Soc. Am.* **93**, 1012–1033.

Campbell, K. W. (2004). Erratum: Prediction of strong ground motion using the hybrid empirical method and its use in the development of ground motion (attenuation) relations in eastern North America, *Bull. Seismol. Soc. Am.* **94**, 2418.

Campbell, K. W. (2009). Estimates of shear-wave *Q* and κ_0 for unconsolidated and semiconsolidated sediments in eastern North America, *Bull. Seismol. Soc. Am.* **99**, 2365–2392.

Castro, R., F. Pacor, A. Sala, and C. Petrangaro (1996). *S* wave attenuation and site effects in the region of Friuli, Italy, *J. Geophys. Res.* **101**, 22,355–22,369.

Chandler, A. M., N. T. K. Lamb, and H. H. Tsang (2006). Near-surface attenuation modelling based on rock shear-wave velocity profile, *Soil Dynam. Earthq. Eng.* **26**, 1004–1014.

Cotton, F., F. Scherbaum, J. J. Bommer, and H. Bungum (2006). Criteria for selecting and adjusting ground-motion models for specific target regions: Application to Central Europe and rock sites, *J. Seismol.* **10**, 137–156.

- Delavaud, E., F. Cotton, S. Akkar, F. Scherbaum, L. Danciu, C. Beauval, S. Drouet, J. Douglas, R. Basili, M. Abdullah Sandikkaya, M. Segou, E. Faccioli, and N. Theodoulidis (2012). Towards a ground-motion logic tree for probabilistic seismic hazard assessment in Europe, *J. Seismol.* **16**, 451–473.
- Douglas, J., P. Gehl, L. F. Bonilla, and C. Gélis (2010). A κ model for mainland France, *Pure Appl. Geophys.* **167**, 1303–1315.
- Drouet, S., F. Cotton, and P. Gueguen (2010). V_{S30} , κ , regional attenuation and M_w from accelerograms: Application to magnitude 3–5 French earthquakes, *Geophys. J. Int.* **182**, 880–898.
- Edwards, B., D. Faeh, and D. Giardini (2011). Attenuation of seismic shear wave energy in Switzerland, *Geophys. J. Int.* **185**, 967–984.
- Fernández-Heredia, A. I., C. I. Huerta-Lopez, R. R. Castro-Escamilla, and J. Romo-Jones (2012). Soil damping and site dominant vibration period determination, by means of random decrement method and its relationship with the site-specific spectral decay parameter κ , *Soil Dynam. Earthq. Eng.* **43**, 237–246.
- Foster, K. M., B. Halldorsson, R. A. Green, and M. C. Chapman (2012). Calibration of the specific barrier model to the NGA dataset, *Seismol. Res. Lett.* **83**, 566–574.
- Frankel, A. (1982). The effects of attenuation and site response on the spectra of microearthquakes in the northeastern Caribbean, *Bull. Seismol. Soc. Am.* **72**, 1379–1402.
- Frankel, A., D. Carver, E. Cranswick, M. Meremonte, T. Bice, and D. Overturn (1999). Site response for Seattle and source parameters of earthquakes in the Puget Sound region, *Bull. Seismol. Soc. Am.* **89**, 468–483.
- Gariel, J.-C., and M. Campillo (1989). The influence of the source on the high-frequency behaviour of the near-field acceleration spectrum: A numerical study, *Geophys. Res. Lett.* **16**, 279–282.
- Gentili, S., and G. Franceschina (2011). High frequency attenuation of shear waves in the southeastern Alps and northern Dinarides, *Geophys. J. Int.* **185**, 1393–1416.
- Ghofrani, H., G. Atkinson, and K. Goda (2013). Implications of the 2011 M 9.0 Tohoku Japan earthquake for the treatment of site effects in large earthquakes, *Bull. Earthq. Eng.* **11**, 171–203.
- Graizer, V. (2012). Effect of low-pass filtering and re-sampling on spectral and peak ground acceleration in strong-motion records, *Proc. 15th World Conference of Earthquake Engineering*, Lisbon, Portugal, 24–28 September, 10 pp.
- Graves, R. (1996). Simulating seismic wave propagation in 3D elastic media using staggered grid finite differences, *Bull. Seismol. Soc. Am.* **86**, 1091–1106.
- Graves, R. W., and A. Pitarka (2010). Broadband ground-motion simulation using a hybrid approach, *Bull. Seismol. Soc. Am.* **100**, 2095–2123.
- Halldorsson, B., and A. S. Papageorgiou (2005). Calibration of the specific barrier model to earthquakes of different tectonic regions, *Bull. Seismol. Soc. Am.* **95**, 1276–1300.
- Hanks, T. C. (1982). f_{\max} , *Bull. Seismol. Soc. Am.* **72**, 1867–1879.
- Hanks, T. C., and R. K. McGuire (1981). The character of high-frequency strong ground motion, *Bull. Seism. Soc. Am.* **71**, 2071–2095.
- Hiemer, S., F. Scherbaum, D. Roessler, and N. Kuehn (2011). Determination of τ_0 and rock site κ from records of the 2008/2009 earthquake swarm in western Bohemia, *Seismol. Res. Lett.* **82**, 387–393.
- Hough, S. E. (1997). Empirical Green's function analysis: Taking the next step, *J. Geophys. Res.* **102**, 5369–5384.
- Hough, S. E., and J. G. Anderson (1988). High-frequency spectra observed at Anza, California: Implications for Q structure, *Bull. Seismol. Soc. Am.* **78**, 692–707.
- Hough, S. E., J. G. Anderson, J. Brune, F. Vernon III, J. Berger, J. Fletcher, L. Haar, T. Hanks, and L. Baker (1988). Attenuation near Anza, California, *Bull. Seismol. Soc. Am.* **78**, 672–691.
- Hough, S. E., J. Lees, and F. Monastero (1999). Attenuation and source properties at the Coso geothermal area, California, *Bull. Seismol. Soc. Am.* **89**, 1606–1619.
- Humphrey, J. R., Jr., and J. G. Anderson (1992). Shear wave attenuation and site response in Guerrero, Mexico, *Bull. Seismol. Soc. Am.* **81**, 1622–1645.
- Irikura, K. (1986). Prediction of strong acceleration motion using empirical Green's function, *Proc. 7th Japan Earthq. Eng. Symp.*, 10–12 December 1986, Tokyo, 151–156.
- Iwakiri, K., and M. Hoshihara (2012). High-frequency (> 10 Hz) content of the initial fifty seconds of waveforms from the 2011 Off the Pacific Coast of Tohoku Earthquake, *Bull. Seismol. Soc. Am.* **102**, 2232–2238.
- Kilb, D., G. Biasi, J. G. Anderson, J. Brune, Z. Peng, and F. L. Vernon (2012). A comparison of spectral parameter κ from small and moderate earthquakes using southern California ANZA seismic network data, *Bull. Seismol. Soc. Am.* **102**, 284–300.
- Ktenidou, O.-J., and C. Van Houtte (2012). *Empirical Estimation of κ from Rock Velocity Profiles at the Swiss NPP Sites* (19.02.2012), Report TP2-TB-1090, PEGASOS Refinement Project.
- Ktenidou, O.-J., S. Drouet, N. Theodoulidis, M. Chaljub, S. Arnaouti, and F. Cotton (2012). Estimation of κ (κ) for a sedimentary basin in Greece (EUROSEISTEST): Correlation to site characterization parameters, *Proc. 15th World Conference of Earthquake Engineering*, Lisbon, Portugal, 24–28 September, 10 pp.
- Ktenidou, O.-J., C. Gélis, and F. Bonilla (2013). A study on the variability of κ in a borehole, Implications on the computation method used, *Bull. Seismol. Soc. Am.* **103**, 1048–1068.
- Lancieri, M., R. Madariaga, and F. Bonilla (2012). Spectral scaling of the aftershocks of the Tocopilla 2007 earthquake in northern Chile, *Geophys. J. Int.* **189**, 469–480.
- Laurendeau, A., F. Cotton, O.-J. Ktenidou, L.-F. Bonilla, and F. Hollender (2013). Rock and stiff-soil site amplification: Dependencies on V_{S30} and κ (κ_0), *Bull. Seismol. Soc. Am.* **103**, no. 6, doi: 10.1785/0120130020.
- Mai, P. M., W. Imperatori, and K. B. Olsen (2010). Hybrid broadband ground-motion simulations: Combining long-period deterministic synthetics with high-frequency multiple S-to-S back-scattering, *Bull. Seismol. Soc. Am.* **100**, 2124–2142.
- Margaris, B. N., and D. M. Boore (1998). Determination of $\Delta\sigma$ and κ_0 from response spectra of large earthquakes in Greece, *Bull. Seismol. Soc. Am.* **88**, 170–182.
- Mayeda, K., and W. Walter (1996). Moment, energy, stress drop, and source spectra of western United States earthquakes from regional coda envelopes, *J. Geophys. Res.* **101**, 11,195–11,208.
- Moss, R. E. S. (2008). Quantifying measurement uncertainty of thirty-meter shear-wave velocity, *Bull. Seismol. Soc. Am.* **98**, 1399–1411.
- Motazedian, D. (2006). Region-specific key seismic parameters of earthquakes in northern Iran, *Bull. Seismol. Soc. Am.* **96**, 1383–1395.
- Nava, F. A., R. García, R. R. Castro, C. Suárez, B. Márquez, F. Núñez-Cornú, G. Saavedra, and R. Toscano (1999). S wave attenuation in the coastal region of Jalisco-Colima, Mexico, *Phys. Earth Planet. In.* **115**, 247–257.
- Oth, A., D. Bindi, S. Parolai, and D. Di Giacomo (2011). Spectral analysis of K-NET and KiK-net data in Japan, Part II: On attenuation characteristics, source spectra, and site response of borehole and surface stations, *Bull. Seismol. Soc. Am.* **101**, 667–687.
- Papageorgiou, A. S. (1988). On two characteristic frequencies of acceleration spectra: Patch corner frequency and f_{\max} , *Bull. Seismol. Soc. Am.* **78**, 509–529.
- Papageorgiou, A. S. (2003). The barrier model and strong ground motion, *Pure Appl. Geophys.* **160**, 603–634.
- Papageorgiou, A. S., and K. Aki (1983). A specific barrier model for the quantitative description of inhomogeneous faulting and the prediction of strong ground motion. Part I: Description of the model, *Bull. Seismol. Soc. Am.* **73**, 693–722.
- Parolai, S., and D. Bindi (2004). Influence of soil-layer properties on k evaluation, *Bull. Seismol. Soc. Am.* **94**, 349–356.
- Purvanche, M. D., and J. G. Anderson (2003). A comprehensive study of the observed spectral decay in strong-motion accelerations recorded in Guerrero, Mexico, *Bull. Seismol. Soc. Am.* **93**, 600–611.
- Rathje, E. M., A. R. Kottke, and M. C. Ozbey (2005). Using inverse random vibration theory to develop input Fourier amplitude spectra

- for use in site response, *Proc. 16th Int. Conf. Soil Mechanics and Geotechnical Engineering: TC4 Earthquake Geotechnical Engineering Satellite Conf.*, 10 September 2005, Osaka, Japan, 160–166.
- Rovelli, A., O. Bonamassa, M. Cocco, M. Di Bona, and S. Mazza (1988). Scaling laws and spectral parameters of the ground motion in active extensional areas in Italy, *Bull. Seismol. Soc. Am.* **78**, 530–560.
- Scherbaum, F. (1990). Combined inversion for the three-dimensional Q structure and source parameters using microearthquake spectra, *J. Geophys. Res.* **95**, 12,423–12,438.
- Scherbaum, F., F. Cotton, and H. Staedtke (2006). The estimation of minimum-misfit stochastic models from empirical ground-motion prediction equations, *Bull. Seismol. Soc. Am.* **96**, 427–445.
- Schmedes, J., R. J. Archuleta, and D. Lavallée (2010). Correlation of earthquake source parameters inferred from dynamic rupture simulations, *J. Geophys. Res.* **115**, no. B03304, doi: [10.1029/2009JB006689](https://doi.org/10.1029/2009JB006689).
- Silva, W. J., N. Abrahamson, G. Toro, and C. Costantino (1997). *Description and Validation of the Stochastic Ground Motion Model*, Report submitted to Brookhaven National Laboratory, Associated Universities, Inc., Upton, New York 11973, Contract No. 770573.
- Silva, W. J., and R. Darragh (1995). *Engineering Characterization of Earthquake Strong Ground Motion Recorded at Rock Sites*, Palo Alto, Electric Power Research Institute, TR-102261.
- Silva, W. J., and R. Darragh (2012). *Assessment of kappa for Vertical and Horizontal Motions at Rock Sites Using Spectral Shapes*, Final Report no. EXT-TB-1089, Pegasos Refinement Project.
- Silva, W., R. Darragh, N. Gregor, G. Martin, N. Abrahamson, and C. Kircher (1998). *Reassessment of Site Coefficients and Near-Fault Factors for Building Code Provisions*, Technical Report Program Element II: 98-HQGR-1010, Pacific Engineering and Analysis, El Cerrito, U.S.A.
- Toro, G. R., N. A. Abrahamson, and J. F. Schneider (1997). Model of strong ground motions from earthquakes in central and eastern North America: Best estimates and uncertainties, *Seismol. Res. Lett.* **68**, 41–57.
- Trifunac, M. D. (1994). Q and high-frequency strong motion spectra, *Soil Dynam. Earthq. Eng.* **13**, 149–161.
- Tsai, C.-C. P., and K.-C. Chen (2000). A model for the high-cut process of strong motion accelerations in terms of distance, magnitude, and site condition: An example from the SMART 1 array, Lotung, Taiwan, *Bull. Seismol. Soc. Am.* **90**, 1535–1542.
- Tsurugi, M., T. Kawaga, and K. Irikura (2008). Study on high-cut frequency characteristics of ground motions for inland crustal earthquakes in Japan, *Proc. 14th WCEE*, Beijing, 12–17 October.
- Van Houtte, C., S. Drouet, and F. Cotton (2011). Analysis of the origins of κ (kappa) to compute hard rock to rock adjustment factors for GMPEs, *Bull. Seismol. Soc. Am.* **101**, 2926–2941.
- Van Houtte, C., O. -J. Ktenidou, and T. Larkin (2013). Near-source kappa estimates from the Canterbury earthquake sequence, New Zealand, *SSA Annual Meeting*, Salt Lake City, 17–19 April 2013.
- Wen, J., and X. Chen (2012). Variations in f_{\max} along the ruptured fault during the M_w 7.9 Wenchuan earthquake of 12 May 2008, *Bull. Seismol. Soc. Am.* **102**, 991–998.
- Wessel, P., and W. H. F. Smith (1998). New, improved version of the Generic Mapping Tools Released, *Eos Trans. AGU* **79**, 579.
- Zeng, Y., J. G. Anderson, and G. Yu (1994). A composite source model for computing realistic synthetic strong ground motions, *J. Res. Lett.* **21**, 725–728.

Olga-Joan Ktenidou
Fabrice Cotton
ISTerre
Université de Grenoble 1
CNRS, F-38041 Grenoble
France
olga.ktenidou@ujf-grenoble.fr

Norman A. Abrahamson
Department of Civil and Environmental Engineering
University of California, Berkeley
447 Davis Hall
Berkeley, California 94720 U.S.A.

John G. Anderson
Nevada Seismological Laboratory
and Department of Geological Sciences and Engineering
MS 174
University of Nevada
Reno, Nevada 89557 U.S.A.

3. IMPROVING OUR UNDERSTANDING OF THE PHYSICS OF KAPPA

3.1 κ_0 in Christchurch: directional dependencies, nonlinearity, and magnitude considerations

The 2010-2012 Canterbury earthquake sequence generated a large number of near-source earthquake recordings, with the vast majority of large events occurring within 30 km of Christchurch. We utilize the dataset to estimate κ_0 at seven rock and stiff soil stations in New Zealand's GeoNet seismic network. As part of this study, an orientation-independent definition of κ_0 is proposed to minimize the influence of observed high-frequency 2D site effects. Minimum magnitude limits for the traditional high-frequency fitting method are proposed, based on the effect of the source corner frequency. It is also the first time that a dependence of κ_0 on ground shaking level (PGA) is observed. This observation is not yet well constrained or explained, but if it is found to be systematic, it could influence the use of κ_0 in future hazard assessments for critical facilities. κ_0 values measured from Fourier amplitude spectra (κ_{0_AS}) are compared with the 'native' κ_0 of local, empirical, ground motion prediction equations (GMPEs), measured using the inverse random vibration theory method (κ_{0_IRVT}). We find that κ_{0_IRVT} of current GMPEs is independent of magnitude and distance, and generally agrees with the average κ_{0_AS} for the region. The correlation between κ_{0_IRVT} and V_{s30} is not strong, indicating that current GMPEs capture the average κ_0 effect through their V_{s30} scaling. The results are of particular interest for site-specific ground motion prediction studies, and for adjustments between different regions or rock types using the host-to-target method.

This chapter reports the work shown in publications J3, and its earlier versions : A1, C1 (see Annex).

Hard-site κ_0 (kappa) measurements for Christchurch, New Zealand, and comparison with local ground motion prediction models

Chris Van Houtte*, Olga-Joan Ktenidou†, Tam Larkin*, Caroline Holden‡

April 26, 2014

*Department of Civil Engineering, University of Auckland, New Zealand

†ISTerre, Université Joseph Fourier, CNRS, BP53, 38041 Grenoble Cedex 9, France

‡GNS Science, Lower Hutt, New Zealand

1 ABSTRACT

2 The 2010-2012 Canterbury earthquake sequence generated a large number of near-source
3 earthquake recordings, with the vast majority of large events occurring within 30 km of
4 Christchurch, New Zealand's second largest city. We utilize the dataset to estimate the site
5 attenuation parameter, κ_0 , at seven rock and stiff-soil stations in New Zealand's GeoNet
6 seismic network. As part of this study, an orientation-independent definition of κ is proposed
7 to minimize the influence of observed high-frequency 2D site effects. Minimum magnitude
8 limits for the traditional high-frequency fitting method are proposed, based on the effect of
9 the source corner frequency. A dependence of κ_0 on ground-shaking level is also observed,
10 where events with large peak ground accelerations (PGAs) have lower κ_0 values than events
11 with small PGAs. This observation is not fully understood, but if such a trend holds in
12 future investigations, it may influence how κ_0 is used in hazard assessments for critical
13 facilities.

14 κ_0 values measured from Fourier amplitude spectra ($\kappa_{0,AS}$) are compared with the 'na-
15 tive' κ_0 of local, empirical, ground-motion prediction equations (GMPEs), calculated using
16 the inverse random vibration theory method ($\kappa_{0,IRVT}$). $\kappa_{0,IRVT}$ is found to be independent
17 of magnitude and distance, and agrees with the average $\kappa_{0,AS}$ for the region. $\kappa_{0,IRVT}$ does
18 not scale strongly with V_{S30} , indicating that current GMPEs may be capturing the average
19 kappa effect through the V_{S30} scaling. The results from this study are of particular inter-
20 est for site-specific ground motion prediction studies, and for GMPE adjustments between
21 different regions or rock types.

22 INTRODUCTION

23 The Canterbury earthquake sequence began with the M_w 7.1 Darfield earthquake on 3
24 September 2010 and since then, over 11,000 aftershocks have been recorded (Bannister
25 & Gledhill, 2012). The majority of the events were in close proximity to Christchurch, New
26 Zealand’s second largest city (population c. 377,000), and as a result, an exceptionally large
27 dataset of near-source strong motion recordings has been collected. This study uses the
28 available data to estimate the spectral decay parameter, κ (“kappa”, Anderson and Hough,
29 1984). κ controls the rate of high-frequency decay of the Fourier amplitude spectrum (FAS)
30 and can be modeled as per equation (1):

$$A(f) = A_0 \exp(-\pi \kappa f), \quad f > f_e \quad (1)$$

31 where f_e is the frequency above which the decay is approximately linear on a plot of log
32 Fourier amplitude vs linear frequency. κ is typically considered to be a function of epicentral
33 distance (R) and a site variable (S), mathematically formulated as:

$$\kappa(R, S) = \kappa_0(S) + \tilde{\kappa}(R) \quad (2)$$

34 where $\kappa_0(S)$ represents the attenuation in the near-surface geology and is specific to every
35 site, and $\tilde{\kappa}(R)$ is the distance-dependence of κ , constrained to equal zero at zero epicentral
36 distance (Anderson, 1991). While the majority of recent κ studies adopt the parameteriza-
37 tion in equation (2), the physical interpretation of κ has been a contentious issue ever since
38 it was first observed. The pioneering studies that first modeled high-frequency attenuation
39 (Hanks, 1982; Anderson and Hough, 1984) interpreted the high-frequency decay as a site
40 effect (i.e. a sharp increase in attenuation in near-surface layers), while others attributed
41 the decay to source effects (e.g. Papageorgiou and Aki, 1983; Aki, 1987). Some more re-
42 cent studies have suggested there may be both a source and site component contributing to
43 the measured κ value (e.g. Tsai and Chen, 2000; Purvance and Anderson, 2003), however
44 current understanding is that κ primarily depends on path and site attenuation.

45 Under the assumption that it represents site attenuation, $\kappa_0(S)$, hereafter referred to
46 as κ_0 , has become a widely used parameter in a range of engineering and seismological
47 applications. In some ground-motion simulation codes (e.g. Boore, 2003; Motazedian and
48 Atkinson, 2005), κ_0 is an input parameter to model the high-frequency shape of the sim-
49 ulated spectra, by controlling the rate of decay of an exponential low-pass filter applied
50 across the entire frequency band. In conjunction with V_{S30} (the time-averaged shear-wave
51 velocity in the first 30 m below ground surface), the κ_0 parameter has recently been used
52 to more accurately model rock site amplification functions, and has been implemented as
53 a predictor variable in an empirical ground motion prediction equation (GMPE) for rock
54 sites (Laurendeau et al., 2013). For the purposes of site-specific ground-motion prediction,
55 κ_0 is used as a GMPE adjustment parameter in the host-to-target method of Campbell
56 (2003), accounting for regional differences in rock site attenuation between the host and
57 target regions (Cotton et al., 2006; Douglas et al., 2006; Van Houtte et al., 2011).

58 Recently, the question has been raised, how should κ_0 be estimated for each of these
59 applications? Several different measurement methods exist, which are not necessarily equiv-
60 alent to each other. Ktenidou et al. (2014) identified different approaches to measure κ_0
61 and grouped them into families based on consistency: 1) the high-frequency family, where κ
62 is measured on the high-frequency part of the data, then an extrapolation to zero distance
63 is made to derive κ_0 , and 2) the broadband family, where κ_0 is derived as one of a set of
64 parameters over the entire frequency band. These authors also introduced the notion that
65 these families may be better suited to different applications. They suggest that a κ_0 value
66 derived across the entire frequency band may be more suitable to use as input in stochastic
67 simulations, while a κ_0 measured only on the high-frequency part of the data may be bet-
68 ter suited for host-to-target adjustments of GMPEs. This paper is concerned with GMPE
69 adjustments and the high-frequency family of κ estimation methods.

70 κ_0 scaling (i.e. applying adjustment factors to a GMPE to account for site or regional
71 differences in κ effects) is currently a challenging task (e.g. Biro and Renault, 2012). While
72 a representative κ_0 value for the host GMPE’s dataset can be directly measured using an
73 inverse random vibration theory approach ($\kappa_{0,IRVT}$, Al Atik et al., 2014), this method is not

74 applicable for a low-seismicity target region, where local, empirically-derived GMPEs are
75 typically unavailable. Direct measurement of a representative κ_0 value in the target region
76 is inherently difficult, given a general lack of data. The typical alternative is inference of κ_0
77 from correlations with V_{S30} (Silva et al., 1998; Chandler et al., 2006; Edwards et al., 2011;
78 Van Houtte et al., 2011; Edwards and Fäh, 2013). The overall correlation of κ_0 with V_{S30} is
79 poor, with different studies yielding significantly different results, especially for rock sites.
80 This makes inferring a representative κ_0 value for the target region difficult and unreliable.
81 In this study, we examine ways to improve the robustness of target region κ_0 estimates,
82 particularly by measuring κ_0 directly from local small magnitude data.

83 Aside from the uncertainties that stem from the different methods used to estimate κ_0
84 across different studies, there is also considerable uncertainty due to the variability of κ
85 measurements within a single study. Most studies identify significant scatter between their
86 calculated κ results and the parameterization in equation (2). This has facilitated the debate
87 regarding the physical mechanism causing κ . Kilb et al. (2012) speculate that the scatter
88 is due to a combination of physical parameters such as focal mechanism, near-source path
89 effects and near-surface heterogeneities. Ktenidou et al. (2013) examined the variability
90 arising from different assumptions in the computational process (e.g. choice of distance
91 metric, correction for site amplification, signal-to-noise ratio) and offered guidelines for a
92 more robust computational process. Despite their standardized computation process, the
93 variability in obtained κ measurements was still substantial. This raises the question, what
94 is causing the scatter of κ measurements?

95 The first motivation of this study is to identify sources of scatter in κ measurements
96 from FAS of acceleration (i.e. κ_{AS}), and provide recommendations for computing more
97 stable values in future studies. The second aim of the article is to compare measured $\kappa_{0,AS}$
98 estimates from Christchurch with $\kappa_{0,IRVT}$ from local ground motion prediction models, to
99 investigate whether these two methods for calculating κ_0 are consistent. Both methods
100 belong to the high-frequency family of methods suitable for GMPE adjustments.

101 DATA

102 The dataset used for this study comprises events recorded at seven GeoNet rock and stiff soil
103 stations (AKSS, CRLZ, D14C, GODS, HVSC, MQZ and MTPS; see www.geonet.org.nz for
104 further information) from the Canterbury region in the South Island of New Zealand. All
105 are free-field, surface stations, except for CRLZ, which is located in a cavern approximately
106 30 meters below ground surface. The locations of these stations are shown in Figure 1.
107 The sites have been previously characterized in terms of resonant site period using the
108 horizontal-to-vertical spectral ratio (HVSR) method for S-wave shaking (Van Houtte et al.,
109 2012). Additionally, approximate shear-wave velocity profiles were obtained via geophysical
110 investigations as part of this study. With only vertical geophones available, the geophysical
111 investigation techniques were limited to P-wave and Rayleigh wave analyses. The Rayleigh
112 wave analysis was limited to high frequencies (greater than 14 Hz), hence the penetration
113 depth typically only reached 10 to 20 meters. Therefore it must be noted that the V_{S30}
114 values used in this study are partially inferred, based on the assumption that the V_S of the
115 bedrock is constant down to 30 m. For the MQZ station, no V_S measurements were possible,
116 hence the V_{S30} value of 1000 m/s is inferred based on correlations with geological data in
117 the region. HVSC has been previously characterized by Wood et al. (2011), and we adopt
118 their profile for this study. Table 1 shows all site information available for each station in
119 this study, including resonant frequencies, newly assessed V_{S30} values and NZS1170.5:2004
120 site classifications (Standards New Zealand, 2004).

121 Two stations (CRLZ, MQZ) comprise both a strong-motion accelerometer and a co-
122 located broadband velocity sensor, while AKSS, D14C, GODS, HVSC and MTPS are strong-
123 motion accelerometers. The accelerometer at MQZ samples at 50 Hz, while the remaining
124 strong-motion instruments sample at 200 Hz. The large number of near-source recordings
125 from the Canterbury earthquake sequence enable us to work with the subset of records at
126 epicentral distance (R) less than 30 km. This allows us to neglect any path-dependence of
127 κ i.e. the $\tilde{\kappa}(R)$ term in equation (2), and assume that each individual measured κ value
128 from an event with epicentral distance less than 30 km corresponds to a zero-distance κ_0

129 value, similar to Rebollar (1990) and Kilb et al. (2012). We justify using this assumption
130 in a later section entitled ‘Distance-dependence of κ_{AS} ’. Therefore, we obtained a dataset
131 of 508 accelerograms recorded at the seven stations, of which 424 have $R < 30$ km.

132 Broadband velocity instruments tend to have a smaller usable frequency range than
133 modern accelerometers. Both of the two stations with co-located broadband instruments
134 (CRLZ and MQZ) sample at 100 Hz, and after correction for instrument response, the pass-
135 band (i.e. unity gain) for these instruments is approximately 1 to 40 Hz. However, the
136 CRLZ site exhibits strong high-frequency site amplification and deamplification effects due
137 to its location in a cavern (Van Houtte et al., 2012), which renders measuring κ unreliable
138 in this pass-band. We therefore discard the velocity channel of CRLZ and only consider the
139 acceleration channel, which has a higher maximum usable frequency (>70 Hz). The greater
140 pass-band for the CRLZ accelerometer enables measurement of κ at frequencies higher than
141 that of the site effects. Thus, MQZ has the only available broadband instrument to robustly
142 measure κ for small magnitude events, and from this station we obtain 1655 events, of
143 which 1099 have epicentral distances less than 30 km. Table 1 shows the total number of
144 recordings at each station, instrument types and their sampling rates. A magnitude-distance
145 plot of the dataset is shown in Figure 2. The four largest events have published moment
146 magnitude (M_w) estimates, while the smaller events have been converted from GeoNet local
147 magnitudes (M_L ; Haines, 1981) to M_w using the correlation of Ristau (2013). An issue with
148 using the Ristau (2013) M_L - M_w relationship is that only events with $M_w > 3$ were used to
149 create the correlation, while our dataset contains many events with $M_w < 3$. While it is
150 unclear whether the relationship will hold for $M_w < 3$, we have no definitive evidence to the
151 contrary, and using it is unlikely to introduce significant bias to the results. Therefore, we
152 extrapolate and apply the M_L - M_w correlation to all events in the dataset.

153 All earthquakes analyzed in this study have focal depths less than 15 km. Metadata for
154 the fine-scale relocations of events are from Bannister et al. (2011). The key advantage of
155 the dataset is the good coverage of events across a wide magnitude range at near-source
156 distances, which allows us to empirically investigate the sensitivity of $\kappa_{0,AS}$ estimates to
157 magnitude and distance.

158 METHOD

159 Data processing and calculation of κ_{AS}

160 For each recording in the dataset, the waveforms were baseline-corrected, the instrument
161 response was removed, the data was converted to units of acceleration (where applicable),
162 and then time windows for S-wave shaking and pre-event noise were selected. Signal windows
163 were selected to encapsulate the main portion of S-wave shaking, with a fixed window
164 duration of five seconds. Noise windows were selected either from pre-event noise, or if this
165 was unavailable, from the last part of the trace to minimize any wave reflections in the noise
166 window. Both signal and noise windows were 5% cosine-tapered at both edges and Fourier
167 transformed. Only amplitudes (i.e. FAS) were retained for the analysis.

168 We use the Anderson and Hough (1984) method to estimate κ directly on the high-
169 frequency part of FAS (κ_{AS}). This method was selected based on its relevance for the
170 host-to-target method for empirical GMPE adjustments. The process we follow is based
171 on the recommended procedure of Ktenidou et al. (2013), in terms of accounting for source
172 corner frequency (f_c), signal-to-noise ratio (SNR) and minimum usable frequency range.
173 As a first step, f_c was manually picked from displacement spectra. The lower bound of
174 the high-frequency slope, f_e , was selected to always be higher than f_c , to avoid any source
175 effects on the frequency band used to estimate κ_{AS} . The upper bound, f_x , was defined as the
176 smallest of: the frequency at which three times the level of noise exceeds the signal (i.e. SNR
177 > 3); where the high-frequency slope clearly plateaus; or the maximum usable frequency
178 of data from the particular instrument (e.g. 80 % of the Nyquist frequency or maximum
179 value of flat instrument response). The site response for each station was also considered
180 in the selection of f_e and f_x , using the horizontal-to-vertical spectral ratios (HVSR) from
181 recorded earthquake motions obtained in Van Houtte et al. (2012), as any amplification or
182 deamplification effects in the chosen frequency band can adversely affect κ measurements
183 (Parolai & Bindi, 2004). In the interest of robustness, a minimum Δf (i.e., $f_x - f_e$) of 10
184 Hz was applied.

185 Figures 3a, b and c show an example of S-wave and noise time windows, FAS, and picks

186 of f_c , f_e and f_x respectively for an event in the Canterbury sequence. Note that in this
187 study, only κ measurements for horizontal shaking are analyzed, and the vertical component
188 is not considered.

189 **Orientation-independent κ_{AS} definition**

190 Thus far, we have detailed a method to compute κ_{AS} from a single earthquake FAS, i.e.
191 one horizontal component of motion. In several previous studies, κ_{AS} is measured on each
192 of the two horizontal components using a similar method to that described here, then av-
193 eraged to obtain one κ_{AS} value per station per event (Douglas et al., 2010; Gentili and
194 Franceschina, 2011; Van Houtte et al., 2011; Ktenidou et al., 2013). Some of these studies
195 also apply criteria that reject data whose κ_{AS} values differ greatly between the two compo-
196 nents (Van Houtte et al., 2011; Ktenidou et al., 2013). Given that such rejection criteria are
197 somewhat arbitrary and may bias results, we investigate whether the orientation of the two
198 horizontal components affects κ_{AS} measurements, using the accelometric data from events
199 at less than 30 km epicentral distance. For each triaxial recording, the two horizontal com-
200 ponents are rotated at five degree increments through 90° , giving a total of 36 individual
201 time series per station per event. κ is then calculated on each rotation increment of the 36
202 time series using the method described in the previous section (with f_e and f_x fixed for all
203 36 spectra).

204 In Figure 4, each line of data points represents κ_{AS} results for one station, as the hori-
205 zontal components are rotated. Each data point shows the average value of κ_{AS} , averaged
206 over all events at that station, for the specific orientation of the sensor. Orientations are
207 shown on the x axis in 5° increments, first for the north component (from 0 to 85°) and
208 then for the east component (from 90 to 175°). As we are examining a mean κ_{AS} value
209 of all recordings, and the recordings at each station have a wide range of event-to-station
210 azimuths, we assume that any variation in κ_{AS} with component orientation is a local effect,
211 rather than relating to event azimuth. While the AKSS, CRLZ and MTPS stations show
212 little variation in κ_{AS} with component orientation, the D14C, GODS, HVSC and MQZ sta-
213 tions show large differences (approximately 20% and 25% between minimum and maximum

214 at GODS and MQZ respectively). Particularly strong topographic site effects have already
215 been observed at the GODS station on the N150° component (Van Houtte et al., 2012), and
216 this orientation of the horizontal component corresponds to the maximum average κ_{AS} mea-
217 surement. This may be an indication that in the frequency band of measurement (roughly
218 12 to 30 Hz), 2D site effects may still interfere with κ_{AS} measurements.

219 This highlights the difficulty in separating the effects of site attenuation and site ampli-
220 fication in κ_{AS} measurements. To average over 2D site effects in future κ_{AS} estimates and
221 derive a more robust value, we propose the following orientation-independent approach for
222 measuring κ_{AS} :

- 223 1. Obtain the north and east horizontal (i.e. $\theta_1 = 0$ and $\theta_2 = 90^\circ$) time series for each
224 recorded event, and select S-wave time windows.
- 225 2. Cosine-taper and Fourier transform time windows, then pick f_e and f_x on the S-wave
226 spectra to obtain κ_θ .
- 227 3. Increment the rotation angle θ by $\Delta\theta$, where $\Delta\theta_{min} = 5^\circ$.
- 228 4. Repeat steps 2 and 3, holding f_e and f_x constant for each κ_θ measurement, until
229 $\theta_1 = 90$ and $\theta_2 = 180^\circ$ respectively.
- 230 5. Calculate the mean of all the obtained κ_θ measurements. The standard deviation of
231 κ_θ is a measure of the scatter of κ due to component orientation.

232 This suggested method is more robust than the current practice of calculating κ_{AS} as the
233 average of κ_{AS} measured on two arbitrarily-orientated components. We prefer this definition
234 of an orientation-independent mean κ_θ value over measuring κ_{AS} from a single orientation-
235 independent FAS (e.g. the quadratic mean spectrum or the Gonella (1972) rotary spectrum),
236 as our definition also offers a measure of the scatter in κ_{AS} estimates due to component
237 orientation, indicating whether effects such as high-frequency 2D site-response may affect
238 the obtained κ results. For this study, we adopt the previously discussed data processing
239 techniques to calculate κ_{AS} from the FAS of a single horizontal recording, then use this

240 orientation-independent approach to calculate one value for horizontal κ_{AS} per event per
241 station.

242 **DISTANCE-DEPENDENCE OF κ_{AS}**

243 Using this method, including the orientation-independent definition, we evaluate the dis-
244 tance dependence of κ_{AS} in the Canterbury region. Given that the strong motion stations
245 did not record a sufficient number of events at epicentral distances greater than 30 km to
246 examine any trends with distance (see Figure 2), only the velocity channel of the MQZ
247 station is used to assess distance-dependence of κ_{AS} in the Canterbury region. Figure 5a
248 plots κ_{AS} against epicentral distance, R_e , with squares indicating the mean and standard
249 deviation of 5 km distance bins. Note that κ_{AS} here represents the mean κ_{AS} of the 36
250 different horizontal component orientations for each event. While the scatter is large (as is
251 typical of most κ studies), the mean binned mean κ_{AS} values are relatively constant up to
252 approximately 30-40 km epicentral distance, above which there is a slight increase in κ_{AS}
253 with distance. This justifies an approximation (such as the one made in the previous sec-
254 tion) where $\kappa_{0,AS}$ is calculated as an average of all κ_{AS} from between 0 and 30 km epicentral
255 distance.

256 Figure 5b shows the standard deviation of κ_{AS} (i.e. the standard deviation of κ_{AS} from
257 the 36 different horizontal component orientations per event, a measure of the scatter due
258 to component orientation), plotted against epicentral distance. We find the distribution of
259 the standard deviation of κ_{AS} to be lognormal, and the lognormally distributed mean and
260 standard deviation across 5 km distance bins are indicated as squares in Figure 5b. At
261 epicentral distances less than 20 km, there is a larger scatter for the κ_{AS} estimates due to
262 component orientation. This indicates that at short distances, finite-fault effects may affect
263 the high-frequency slope, even for small magnitude events. Despite the increased scatter
264 in κ_{AS} estimates, there is no corresponding change in the mean κ_{AS} at distances less than
265 20 km, hence it is considered that this effect will have little influence on the obtained κ_0
266 calculations.

267 CONSTRAINTS ON κ_{AS} ESTIMATION DUE TO MA- 268 GNITUDE

269 The broadband instrument at the MQZ station recorded a large amount of near-source
270 data across a wide range of magnitudes, from 0.5 to 5.5. This is an unusually wide range
271 and allows us to explore the limitations and applicability of the κ_{AS} approach, which is
272 typically used for large magnitudes. The range of frequencies used to compute κ_{AS} may
273 depend on magnitude, as shown in Ktenidou et al. (2013) (see their Figure 4a): the lower
274 the magnitude, the higher the source corner frequency, f_c , and the higher the frequency
275 band needed to measure κ_{AS} . This frequency band is constrained from below by f_c and
276 from above by the noise level ($\text{SNR} > 3$), instrument sampling rate and instrument response.
277 Here, we investigate what the lowest usable magnitude is for determining κ_{AS} given the
278 existing instrument constraints. First we bin data according to magnitude. In Figure 6a,
279 the dotted lines indicate the boundaries of the magnitude bins, with a similar number of
280 events in each bin. The MQZ velocity channel has a sampling rate of 100 Hz (Nyquist
281 frequency of 50 Hz), and after correction for instrument response, we consider the data to
282 be reliable up to 40 Hz. Adopting this as the upper usable frequency limit of the data,
283 Figure 6b shows the f_c , f_e and f_x values for the data. f_c is only picked for events smaller
284 than magnitude 4, since it will not pose problems for large magnitudes, for which the κ_{AS}
285 method is well-validated. As f_c depends on magnitude, the f_e pick must also be magnitude-
286 dependent to avoid trade-off between κ_{AS} and source parameters. The f_x pick is made
287 visually but is always limited by the maximum usable frequency of 40 Hz, and therefore Δf
288 tends to decrease with decreasing magnitude, but always remains above 10 Hz. Using these
289 Δf ranges, Figure 6c shows the corresponding $\kappa_{0,AS}$ values against magnitude, along with
290 the mean and ± 1 standard deviation of $\kappa_{0,AS}$ per bin. There is no significant magnitude
291 dependence of $\kappa_{0,AS}$ for magnitudes greater than 2.5 when using these frequency picks.
292 Below this magnitude threshold, the influence of f_c becomes more pronounced and there
293 is an increasing tradeoff between f_c and $\kappa_{0,AS}$, resulting in a decrease in the mean $\kappa_{0,AS}$.
294 This decrease indicates an erroneous measurement, as the measured slope no longer solely

295 represents the site attenuation effect.

296 We now perform a sensitivity analysis on the effect of the maximum usable frequency of
297 the data on κ_{AS} for small magnitudes i.e. maximum possible f_x . The maximum possible
298 f_x is decreased from 40 Hz to 30 Hz and 23 Hz, simulating lower sampling rates or different
299 instrument responses. Figure 6d compares obtained $\kappa_{0,AS}$ values for the same dataset, for
300 the different maximum usable frequencies. Only the mean $\kappa_{0,AS}$ values across the magnitude
301 bins are shown for clarity. When the maximum usable frequency decreases, the trade-off
302 between f_c and κ_{AS} becomes more evident at larger magnitudes, manifesting as a decrease
303 in measured $\kappa_{0,AS}$. If the maximum usable frequency is 40 Hz, $\kappa_{0,AS}$ cannot be measured
304 reliably for events with magnitude less than 2.5. When the maximum usable frequency
305 is 30 Hz, $\kappa_{0,AS}$ measurements should be kept to magnitudes greater than 3, and if the
306 maximum is 23 Hz (which may be typical for instruments sampling at 50 Hz), the minimum
307 usable magnitude is 3.5. Above these magnitude thresholds, the data can be used to get
308 good estimates of the mean value of $\kappa_{0,AS}$, however the standard deviation of the estimates
309 incrementally increases as the maximum usable frequency decreases. In order to avoid such
310 trade-offs in future studies, we suggest some magnitude limits for the κ_{AS} method, based on
311 the effects of f_c and maximum usable frequencies of available data. These limits are shown
312 in Table 2. Note that as κ_{AS} increases, the Fourier amplitudes decay more rapidly and
313 may reach the noise level before the maximum usable frequency of the data. The minimum
314 magnitudes indicated in Table 2 assume the S-wave Fourier amplitudes are greater than
315 three times the noise amplitudes across the usable frequency band, as was generally the
316 case in this study. In reality, there may be a tendency for the minimum usable magnitude
317 to increase with κ_{AS} , and thus the minimum magnitudes in Table 2 should be considered
318 indicative only, and applicable for $\kappa_{AS} \leq 0.03$ s.

319 A further note from Figure 6d is that some error bars for maximum $f_x = 23$ and 30
320 Hz extend to negative $\kappa_{0,AS}$ values, indicating that many records have $\kappa_{AS} < 0$. This is
321 not observed for any of the data points in Figure 6c where the maximum $f_x = 40$ Hz, and
322 highlights the adverse effects of measuring κ_{AS} from data with lower sampling rates.

323 CORRELATION WITH SITE PARAMETERS

324 κ_0 is commonly assumed to represent the attenuation of seismic waves due to the geology
325 in the upper few kilometers of the Earth’s crust. κ_0 is often correlated with V_{S30} , under the
326 assumption that V_{S30} is indicative of the deeper V_s and Q (seismic quality factor) profile
327 that causes the site attenuation. There is considerable scatter in such correlations. Figure
328 7a plots the mean $\kappa_{0,AS}$ values for the seven stations analyzed in this study against V_{S30} .
329 The standard deviation of $\kappa_{0,AS}$ is also indicated. The range of V_{S30} values and quantity
330 of stations in the dataset are too small to offer a quantitative correlation, however it is
331 reasonable to conclude that the softer sites have higher $\kappa_{0,AS}$ values than the harder sites.
332 $\kappa_{0,AS}$ still varies significantly (roughly 0.025–0.039 s) amongst the NZS 1170.5:2004 class B
333 sites with similar V_{S30} values, indicating that V_{S30} alone cannot be used to accurately infer
334 $\kappa_{0,AS}$.

335 The average $\kappa_{0,AS}$ value for rock sites in the region is approximately 0.03 s. However, the
336 error bars indicate large standard deviations ranging from 0.005 to 0.01 s, depending on the
337 station. The standard deviation decreases for harder sites but again V_{S30} is not sufficient
338 to describe the variability. Van Houtte et al. (2012) found that several of these sites are
339 located at sites with complex geology e.g. ridges, tunnels etc. that result in significant 2D
340 response. Hence, in Figure 7b, we plot the standard deviation of $\kappa_{0,AS}$ against a simple
341 binary measure of 2D site effects, where a value of 1 corresponds to sites with complex 2D
342 geological structures that influence the site response, and 0 is for stations with site response
343 that can be approximated as 1D. The scatter in $\kappa_{0,AS}$ is significantly higher for stations
344 with strong 2D site effects, hence 2D site effects may explain some of the variability of $\kappa_{0,AS}$
345 measurements, both in this study and in previous studies on κ .

346 VARIATION WITH GROUND MOTION AMPLITUDE

347 The Canterbury earthquake sequence resulted in several rock and stiff soil recordings with
348 very large horizontal ground motion amplitudes. This section examines the dependence of
349 $\kappa_{0,AS}$ with the level of horizontal ground shaking. Figures 8a to 8f plot $\kappa_{0,AS}$ against peak

350 ground acceleration (PGA) for the six strong motion stations in this study. Events with
351 large PGAs have smaller values of $\kappa_{0,AS}$ than small PGA events, particularly evident at
352 the D14C, GODS, HVSC and MTPS stations. While the AKSS and CRLZ stations do not
353 show a trend with PGA, all events recorded at these sites had PGAs of less than 0.2 g. PGA
354 is used here to indicate the amplitude of ground motion, as we observe similar behaviour
355 when plotting $\kappa_{0,AS}$ against all pseudo spectral acceleration ordinates.

356 This is the first time that such a result is reported. To our knowledge, there is only one
357 previous κ study that examines dependence with PGA (Dimitriu et al., 2001), which found
358 an increase in $\kappa_{0,AS}$ with PGA on soft soil sites. If we consider that part of κ_0 can be seen
359 as damping in the top layers, then it would be expected to increase with the level of shaking
360 if it reached nonlinear soil behaviour (as observed in Dimitriu et al. (2001)). However, we
361 find the opposite effect here for stiff soil and soft rock sites. As we were also unable to
362 attribute the observed variation to a distance effect (the high-PGA events did not occur at
363 shorter distances), one possible alternative interpretation is that part of the site attenuation
364 described by $\kappa_{0,AS}$ may be related to local heterogeneities in the geological profile that cause
365 high-frequency scattering (Faccioli et al., 1989). Under very high amplitude motion, small-
366 scale heterogeneities in the profile causing such scattering may be smoothed out, leading to
367 a decrease in $\kappa_{0,AS}$. Furthermore, the wavelengths associated with large amplitude motion
368 may be much longer compared to the dimension of the scatterers. The effects of the decrease
369 in scattering attenuation would need to be greater than the increase in material damping for
370 this interpretation to fit our observations. Another possible explanation for $\kappa_{0,AS}$ decreasing
371 with PGA is that the correlation is physically representing a dependence with the rate of
372 shear strain, rather than the ground motion amplitude. Tatsuoka et al. (2008) performed
373 laboratory experiments on the effect of strain rate on damping, and found that very high
374 strain rates can actually decrease material damping, and therefore may cause κ_0 to decrease.
375 Note that PGA here is a proxy for strain rate rather than strain amplitude.

376 These interpretations are only speculative, and there are no comparable κ studies that
377 analyze such large PGAs (even the Dimitriu et al. (2001) study only included one recording
378 with PGA > 0.3 g). However, it might be prudent to consider the possible decrease in $\kappa_{0,AS}$

379 with increasing ground-motion amplitude in hazard assessments for important structures,
 380 particularly where large, nearby sources have significant contributions to the hazard. Cur-
 381 rent practice assumes that κ_0 is independent of the level of ground shaking, however these
 382 results suggest that such an assumption may be unconservative. It is possible that these
 383 large, nearby events could produce lower values for $\kappa_{0,AS}$ and therefore increase the seismic
 384 hazard at short periods.

385 COMPARISON WITH $\kappa_{0,IRVT}$ FROM LOCAL GMPEs

386 In the previous sections, we studied κ_0 using the Anderson and Hough (1984) approach
 387 ($\kappa_{0,AS}$). This section compares these results with the native κ_0 of local empirical GMPEs,
 388 calculated using inverse random vibration theory (IRVT, Gasparini and Vanmarcke, 1976).
 389 These two approaches belong to the high-frequency family of methods, defined by Ktenidou
 390 et al. (2014) as being compatible with empirical GMPE adjustments, however to date no
 391 published study has compared the two approaches.

392 Background

393 Given that this is a nascent approach for calculating κ , here we provide a background to
 394 the method. Al Atik et al. (2014) first used IRVT to compute κ_0 from response spectra
 395 compatible FAS. The purpose of this approach is to allow a value for κ_0 to be computed
 396 from an existing GMPE, representing an average value of κ_0 for the dataset that was used
 397 to create the GMPE (hereafter referred to as $\kappa_{0,IRVT}$). The IRVT process is relatively
 398 complex, and to date is yet to be widely implemented in this context. While a detailed
 399 explanation can be found in Rathje et al. (2005), a simplified summary of the methodology
 400 is included here. Using random vibration theory (RVT), the spectral acceleration (Sa) is
 401 related to the root mean square spectral acceleration (Sa_{rms}) by the peak factor (p):

$$(Sa)^2 = p^2(Sa_{rms})^2 . \tag{3}$$

402 For a single degree of freedom (SDOF) system, Sa_{rms} can be determined using Parseval's

403 theorem, which states that power is conserved in the time and frequency domains, and thus
 404 the total power of a signal can be calculated in either domain:

$$(S_{a_{rms}})^2 = \frac{2}{T_d} \int_0^\infty |A(f)|^2 |H_{f_n}(f)|^2 df, \quad (4)$$

405 where T_d is the signal duration, $A(f)$ is the FAS and $|H_{f_n}(f)|$ is the transfer function of a
 406 SDOF oscillator with natural frequency f_n and critical damping ratio ξ . The difficulty with
 407 solving equation (4) is that a given spectral ordinate is influenced by a range of frequencies in
 408 the FAS, and cannot be used directly to calculate a value in the FAS. To address this issue,
 409 the characteristics of lightly damped (e.g. 5%) SDOF transfer functions are used, namely
 410 three important properties: they are equal to unity beneath the natural frequency of the
 411 SDOF system, they contain large amplification in a narrow band near the natural frequency,
 412 and they quickly tend to zero for frequencies greater than the fundamental frequency. These
 413 properties allow the integral in equation (4) to be approximated in terms of the Fourier
 414 amplitude at the natural frequency of the oscillator, $|A(f_n)|$, by using a constant value
 415 of $|A(f)|^2$ equal to its value at the natural frequency. Using the approximated integral,
 416 equation (4) is combined with equation (3) to solve for $|A(f_n)|^2$, giving:

$$|A(f_n)|^2 \approx \frac{1}{\int_0^\infty |H_{f_n}(f)|^2 df - f_n} \left(\frac{T_d \cdot S_a^2}{2 \cdot p^2} - \int_0^{f_n} |A(f)|^2 df \right), \quad (5)$$

417 The integral of the transfer function is constant for a given natural frequency and damp-
 418 ing ratio, which simplifies equation (5) to:

$$|A(f_n)|^2 \approx \frac{1}{f_n \left(\frac{\pi}{4\xi} - 1 \right)} \left(\frac{T_d \cdot S_a^2}{2 \cdot p^2} - \int_0^{f_n} |A(f)|^2 df \right), \quad (6)$$

419 Before using equation (6) to invert from a response spectrum to a FAS, an initial estimate
 420 of the peak factor, p , is required. The peak factor depends on the statistical moments of the
 421 FAS and the duration of motion, and is therefore unknown. By assuming an initial value
 422 for p , an estimated FAS can be determined and subsequently used for a second calculation
 423 of peak factors for the inversion. To calculate the response spectrum compatible FAS,

424 equation (6) is first applied at low frequencies, where the integral term is approximately
425 equal to zero, then at incrementally higher frequencies. κ can then be measured from the
426 obtained FAS in the classic definition of linear high-frequency decay, following Anderson
427 and Hough (1984). To avoid path effects, the input response spectra should be generated
428 for near-source distances (i.e. less than 30 km), but not for very small distances (less than
429 5 km), where empirical GMPEs are not well constrained.

430 **Application**

431 We use the IRVT process to calculate κ_{IRVT} for two New Zealand crustal GMPEs (McVerry
432 et al., 2006; Bradley, 2013). Response spectra are derived using the two GMPEs for various
433 magnitude, distance and site scenarios, in accordance with Al Atik et al. (2014). For the
434 distance parameter, the McVerry et al. (2006) GMPE uses the closest distance to the rupture
435 plane, R_{rup} , while the Bradley (2013) GMPE uses R_{rup} and the Joyner-Boore distance, R_{jb} .
436 For the site term, Bradley (2013) uses V_{S30} and depth to bedrock, $Z_{1,0}$, while McVerry et
437 al. (2006) use NZS1170.5:2004 site classifications (Standards New Zealand, 2004). Both
438 GMPEs are in terms of moment magnitude, M_w .

439 Here, response spectra are generated for vertical strike-slip scenarios with $M_w=5.5, 6$
440 and 6.5 , $R_{rup}=5, 10, 15$ and 20 km and a fixed hypocentral depth $H=5$ km. We infer
441 approximate R_{jb} values from these parameters, guided by the R_{rup} and R_{jb} simulation
442 results from Chiou and Youngs (2006). To calculate the depth to the top of the rupture
443 plane, Z_{TOR} , the down-dip rupture width is estimated from H , M_w and focal mechanism,
444 using the relation of Wells and Coppersmith (1994), and Z_{TOR} is approximated as half the
445 down-dip rupture width, following Scasserra et al. (2009) and Bradley (2013). For these
446 scenarios we calculate response spectra for each seismic station previously analyzed in this
447 study, using the site information given in Table 1. Where the depth to bedrock, $Z_{1,0}$, was
448 not directly measured from the geophysical investigations, the $Z_{1,0}$ relationship with V_{S30}
449 from Chiou and Youngs (2008) was adopted.

450 Response spectra compatible FAS were then calculated using the IRVT procedure. For
451 the duration input, we use the Western United States point source model (Campbell, 2003)

452 relations:

$$T_d = \frac{1}{f_c} + 0.05R, \quad (7)$$

453 where f_c is the source corner frequency in Hz and R is distance in km. Our estimates of
454 f_c are based on the findings of Oth and Kaiser (2013) for similarly large magnitude events
455 in the Canterbury sequence.

456 Figure 9a shows the response spectra generated using the Bradley (2013) and McVerry
457 et al. (2006) GMPEs for a $M_w=6$, $R_{rup}=10$ km, $V_{S30}=1000$ m/s scenario. Figure 9b shows
458 the response spectra compatible FAS for this scenario, with a linear slope fitted to the high-
459 frequency decay of each spectrum. As the smallest spectral ordinate in the McVerry et al.
460 (2006) model is at $T = 0.075$ s, this study assumed that PGA in the GMPE corresponded
461 to $T = 0.04$ s to better constrain the FAS at high frequencies. We judged 0.04 s to be most
462 appropriate, as the majority of the data used to develop the McVerry et al. (2006) GMPE
463 had a sampling rate of 50 Hz and hence a Nyquist frequency of 25 Hz. f_e and f_x were
464 picked individually on each spectrum, with $f_x \leq 20$ Hz. Figures 10a to 10g show $\kappa_{0,IRVT}$
465 estimates from the Bradley (2013) GMPE, for the seven sites in this study. Triangles,
466 circles and crosses correspond to the $M_w=6.5$, 6 and 5.5 scenarios respectively. There is
467 no apparent dependence with distance or magnitude for the rock sites, while for stiff soil
468 site, HVSC, $\kappa_{0,IRVT}$ decreases slightly as magnitude increases. Figures 10h and 10i show
469 $\kappa_{0,IRVT}$ from the McVerry et al. (2006) GMPE, for NZS 1170.5:2004 class B and class C
470 sites respectively (Standards New Zealand, 2004), using the same magnitude and distance
471 scenarios. $\kappa_{0,IRVT}$ is higher for McVerry et al. (2006) than for Bradley (2013). However,
472 these values are likely to be influenced by our assumption that PGA in the McVerry et al.
473 (2006) model is equivalent to $T = 0.04$ s, as the choice of spectral period would significantly
474 change the slope. There is also an increase in $\kappa_{0,IRVT}$ at small distances, especially for
475 the smaller magnitude scenarios. This may be because at the time of the development of
476 the McVerry et al. (2006) GMPE, there were a lack of New Zealand data for distances less
477 than 10 km, and the dataset was therefore supplemented with foreign PGA data. The high-
478 frequency range of the McVerry et al. (2006) model appears to be too limited to obtain an

479 accurate estimate of $\kappa_{0,IRVT}$, however it is unlikely that the GMPE was ever intended to
480 be used in this way. Given that we are pushing the McVerry et al. (2006) model somewhat
481 beyond its limits, the Bradley (2013) GMPE may be a more reliable representation of the
482 high frequency characteristics of the Canterbury data.

483 **Comparison of $\kappa_{0,AS}$ and $\kappa_{0,IRVT}$**

484 In order to compare the $\kappa_{0,IRVT}$ values with the $\kappa_{0,AS}$ estimates from the previous sections,
485 Figure 11 plots both against V_{S30} for the seven stations in this study. Table 3 shows the
486 values for each station. In general, $\kappa_{0,IRVT}$ from the Bradley (2013) GMPE matches well
487 with the $\kappa_{0,AS}$ values, mostly within one standard deviation of the mean $\kappa_{0,AS}$. There
488 appears to be a slight correlation between $\kappa_{0,IRVT}$ and V_{S30} , however the trend of $\kappa_{0,IRVT}$
489 with V_{S30} has a significantly shallower slope than the general trend of $\kappa_{0,AS}$ with V_{S30} .
490 This suggests that current GMPEs do not scale adequately with κ , possibly due to their
491 form. A small change in κ may significantly modify the high-frequency shape of a FAS,
492 however GMPEs are typically fitted to response spectra (rather than FAS), where the high
493 frequencies are smoothed and hence less sensitive to κ . Therefore, to better model high
494 frequencies in GMPEs, it may be beneficial to empirically fit the FAS, then compute a
495 response spectrum using random vibration theory (e.g. Bora et al., 2013).

496 **DISCUSSION**

497 The most significant finding from our analysis is the apparent decrease in $\kappa_{0,AS}$ with large
498 ground-motion amplitudes. While the physical mechanism (or mechanisms) causing this
499 trend are currently unclear, the potential implications for hazard assessments at critical
500 installations are large. These facilities are often designed to resist events with very low
501 probabilities of occurrence but high ground-motion intensities. Direct measurements of κ are
502 predominantly obtained from low-intensity earthquake records that are not of engineering
503 interest, then applied to predict ground-motion for high-intensity events, either through
504 host-to-target adjustments, stochastic simulations or GMPEs. This process is invalid if

505 ‘high-intensity κ ’ values are different from ‘low-intensity κ ’ values, as our findings may
506 suggest. Given its importance for the earthquake-resistant design of critical facilities, future
507 research should focus on the variation of κ with ground-motion amplitude. The $\kappa_{0,AS}$ -PGA
508 correlation we present here is still relatively weak, and requires further analysis with a larger
509 dataset of high-intensity rock site recordings. Additional research could focus on developing
510 a method to infer high-intensity $\kappa_{0,AS}$ from low-intensity $\kappa_{0,AS}$.

511 The variation in $\kappa_{0,AS}$ with ground-motion amplitude also means that the minimum
512 magnitude recommendations for estimating κ_{AS} in Table 2 are guidelines for measuring
513 low-intensity κ_{AS} only. The recommendations have been proposed to prevent trade-off
514 between source parameters and κ_{AS} in future studies. Events larger than our minimum
515 magnitude recommendations can still be used to calculate low-intensity κ_{AS} , however they
516 may overestimate high-intensity κ_{AS} .

517 A further recommendation of this study is an orientation-independent definition of κ_{AS} ,
518 to average over possible high-frequency 2D site effects. Such effects may be significant at
519 sites with strong 2D geological structures, with $\kappa_{0,AS}$ varying by up to 25% depending on the
520 horizontal component orientation. Using an orientation-independent definition for κ_{AS} is
521 more robust than calculating κ_{AS} as the mean from two arbitrarily-orientated components,
522 and therefore can be used to compute a more stable mean as well as an estimate of uncer-
523 tainty due to component orientation. However, it should be noted that the variation due to
524 component orientation is still less than the standard deviation of $\kappa_{0,AS}$ at each station, i.e.
525 despite our attempts to reduce and understand the scatter in κ_{AS} , the observed variability
526 is still very high at all stations. Future research should focus on further understanding the
527 physical mechanisms behind κ and identifying other sources of scatter contributing to the
528 variation in κ .

529 In addition to analyzing the scatter in κ_{AS} measurements, this study also compares
530 results from Christchurch with the ‘native’ κ_0 values of local GMPEs. $\kappa_{0,IRVT}$ from the
531 Bradley (2013) GMPE is relatively independent of distance and V_{S30} , indicating that is
532 mostly decoupled from these effects. While this suggests that the GMPE is smoothing the
533 high-frequency effect, it also means that the Bradley (2013) model, and therefore the Chiou

534 and Youngs (2008) model, on which the Bradley (2013) model is based, are good candidate
535 GMPEs for κ adjustments. $\kappa_{0,AS}$ from Christchurch rock sites are similar to $\kappa_{0,IRVT}$ from
536 Bradley (2013), therefore this model is likely to give relatively reliable predictions for short
537 period rock motions in Christchurch.

538 DATA AND RESOURCES

539 We acknowledge the New Zealand GeoNet project (www.geonet.org.nz, last accessed Septem-
540 ber 2013) and its sponsors, the Earthquake Commission (EQC), GNS Science and Land In-
541 formation New Zealand (LINZ), for providing the data used in this study. Signal processing
542 benefited greatly from the use of SAC (Goldstein & Snoke, 2005; www.iris.edu/software/sac,
543 last accessed February 2013), and figures were created using Generic Mapping Tools (Wessel
544 & Smith, 1998; www.gmt.soest.hawaii.edu, last accessed February 2013). We thank Dr
545 Graeme McVerry for kindly providing Fortran scripts to generate response spectra for
546 the McVerry et al. (2006) GMPE. Response spectra for the Bradley (2013) GMPE were
547 generated using code from [https://sites.google.com/site/brendonabradley/research/ground-](https://sites.google.com/site/brendonabradley/research/ground-motion-prediction)
548 [motion-prediction](https://sites.google.com/site/brendonabradley/research/ground-motion-prediction), last accessed July 2013. The software used to perform the IRVT calcu-
549 lations is publically available from: <https://github.com/arkottke/irvt> (Kottke and Rathje,
550 2008, last accessed June 2013). Geophysical software Geopsy and Dinver (Wathelet, 2008;
551 www.geopsy.org, last accessed May 2013) were used to respectively calculate and invert
552 dispersion curves to obtain V_S profiles.

553 ACKNOWLEDGMENTS

554 The orientation-independent definition of κ was inspired by the work of Boore et al. (2006).
555 The authors would like to thank N. Abrahamson, P.-Y. Bard, S. Iai and A. Kottke for
556 fruitful discussions and suggestions. We are grateful for the assistance of L. Wotherspoon,
557 L. Storie and S. Garambois in collecting and analyzing geophysical data for the V_S profiles.
558 CVH is funded by a University of Auckland Doctoral Scholarship, while OJK is funded by

559 the French SIGMA project. The authors would like to thank F. Cotton for reading an early
560 version of this manuscript and providing useful comments. This work greatly benefitted
561 from the thoughtful reviews of two anonymous reviewers.

References

- 563 Aki, K. (1987). Magnitude-frequency relation for small earthquakes: A clue to the origin of
564 f_{max} of large earthquakes. *Journal of Geophysical Research: Solid Earth (1978–2012)*,
565 92(B2), 1349–1355.
- 566 Al Atik, L., Kottke, A., Abrahamson, N., & Hollenback, J. (2014). Kappa (κ) scaling
567 of Ground Motion Prediction Equations using Inverse Random Vibration Theory ap-
568 proach. *Bulletin of the Seismological Society of America*, 104(1), -.
- 569 Anderson, J. G. (1991). A preliminary descriptive model for the distance dependence of the
570 spectral decay parameter in southern California. *Bulletin of the Seismological Society
571 of America*, 81(6), 2186–2193.
- 572 Anderson, J. G., & Hough, S. E. (1984). A model for the shape of the Fourier amplitude
573 spectrum of acceleration at high frequencies. *Bulletin of the Seismological Society of
574 America*, 74(5), 1969–1993.
- 575 Bannister, S., Fry, B., Reyners, M., Ristau, J., & Zhang, H. (2011). Fine-scale relocation of
576 aftershocks of the 22 February Mw 6.2 Christchurch earthquake using double-difference
577 tomography. *Seismological Research Letters*, 82(6), 839–845.
- 578 Bannister, S., & Gledhill, K. (2012). Evolution of the 2010–2012 Canterbury earthquake
579 sequence. *New Zealand Journal of Geology and Geophysics*, 55(3), 295–304.
- 580 Biro, Y., & Renault, P. (2012). Importance and Impact of Host-to-Target Conversions
581 for Ground Motion Prediction Equations in PSHA. In *15th World Conference on
582 Earthquake Engineering, Lisbon, Portugal*.
- 583 Boore, D. M. (2003). Simulation of ground motion using the stochastic method. *Pure and
584 applied geophysics*, 160(3-4), 635–676.
- 585 Boore, D. M., Watson-Lamprey, J., & Abrahamson, N. A. (2006). Orientation-independent
586 measures of ground motion. *Bulletin of the Seismological Society of America*, 96(4A),
587 1502–1511.
- 588 Bora, S. S., Scherbaum, F., Kuehn, N., & Stafford, P. (2013). Fourier spectral-and du-
589 ration models for the generation of response spectra adjustable to different source-,

- 590 propagation-, and site conditions. *Bulletin of Earthquake Engineering*, 1–27.
- 591 Bradley, B. A. (2013). A New Zealand specific pseudospectral acceleration groundmotion
592 prediction equation for active shallow crustal earthquakes based on foreign models.
593 *Bulletin of the Seismological Society of America*, 103(3), 1801–1822.
- 594 Campbell, K. W. (2003). Prediction of strong ground motion using the hybrid empirical
595 method and its use in the development of ground-motion (attenuation) relations in
596 eastern North America. *Bulletin of the Seismological Society of America*, 93(3), 1012–
597 1033.
- 598 Chandler, A., Lam, N., & Tsang, H. (2006). Near-surface attenuation modelling based on
599 rock shear-wave velocity profile. *Soil Dynamics and Earthquake Engineering*, 26(11),
600 1004–1014.
- 601 Chiou, B., & Youngs, R. (2006). Chiou and Youngs PEER-NGA empirical ground motion
602 model for the average horizontal component of peak acceleration and pseudo-spectral
603 acceleration for spectral periods of 0.01 to 10 seconds. *Interim Report Issued for USGS*
604 *Review*.
- 605 Chiou, B., & Youngs, R. R. (2008). An NGA model for the average horizontal component
606 of peak ground motion and response spectra. *Earthquake Spectra*, 24(1), 173–215.
- 607 Cotton, F., Scherbaum, F., Bommer, J. J., & Bungum, H. (2006). Criteria for selecting and
608 adjusting ground-motion models for specific target regions: Application to Central
609 Europe and rock sites. *Journal of Seismology*, 10(2), 137–156.
- 610 Dimitriu, P., Theodulidis, N., Hatzidimitriou, P., & Anastasiadis, A. (2001). Sediment
611 non-linearity and attenuation of seismic waves: a study of accelerograms from Lefkas,
612 western Greece. *Soil Dynamics and Earthquake Engineering*, 21(1), 63–73.
- 613 Douglas, J., Bungum, H., & Scherbaum, F. (2006). Ground-Motion Prediction Equations for
614 southern Spain and southern Norway obtained using the composite model perspective.
615 *Journal of Earthquake Engineering*, 10(1), 33–72.
- 616 Douglas, J., Gehl, P., Bonilla, L. F., & Gélis, C. (2010). A κ model for mainland France.
617 *Pure and Applied Geophysics*, 167(11), 1303–1315.
- 618 Edwards, B., & Fäh, D. (2013). Measurements of stress parameter and site attenuation

619 from recordings of moderate to large earthquakes in Europe and the Middle East.
620 *Geophysical Journal International*, 194(2), 1190-1202.

621 Edwards, B., Fäh, D., & Giardini, D. (2011). Attenuation of seismic shear wave energy in
622 Switzerland. *Geophysical Journal International*, 185(2), 967–984.

623 Faccioli, E., Tagliani, A., & Paolucci, R. (1989). Effects of wave propagation in random
624 earth media on the seismic radiation spectrum. *Structural Dynamics and Soil–structure*
625 *Interaction*, 61–75.

626 Gasparini, D. A., & Vanmarcke, E. H. E. J. (1976). *Simulated earthquake motions compatible*
627 *with prescribed response spectra*. Department of Civil Engineering, Research report
628 R76-4, Massachusetts Institute of Technology.

629 Gentili, S., & Franceschina, G. (2011). High frequency attenuation of shear waves in the
630 southeastern Alps and northern Dinarides. *Geophysical Journal International*, 185(3),
631 1393–1416.

632 Goldstein, P., & Snoke, A. (2005). SAC availability for the IRIS community. *Incorporated*
633 *Institutions for Seismology Data Management Center Electronic Newsletter*, 7.

634 Gonella, J. (1972). A rotary-component method for analysing meteorological and oceano-
635 graphic vector time series. In *Deep sea research and oceanographic abstracts* (Vol. 19,
636 pp. 833–846).

637 Haines, A. J. (1981). A local magnitude scale for New Zealand earthquakes. *Bulletin of the*
638 *Seismological Society of America*, 71(1), 275–294.

639 Hanks, T. C. (1982). f_{max} . *Bulletin of the Seismological Society of America*, 72(6A),
640 1867–1879.

641 Kilb, D., Biasi, G., Anderson, J., Brune, J., Peng, Z., & Vernon, F. L. (2012). A comparison
642 of spectral parameter kappa from small and moderate earthquakes using southern Cal-
643 ifornia ANZA seismic network data. *Bulletin of the Seismological Society of America*,
644 102(1), 284–300.

645 Kottke, A. R., & Rathje, E. M. (2008). *Technical manual for STRATA*. Report 2008/10,
646 Pacific Earthquake Engineering Research (PEER) Center, Berkeley, California.

647 Ktenidou, O.-J., Cotton, F., Abrahamson, N., & Anderson, J. (2014). Taxonomy of κ : a

648 review of definitions and estimation approaches targeted to applications. *Seismological*
649 *Research Letters*, 85(1), 135-146.

650 Ktenidou, O.-J., Gélis, C., & Bonilla, L.-F. (2013). A study on the variability of kappa (κ)
651 in a borehole: Implications of the computation process. *Bulletin of the Seismological*
652 *Society of America*, 103(2A), 1048–1068.

653 Laurendeau, A., Cotton, F., Ktenidou, O.-J., Bonilla, L.-F., & Hollender, F. (2013). Rock
654 and stiff soil site amplification: dependency on v_{S30} and kappa (κ_0). *Bulletin of the*
655 *Seismological Society of America*, 103(6).

656 McVerry, G. H., Zhao, J. X., Abrahamson, N. A., & Somerville, P. G. (2006). New Zealand
657 acceleration response spectrum attenuation relations for crustal and subduction zone
658 earthquakes. *Bulletin of the New Zealand Society for Earthquake Engineering*, 39(1),
659 1–58.

660 Motazedian, D., & Atkinson, G. M. (2005). Stochastic finite-fault modeling based on a
661 dynamic corner frequency. *Bulletin of the Seismological Society of America*, 95(3),
662 995–1010.

663 Oth, A., & Kaiser, A. (2013). Stress release and source scaling of the 2010-2011 Canterbury,
664 New Zealand, earthquake sequence from spectral inversion of ground motion data.
665 *Pure and Applied Geophysics*, submitted.

666 Papageorgiou, A. S., & Aki, K. (1983). A specific barrier model for the quantitative
667 description of inhomogeneous faulting and the prediction of strong ground motion.
668 I. Description of the model. *Bulletin of the Seismological Society of America*, 73(3),
669 693–722.

670 Parolai, S., & Bindi, D. (2004). Influence of soil-layer properties on k evaluation. *Bulletin*
671 *of the Seismological Society of America*, 94(1), 349–356.

672 Purvance, M. D., & Anderson, J. G. (2003). A comprehensive study of the observed
673 spectral decay in strong-motion accelerations recorded in Guerrero, Mexico. *Bulletin*
674 *of the Seismological Society of America*, 93(2), 600–611.

675 Rathje, E., Kottke, A., & Ozbey, C. (2005). Using inverse random vibration theory to
676 develop input Fourier amplitude spectra for use in site response. In *16th Interna-*

- 677 *tional Conference on Soil Mechanics and Geotechnical Engineering: TC4 Earthquake*
678 *Geotechnical Engineering Satellite Conference* (pp. 160–166).
- 679 Rebollar, C. J. (1990). Estimates of shallow attenuation of the San Miguel fault, Baja
680 California. *Bulletin of the Seismological Society of America*, 80(3), 743–746.
- 681 Ristau, J. (2013). Update of regional moment tensor analysis for earthquakes in New Zealand
682 and adjacent offshore regions. *Bulletin of the Seismological Society of America*, 103(4),
683 2520–2533.
- 684 Scasserra, G., Stewart, J. P., Bazzurro, P., Lanzo, G., & Mollaioli, F. (2009). A com-
685 parison of NGA ground-motion prediction equations to Italian data. *Bulletin of the*
686 *Seismological Society of America*, 99(5), 2961–2978.
- 687 Silva, W., Darragh, D., Gregor, N., Martin, G., Abrahamson, N., & Kircher, C. (1998).
688 *Reassessment of site coefficients and near fault factors for building code provisions,*
689 *Program Element: II. 98-HQGR-1010*, Report to US Geological Survey (USGS) Re-
690 ston, Virginia.
- 691 Standards New Zealand. (2004). Structural Design Actions Part 5: Earthquake Actions.
692 *Department of Building and Housing, Wellington, New Zealand.*
- 693 Tatsuoka, F., Di Benedetto, H., Enomoto, T., Kawabe, S., & Kongkitkul, W. (2008). Various
694 viscosity types of geomaterials in shear and their mathematical expression. *Soils and*
695 *Foundations*, 48(1), 41–60.
- 696 Tsai, C.-C. P., & Chen, K.-C. (2000). A model for the high-cut process of strong-motion
697 accelerations in terms of distance, magnitude, and site condition: An example from the
698 SMART 1 array, Lotung, Taiwan. *Bulletin of the Seismological Society of America*,
699 90(6), 1535–1542.
- 700 Van Houtte, C., Drouet, S., & Cotton, F. (2011). Analysis of the origins of κ (kappa) to
701 compute hard rock to rock adjustment factors for GMPEs. *Bulletin of the Seismological*
702 *Society of America*, 101(6), 2926–2941.
- 703 Van Houtte, C., Ktenidou, O., Larkin, T., & Kaiser, A. (2012). Reference stations for
704 Christchurch. *Bulletin of the New Zealand Society for Earthquake Engineering*, 45(4),
705 184–195.

- 706 Wathélet, M. (2008). An improved neighborhood algorithm: parameter conditions and
707 dynamic scaling. *Geophysical Research Letters*, 35(9).
- 708 Wells, D. L., & Coppersmith, K. J. (1994). New empirical relationships among magnitude,
709 rupture length, rupture width, rupture area, and surface displacement. *Bulletin of the*
710 *Seismological Society of America*, 84(4), 974–1002.
- 711 Wessel, P., & Smith, W. H. (1998). New, improved version of Generic Mapping Tools
712 released. *Eos, Transactions American Geophysical Union*, 79(47), 579–579.
- 713 Wood, C. M., Cox, B. R., Wotherspoon, L. M., & Green, R. A. (2011). Dynamic site
714 characterization of Christchurch strong motion stations. *Bulletin of the New Zealand*
715 *Society for Earthquake Engineering*, 44(4), 195–204.

716 **Full mailing address for each author**

717 **Chris Van Houtte and Tam Larkin**

718 Faculty of Engineering
719 The University of Auckland
720 Private Bag 92019
721 Auckland Mail Centre
722 Auckland 1142
723 New Zealand

724 **Olga-Joan Ktenidou**

725 ISTerre
726 Université de Grenoble 1
727 CNRS BP53
728 38041 Grenoble Cedex 9
729 France

730 **Caroline Holden**

731 GNS Science
732 PO Box 30-368
733 Lower Hutt 5040
734 New Zealand

TABLES

Table 1: GeoNet sites in this study. All instruments are strong motion accelerometers, except MQZ, which is a broadband instrument.

Station	Sampling rate (Hz)	V_{S30} (m/s)	Fundamental frequency (Hz)	NZS1170.5: 2004 Site Class	Total recordings	Recordings with $R_e < 30$ km
AKSS	200	1073	9	B	46	11
CRLZ	200	900	1	B	143	124
D14C	200	733	1	B	84	70
GODS	200	586	1	B	106	99
HVSC	200	422	3.5	C	34	33
MQZ	100	1000*	8	B	1655	1099
MTPS	200	830	1	B	95	87

* V_{S30} for this station is entirely inferred.

Table 2: Suggested limits of the Anderson and Hough (1984) manual fitting method, for $\kappa_{AS} \leq 0.03$ s.

Maximum usable frequency of available data (Hz)	Minimum magnitude to calculate κ_{AS}
40	2.5
30	3
23	3.5

Table 3: κ_0 results for the seven sites in this study

Station	Mean $\kappa_{0,AS}$ (s)	Standard deviation of $\kappa_{0,AS}$ (s)	$\kappa_{0,IRVT}$ (s) from Bradley (2013)
AKSS	0.0334	0.0039	0.0341
CRLZ	0.0319	0.0059	0.0348
D14C	0.0251	0.0091	0.0355
GODS	0.0497	0.0096	0.0372
HVSC	0.0437	0.0095	0.0377
MQZ	0.0297	0.0089	0.0344
MTPS	0.0393	0.0060	0.0351

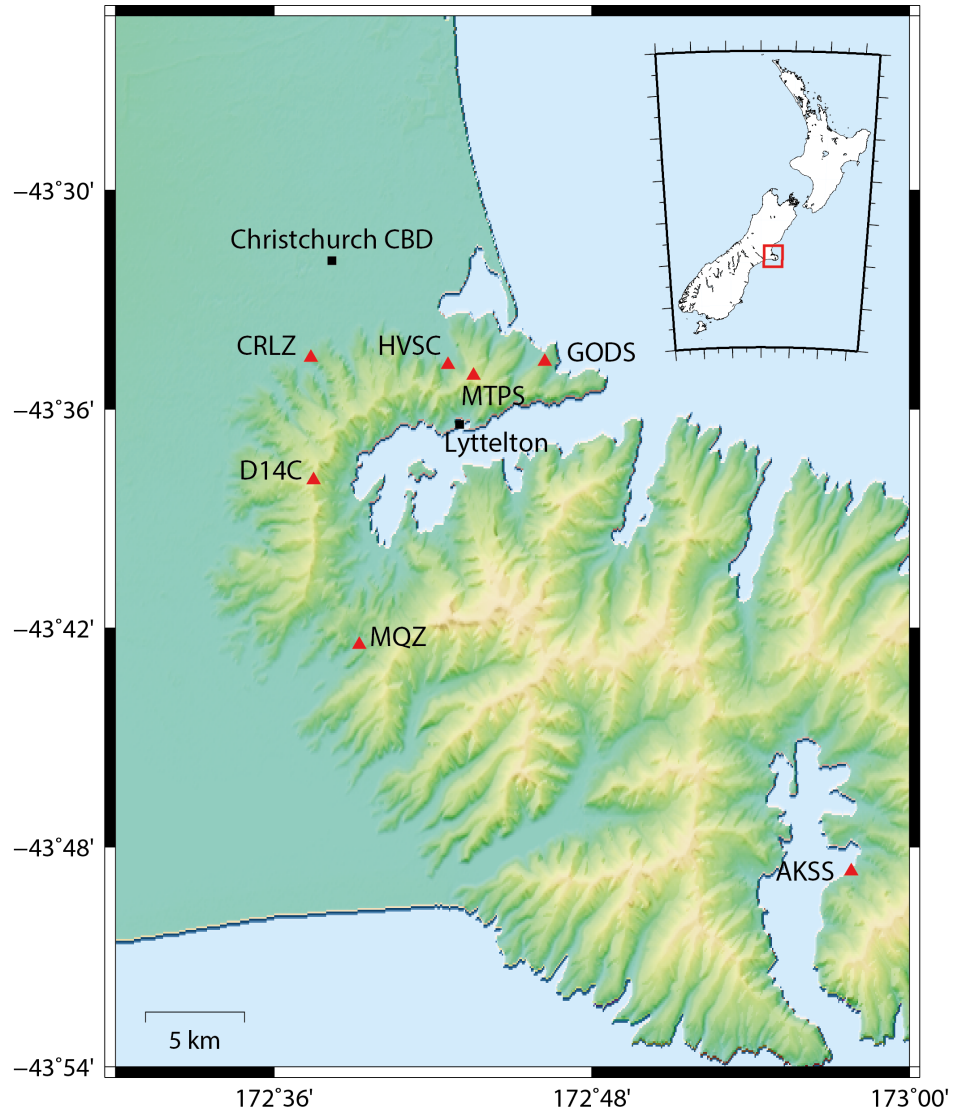


Figure 1: Locations of the seismic stations analyzed in this study. The color version of this figure is available only in the electronic edition.

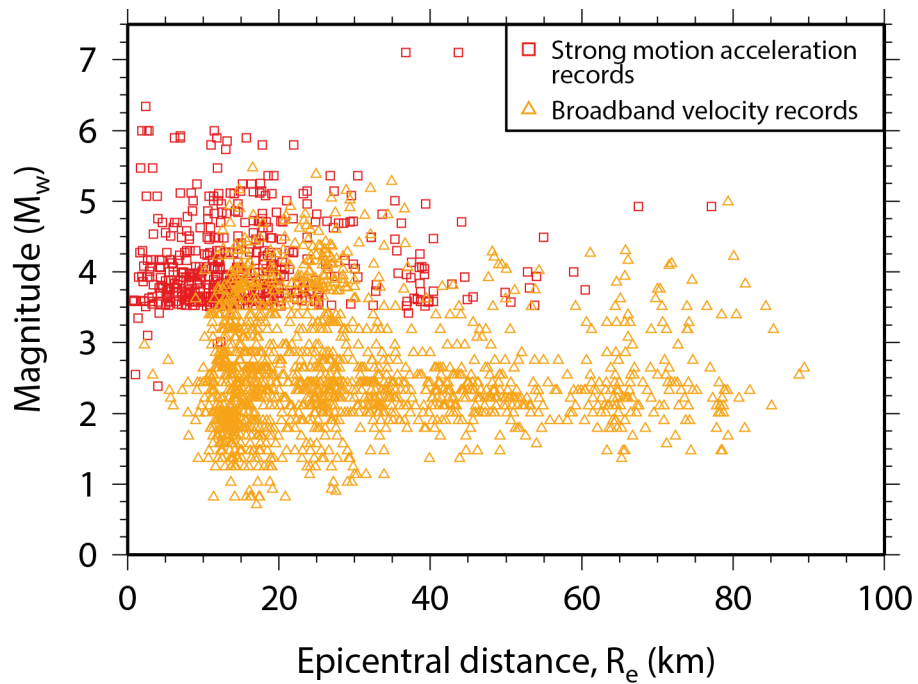


Figure 2: Magnitude - epicentral distance distribution of events analyzed in this study. Squares indicate events recorded by strong motion stations and triangles indicate events recorded by a broadband sensor. The color version of this figure is available only in the electronic edition.

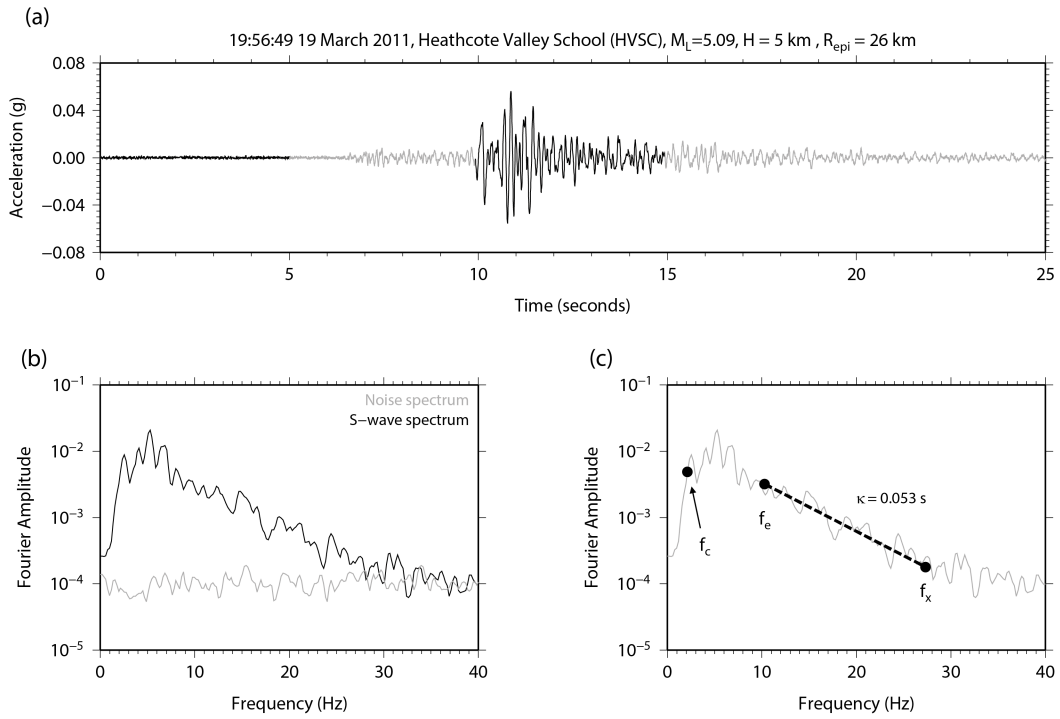


Figure 3: (a) Example S-wave and pre-event noise windows from an event in the Canterbury earthquake sequence (indicated in black), (b) their corresponding Fourier amplitude spectra and (c) f_c , f_e and f_x picks for calculating κ_{AS} . Fourier amplitude units in (b) and (c) are $m/(9.81 \cdot s)$

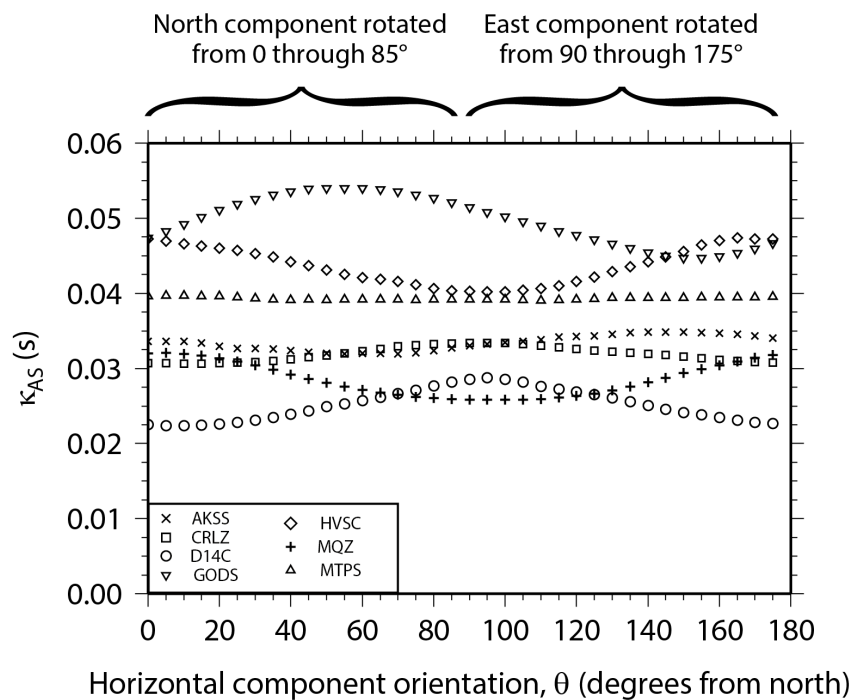


Figure 4: The sensitivity of κ_{AS} measurements to the orientation of the sensor. For every station (see legend), each data point gives the average κ_{AS} for a single component over all events recorded at that station, and for the particular orientation of the component. The north component is rotated in 5° increments from 0 to 85° , and the east component from 90 to 175° . For station MTPS the sensitivity of κ_{AS} to sensor orientation is negligible, while for station GODS it is substantial.

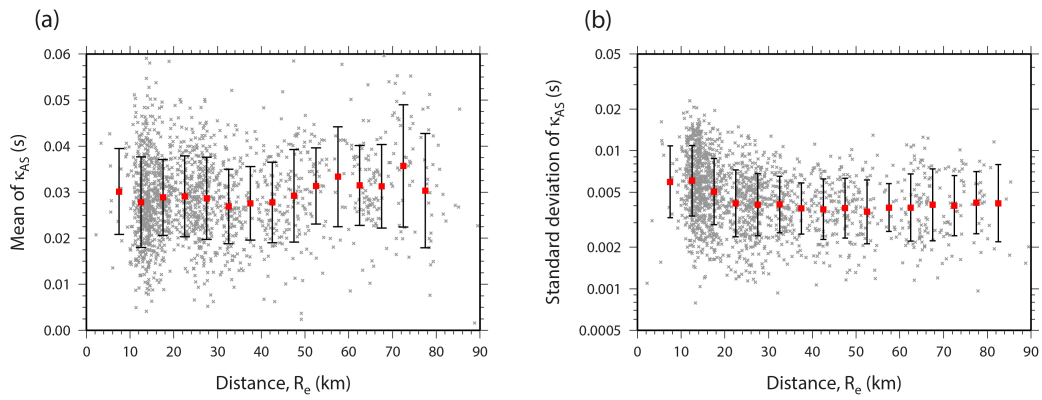


Figure 5: (a) κ_{AS} against epicentral distance, R_e , for recordings at the MQZ station. Squares indicate the mean of 5 km distance bins, with error bars representing ± 1 standard deviation. (b) standard deviation of κ_{AS} (computed from the normal distribution of the 36 κ_θ values per event recorded at MQZ), plotted against epicentral distance. Also indicated are lognormally distributed mean and standard deviation of 5 km distance bins. The color version of this figure is available only in the electronic edition.

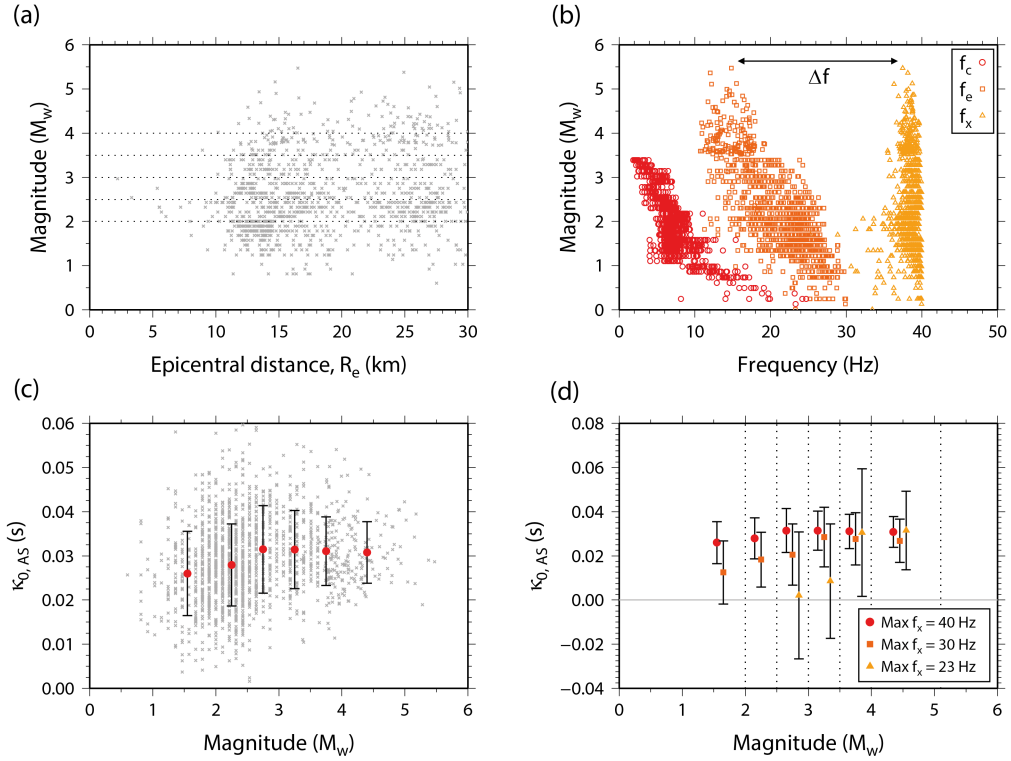


Figure 6: (a) The near-source events recorded by the velocity channel at the MQZ station, with dotted lines indicating the boundaries of magnitude bins that the data is divided into. (b) the distribution of f_c , f_e and f_x picks with magnitude for the events. (c) $\kappa_{0,AS}$ against magnitude, with mean of the magnitude bins indicated as circles, with ± 1 standard deviation indicated by error bars. (d) the effect of the maximum usable frequency of the available data. Note that each bin contains exactly the same data, only the maximum value for f_x has changed. The color version of this figure is available only in the electronic edition.

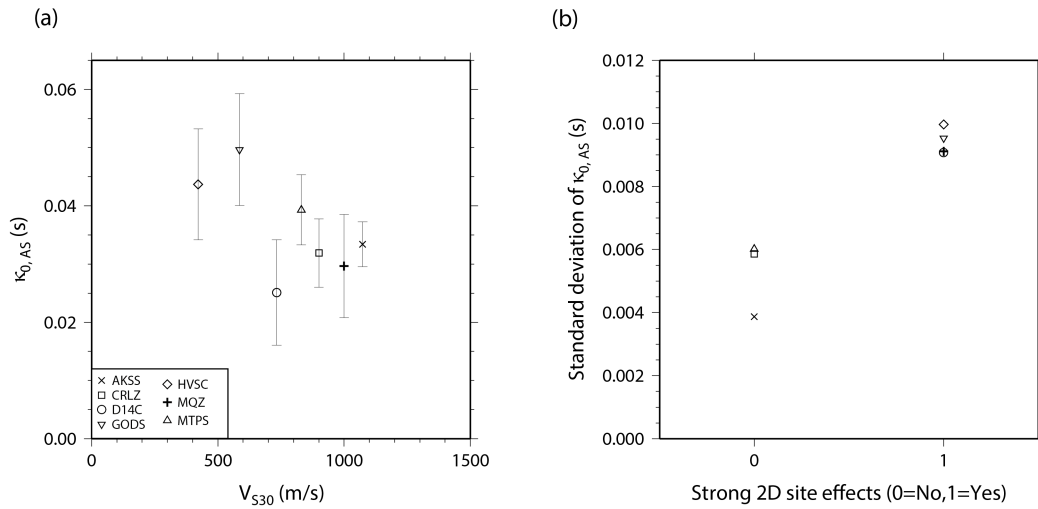


Figure 7: (a) $\kappa_{0,AS}$ against V_{S30} for the seven stations in this study. (b) The standard deviation of $\kappa_{0,AS}$ against a binary measure of 2D site effects. A value of one corresponds to a site with known strong 2D site effects, while a value of zero corresponds to a site where the response can be considered 1D.

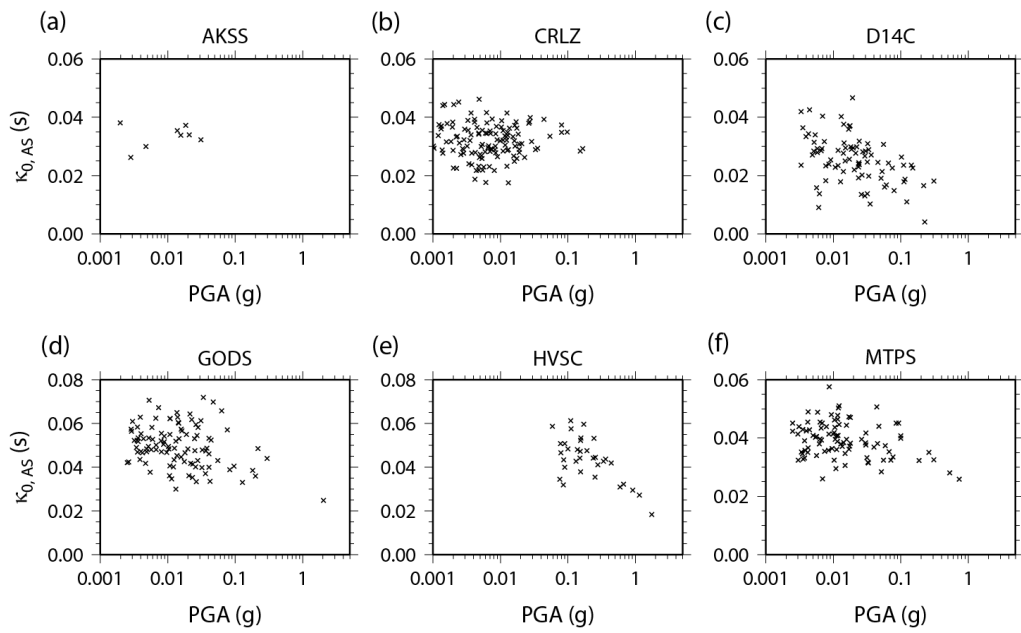


Figure 8: $\kappa_{0,AS}$ against peak ground acceleration for (a) AKSS, (b) CRLZ, (c) D14C, (d) GODS, (e) HVSC and (f) MTPS strong motion stations.

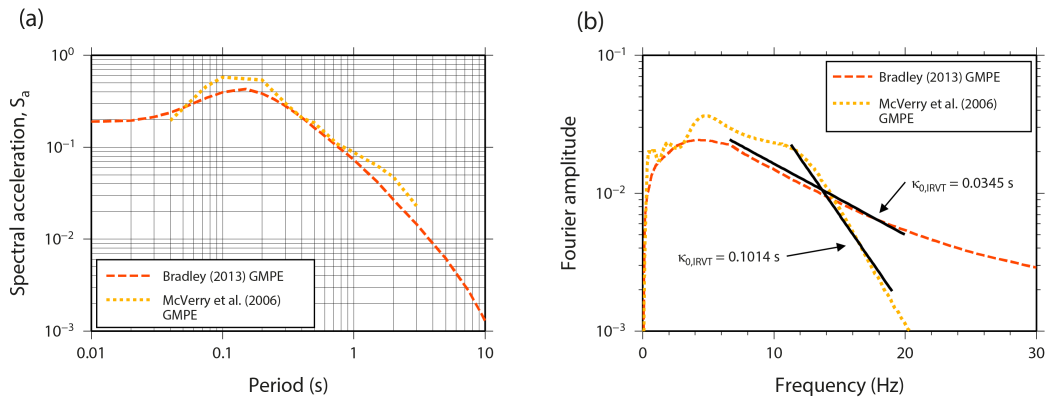


Figure 9: (a) Response spectra for a $M_w=6$, $R=10$ km, $V_{S30}=1000$ m/s scenario using the Bradley (2013) and McVerry et al. (2006) GMPEs, and (b) the two compatible FAS calculated using IRVT, with κ_{IRVT} measurements indicated. Note that PGA in the McVerry et al. (2006) GMPE was assumed to represent $T=0.04$ s. The color version of this figure is available only in the electronic edition.

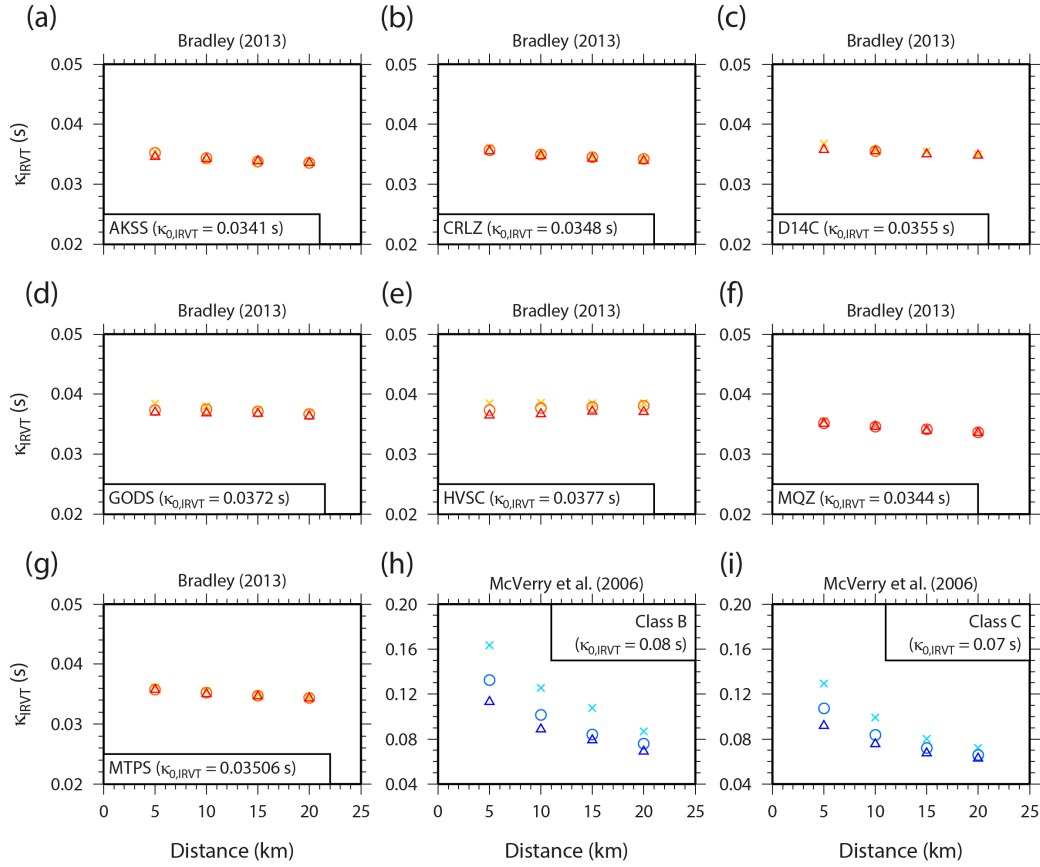


Figure 10: κ_{IRVT} for the magnitude, distance and site scenarios using the Bradley (2013) [(a)-(g)] and the McVerry et al. (2006) [(h) and (i)] GMPEs. Triangles, circles and crosses correspond to $M_w = 6.5$, 6 and 5.5 scenarios respectively. The Bradley (2013) GMPE uses V_{S30} and $Z_{1.0}$ as the site term predictor variables, while McVerry et al. (2006) uses NZS1170.5:2004 site classifications (see Table 1 for the site data of each of the seven stations). Please note the different scale on (h) and (i). The color version of this figure is available only in the electronic edition.

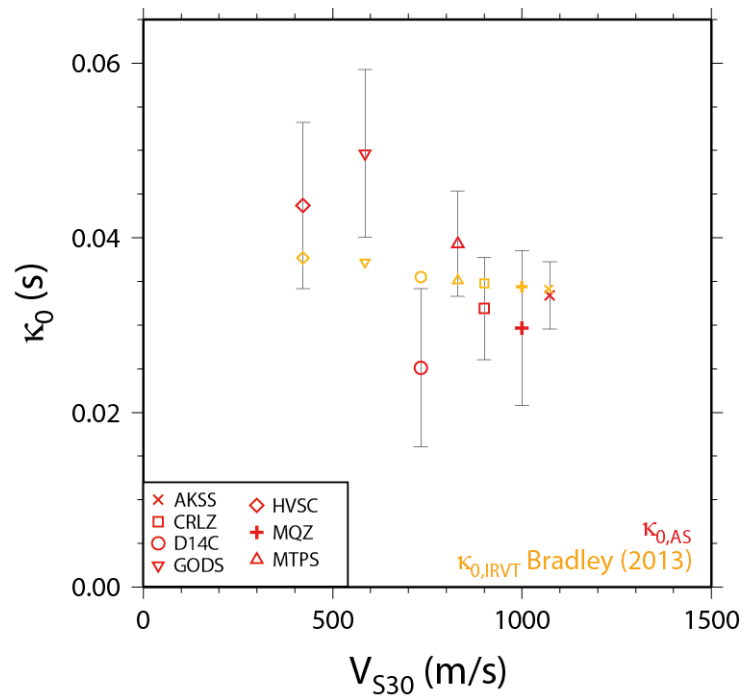


Figure 11: Comparison of $\kappa_{0,AS}$ and $\kappa_{0,IRVT}$ from the Bradley (2013) GMPE, plotted against V_{S30} . The color version of this figure is available only in the electronic edition.

3.2 κ_0 in Euroseistest: possible physical basis for regional dependency and the effect of scattering

Numerous approaches have been proposed to compute κ_0 . In this study we estimate κ for the EUROSEISTEST valley, a geologically complex and seismically active region with a permanent strong motion array consisting of 14 surface and 6 downhole stations. Site conditions range from soft sediments to hard rock. Our goal is three-fold. First, we use two different but conceptually consistent approaches, measuring κ on the high-frequency part of the S-wave acceleration spectra (AS), and on the site transfer function (TF). For the AS approach, we separate the site (κ_{0_AS}) and path (regional Q attenuation) components of κ_{r_AS} . We then compare results from the two approaches. κ_0 results are similar and the differences between the methods provide an estimate of epistemic uncertainty on κ_0 . The regional Q results of both methods are also in agreement with independent crustal attenuation studies. Second, we take advantage of the existing knowledge of the geological profile and material properties to examine the correlation of κ_0 with site characterisation parameters, namely V_{s30} , resonant frequency, and depth-to-bedrock. κ_0 correlates to V_{s30} as expected, though the scatter is large. It also correlates with the geological structure below 30 m (and down to 400 m). Thus, correlations with the entire soil column may complement the correlation of κ_0 with the very shallow geology. Third, we use results to improve our understanding of κ and propose two new notions regarding its physics. On the one hand, and contrary to existing correlations, we observe that κ_0 stabilises for high V_s values. This may indicate the existence of regional minima for rock κ_0 . If so, we propose that borehole measurements (almost never used up to now) may be useful in determining them. On the other hand, we find that material damping, as expressed through travel times, may not suffice to account for the total κ_0 measured at the surface. The uncertainty in the damping does not justify this discrepancy, because our values are well constrained from both lab and in situ tests. We propose that additional attenuation may be due to scattering from small-scale variability in the profile. If this is so, geotechnical damping measurements may not suffice to infer the overall crustal attenuation under a site, but starting with a regional (or borehole) value and adding damping could help define a lower bound for site-specific κ_0 .

This chapter reports the work shown in publications A8 and J4 (see Annex).

1
2
3
4
5
6
7
8
9
10
11
12
13
14
15
16
17
18
19
20
21
22
23
24
25
26
27
28

UNDERSTANDING THE PHYSICS OF KAPPA (K): INSIGHTS FROM EUROSEISTEST

by

Olga-Joan Ktenidou^{1*}, Stephane Drouet³, Fabrice Cotton¹, Norman A. Abrahamson²

¹ ISTerre, Université de Grenoble 1, CNRS, F-38041 Grenoble, France

² University of California, Berkeley, Department of Civil and Environmental Engineering, Berkeley, California 94720 U.S.A.

² Observatório Nacional, R. Gen. José Cristino, 77 - São Cristóvão, Rio de Janeiro, Brazil

To be submitted to:

GJI

Fifth draft

April 2014

* Corresponding author

29 ABSTRACT

30

31 At high frequencies the acceleration spectral amplitude decreases rapidly. Anderson and Hough (1984)
32 modelled this with the spectral decay factor κ , whose site component, κ_0 , is used widely today in
33 ground motion prediction and simulation. Numerous approaches have been proposed to compute κ_0 . In
34 this study we estimate κ for the EUROSEISTEST valley, a geologically complex and seismically
35 active region with a permanent strong motion array consisting of 14 surface and 6 downhole stations.
36 Site conditions range from soft sediments to hard rock. Our goal is three-fold. First, we use two
37 different but conceptually consistent approaches, measuring κ on the high-frequency part of the S-
38 wave acceleration spectra (κ_{r_AS} , after Ktenidou et al., 2013), and on the site transfer function (κ_{0_TF} ,
39 after Drouet et al., 2008a). For the AS approach, we separate the site (κ_{0_AS}) and path (regional Q
40 attenuation) components of κ_{r_AS} . We then compare results from the two approaches. κ_0 results are
41 similar and the differences between the methods provide an estimate of epistemic uncertainty on κ_0 .
42 The regional Q results of both methods are also in agreement with independent crustal attenuation
43 studies. Second, we take advantage of the existing knowledge of the geological profile and material
44 properties to examine the correlation of κ_0 with site characterisation parameters, namely V_{s30} , resonant
45 frequency, and depth-to-bedrock. κ_0 correlates to V_{s30} as expected, though the scatter is large. It also
46 correlates with the geological structure below 30 m (and down to 400 m). Thus, correlations with the
47 entire soil column may complement the correlation of κ_0 with the very shallow geology. Third, we use
48 results to improve our understanding of κ and propose two new notions regarding its physics. On the
49 one hand, and contrary to existing correlations, we observe that κ_0 stabilises for high V_s values. This
50 may indicate the existence of regional minima for rock κ_0 . If so, we propose that borehole
51 measurements (almost never used up to now) may be useful in determining them. On the other hand,
52 we find that material damping, as expressed through travel times, may not suffice to account for the
53 total κ_0 measured at the surface. The uncertainty in the damping does not justify this discrepancy,
54 because our values are well constrained from both lab and in situ tests. We propose that additional
55 attenuation may be due to scattering from small-scale variability in the profile. If this is so,
56 geotechnical damping measurements may not suffice to infer the overall crustal attenuation under a

57 site, but starting with a regional (or borehole) value and adding damping could help define a lower
58 bound for site-specific κ_0 . More precise estimation would necessitate site instrumentation.

59

60 INTRODUCTION

61

62 At high frequencies, the spectral amplitude of acceleration decays rapidly. Hanks (1982) first
63 introduced f_{max} to model the frequency above which the spectrum decreases, while Anderson and
64 Hough (1984) introduced the spectral decay factor (κ) to model the rate of the decrease. Though its
65 physics are still not completely deciphered, κ is a crucial input for describing high frequency motion in
66 various applications, including the simulation of ground motion and the creation and adjustment of
67 GMPEs from one region to another. There are many approaches for estimating κ and it has been
68 suggested that certain approaches may be consistent with one another based on the frequency range
69 over which they measure it (Biro and Renault, 2012; Ktenidou et al., 2014). In this paper, we first
70 examine two such approaches, compare the results and confirm their compatibility. In a second step,
71 we correlate κ to various site characterization parameters in order to better understand the physics
72 behind it. In the last part, we examine new possibilities as to its physical interpretation.

73

74 Anderson and Hough (1984) coined κ based on the observation that, above a given frequency, the
75 amplitude of the Fourier acceleration spectrum (FAS) decays linearly if plotted in lin-log space. κ for a
76 given record at some distance R (termed κ_r) can be related to the slope (λ) of the spectrum (a) as
77 follows:

78

$$79 \quad \kappa_r = -\lambda/\pi \quad \text{where} \quad \lambda = \Delta(\ln a)/\Delta f \quad (1)$$

80

81 The same authors observed that measured κ_r values at a given station scale with distance. The zero-
82 distance intercept of the κ trend with distance (denoted κ_0) corresponds to the attenuation that S waves
83 encounter when travelling vertically through the geological structure beneath the station. The distance
84 dependence corresponds to the incremental attenuation due to predominantly horizontal S-wave

85 propagation through the crust. As a first approximation, the distance dependence may be considered
86 linear and denoted by κ_R , so that the overall κ can be written as follows, in units of time:

87

$$88 \quad \kappa_r = \kappa_0 + \kappa_R \cdot R \quad (s) \quad (2)$$

89

90 This linear simplification cannot always describe the distance dependence, but has proven a good
91 approximation for some (Nava et al., 1999; Douglas et al., 2010; Gentili and Francheschina, 2011;
92 Ktenidou et al., 2013). Several studies also investigate the dependence of κ_r on site and source
93 parameters (e.g. Tsai and Chen, 2000; Purvance and Anderson, 2001; Douglas et al., 2010; Van
94 Houtte et al., 2011). Despite the debate as to the relative importance of these components in different
95 regions, in current applications κ_0 is used primarily to describe site attenuation due to local geological
96 conditions down to a few hundreds of meters, or a few kilometers, beneath the site under study
97 (Anderson and Hough, 1984; Campbell, 2009). Today, interest in κ_0 is renewed because it constitutes
98 an important input parameter when adjusting GMPEs to different regions through the host-to-target
99 method (Cotton et al., 2006; Douglas et al., 2006; Biro and Renault, 2012), and in constraining high
100 frequencies for synthetic ground motion generated either by stochastic, physics-based, or hybrid-
101 method simulations (e.g., Boore, 2003; Graves and Pitarka, 2010; Mai et al., 2010). The latest
102 generation of GMPEs is also expected to incorporate κ_0 as a new predictor variable (e.g. Laurendeau et
103 al., 2013).

104

105 Recently, existing approaches for computing κ from seismic records were identified and grouped into
106 a taxonomy (Ktenidou et al., 2014). Whether κ_0 values derived using different methods are consistent
107 or not may have significant effects on the aforementioned applications that use κ as input. It is
108 important to capture the epistemic uncertainty due to the different approaches for measuring κ before
109 we can attempt to interpret κ values physically. It has not yet been investigated whether all approaches
110 yield equivalent results, but it has been suggested that some may be more consistent due to similar
111 characteristics of the frequency band they examine. For example, one group of approaches uses only
112 the high-frequency range to compute κ , while another group uses the entire frequency band. For this

113 study we choose to apply two of the high-frequency approaches: the ‘acceleration spectrum’ (AS)
114 approach and the ‘transfer function’ (TF) approach. We choose a site marked by complex surface
115 geology, where records are available from a variety of geological conditions ranging from soft soil to
116 hard rock, and where the geometry and dynamic properties of the formations are well known through
117 geotechnical and geological surveys. This will allow us to perform three tasks: 1. Estimate κ_0 at all
118 these sites through these two different approaches, compare results and conclude as to their
119 compatibility. 2. Correlate our κ_0 estimates with parameters used in site characterization (V_{s30} , depth
120 to bedrock, resonant frequency). 3. Use results to better understand the physics of κ and κ_0 ,
121 particularly with respect to its relation with damping, and values for hard rock.

122

123

124 STUDY AREA AND DATA

125

126 The area studied is an elongated sedimentary basin in Northern Greece, situated between lakes
127 Langada and Volvi. It lies 30 km from the city of Thessaloniki and is the nearest active seismic zone
128 affecting it. This is why, over the past two decades, this site has been the object of extensive studies in
129 terms of its geological structure and soil properties (through geological, geophysical and geotechnical
130 in situ surveys) and seismic response (through empirical and numerical methods).

131

132 The basin’s width is around 6 km and the maximum thickness of the sediments is around 200 m at its
133 centre. A permanent accelerometric network named Euroseistest (Pitilakis et al., 2013;
134 <http://euroseis.civil.auth.gr>) has been installed around the basin centre, comprising 14 surface and 6
135 downhole receivers. The surface layout of the array has the shape of a cross, extending in two
136 directions, perpendicular and parallel to the basin axis (Figure 1). The stations have been installed in
137 different formations to sample ground motion in various geological conditions (Figures 2,3). Thus, the
138 soil conditions where κ is investigated range from very soft, deep valley deposits (TST000 station at
139 the valley centre) to weathered rock outcrop (PRO000 and STE stations on the neighbouring hills) and
140 very hard rock (PRO033 and TST196 downhole stations). In terms of shear wave velocity, this

141 corresponds to a range of V_{S30} from 190 m/s to 1840 m/s. In terms of EC8 site classification (CEN,
142 2003), this corresponds to sites ranging from D/C to A respectively.

143

144 We use a dataset of 84 earthquakes, recorded by the surface and downhole stations of the permanent
145 network between 1994 and 2009. The epicentral distribution of these events is shown in Figure 4.
146 Their moment magnitudes range from 2 to 6.5, with distances out to 150 km. All events are crustal,
147 with depths down to 15 km. These parameters are also shown in Figure 4.

148

149

150 APPROACHES FOR KAPPA ESTIMATION

151

152 Ktenidou et al. (2014) identify a group of approaches that measure κ over the high frequency range.
153 We use two of these approaches, measuring κ on the acceleration spectrum (κ AS) of individual
154 records and on the transfer function of each site (κ TF). These approaches are considered compatible
155 due to the similar frequency range in which κ is computed. In what follows we describe the main steps
156 of each approach.

157

158 Acceleration spectra (AS)

159

160 We follow the methodology proposed in Ktenidou et al. (2013) for the estimation of κ . The steps
161 followed are summarised below. Based on a preliminary visual check we choose records of good
162 quality, for which there is also an adequate window of pre-event noise. We pick P and S arrivals
163 manually and choose an S-wave window by visual inspection, taking into account the magnitude and
164 distance of the earthquake. We compute the signal-to-noise ratio using the S-wave and noise windows
165 and only work with records for which SNR is higher than 3. We compute the Fourier amplitude
166 spectrum for the S-window and pick frequencies f_1 and f_2 between which the spectral acceleration
167 amplitude decreases linearly in lin-log space. We take care to pick f_1 well to the right of the corner
168 frequency of the respective earthquakes, in order to avoid trade-off between site and source effects. In

169 picking f_1 we also avoid the resonant peak of the transfer function and the first few overtones, so as to
170 avoid biasing κ_r measurement due to the distortion of the spectral shape coming from local resonance
171 peaks (Parolai and Bindi, 2004). For high-frequency resonance, if we cannot avoid the resonant peaks
172 then we try to cut through some of them. f_2 is chosen within the frequency range for which the
173 instrument response can be considered flat and above the noise. The chosen frequencies f_1 and f_2 vary
174 among records depending on magnitude, resonance pattern, noise level, and spectral shape, but on
175 average the range used is 15-30 Hz. Using the chosen frequency range, we regress the data based on
176 equation (1) to compute the individual value of κ_r for each event at each station. We do this for all
177 three components. We then compute the average horizontal κ_r value from the NS and EW components.
178 Figure 5a shows the picking of f_1 and f_2 and the computation of κ_r for an earthquake (15/07/2004
179 00:40 GMT, M 3.5, R=10 km, EW component) recorded at all stations of the TST downhole array
180 (Figure 5b). The results are shown with depth, starting from TST000, the centre of the basin where
181 $V_{s30}=175$ m/s, down to TST200, the downhole bedrock station where $V_{s30}>1500$ m/s (see station
182 locations in Figure 1). f_2 is determined by the noise level, which is naturally lower the deeper the
183 station. The choice of f_1 is affected by the corner frequency of the event (3-4 Hz) and each station's
184 resonant frequency. The computed κ_r values differ greatly: at depth, κ is less than half with respect to
185 the surface (Figure 5c).

186

187 We now have pairs of values for κ_r and distance for all records (Figure 6). We see an increase of κ_r
188 with epicentral distance, even though not all stations recorded distant events. We observe that κ_r
189 values are correlated with the site conditions. For instance, data from station TST000 (0m, blue points)
190 lie above data from T200 (-200m, red points); however, the scatter is large. We proceed to the
191 regressions with distance to derive the parameters of equation 2. We assume the simplest model, a
192 linear dependence of κ_r with distance. This assumes that regional attenuation in the upper crust is
193 constant with frequency and depth, but has often been shown to be a good first approximation. We use
194 a weighed bisquared scheme for the linear regression and since the slope of the line is considered to
195 represent the regional attenuation effect, we constrain it to be the same for all stations. Thus, we
196 compute a common κ_R using data from all the stations together, regardless of soil type, and then

197 estimate of κ_0 separately for each station, given the different site conditions. The regression results are
198 shown in Figure 6 for TST000 and T200 stations (blue and red respectively), where the lines indicate
199 the mean ± 1 standard deviation. Despite the large scatter in the data points -typical in such studies-,
200 the difference in κ_r values between the shallowest and deepest station of the TST borehole is
201 significant.

202

203

204 Transfer functions (TF)

205

206 In the previous section we computed κ according to the original definition introduced by Anderson
207 and Hough (1984). In this section we follow an alternative approach from the same the ‘high-
208 frequency’ approach group according to the taxonomy. This approach differs from the previous one in
209 that the measured quantity is not κ_r , but is directly the site term, κ_0 , along with a full frequency-
210 dependent Q model estimated separately. Drouet et al. (2008b) implemented a parametric inversion on
211 the same dataset we have studied here and separated the source, path and site contribution. Their
212 technique is detailed in Drouet et al. (2008a) and is based on far-field Fourier spectra of S waves. A
213 Brune (1970) source is assumed and both geometrical and anelastic attenuation are modeled. Then an
214 iterative least squares inversion is applied which uses the derivatives of the modeling function with
215 respect to the different parameters. Drouet et al. (2008b) derived moment magnitudes, corner
216 frequencies, a frequency-dependent model of Q and the site functions for the average horizontal and
217 vertical components. Here we focus on the latter two, in order to derive local and regional high-
218 frequency attenuation. We use the high-frequency part of the amplification functions at each station to
219 derive the site-specific component of κ , namely κ_{0_TF} , as per Drouet et al. (2010). The frequency range
220 in which we consider the decay of the transfer functions linear ranges from $f_1=5-15$ Hz to $f_2=15-25$
221 Hz and is shown in Figure 7 along with κ_0 values.

222

223

224 EPISTEMIC UNCERTAINTY: COMPARING RESULTS BETWEEN APPROACHES AND

225 CONFRONTING WITH REGIONAL Q STUDIES

226

227 Site attenuation (κ_0)

228

229 We have computed κ_0 using two approaches, which we considered a priori as compatible. In this
230 section we verify that this is true and also compare with the results of other κ studies performed in
231 Greece. In Figure 8 we compare the κ_0 values computed for the horizontal components using the two
232 different approaches. The results are well correlated (the coefficient of correlation is 66%). The
233 transfer function approach slightly overestimates κ_0 , which may be related to the frequency-dependent
234 Q of the inversions. However, this difference lies within the scatter of the results. κ_0 ranges from 0.02-
235 0.03 s for the sites on downhole rock (EC8 class A with V_{S30} of 1840 m/s) up to 0.06-0.07 s for the
236 softest sites in the basin (EC8 class C/D, with V_{S30} of 190 m/s).

237

238 Overall, κ_0 values from the two approaches range from 0.02 to 0.08 s for these highly varying site
239 conditions. Hatzidimitriou et al. (1993) proposed an average κ_0 value of 0.057 s after studying a
240 variety of sites across Greece, while Ktenidou et al. (2013) found lower values of 0.02-0.03 s and
241 Tselentis (1993) found values of 0.04 s near the Gulf of Corinth. Papaioannou (2007) also made a
242 study of κ_{AS} for the Euroseistest array. He computed κ_0 values that range from 0.050 s for stiff soil
243 outside the basin to 0.085 s for soft alluvia near its centre, with transition sites near the edges at 0.065
244 s. Our values are lower, and one reason could be trade-off with Q: we constrained κ_R to be the same at
245 all stations, considering it a regional effect, while he allowed it to be guided by the data and vary
246 among stations.

247

248 Regional attenuation (κ_R)

249

250 In this section we compare the values of anelastic regional attenuation derived from the two
251 approaches and from independent Q studies in Greece. Drouet et al. (2008b) found the following
252 power law relation for frequency-dependent Q:

253

$$254 \quad Q(f) = 57.5226 \cdot f^{0.6789} \quad (3)$$

255

256 That study used data up to 25 Hz. At that frequency, Q according to Equation 3 equals 510. The
257 frequency range we used to compute κ following the traditional approach was mostly between 15 and
258 30 Hz. Assuming an average crustal shear wave velocity of 3.5 km/s, the slope we computed in our κ
259 regressions in Figure 6 ($\kappa_R \sim 0.00048$ s/km) corresponds to a frequency-independent regional Q of 590.
260 So the two approaches yield similar results in terms of regional attenuation. This is despite the
261 simplifications made in the traditional approach, where we assumed a linear dependence of κ_r with
262 distance, and thus we consider that assumption justified. We also compare these relatively low Q
263 estimates with independent attenuation studies for Greece. For Northern Greece Hatzidimitriou (1995)
264 proposed $Q=590$ around 8 Hz, while Polatidis et al. (2003) proposed $Q=525$ at 12 Hz. As expected, no
265 studies show results above 20 Hz. For higher frequencies, some κ studies have inferred Q in Greece
266 based on κ_R . Papaioannou (2007) derived κ_R values that correspond to various frequency-independent
267 Q values ranging from 200 to 570 at different stations of the EUROSEISTEST array, and Ktenidou et
268 al. (2013) inferred Q of 500 for the Gulf of Corinth.

269

270 We have shown that the AS and TF approach yield similar results both in terms of local and regional
271 high-frequency attenuation. This supports the notion that the acceleration spectrum and the transfer
272 function approach may be considered as consistent and be classified together in the same group of
273 approaches, the high-frequency group, as postulated in Ktenidou et al (2014). The matching of the two
274 methods also indicates that -at least in this case- κ_0 of equation 2 is indeed primarily a site effect (since
275 our κ_{0_AS} are similar to the κ_{0_TH} and the latter were computed purely on the site amplification
276 functions) and κ_R is indeed primarily a path effect, since our κ_{r_AS} corresponds well to the Q results of
277 the TF method and other independent studies.

278

279

280 CORRELATION WITH SITE CHARACTERISATION PARAMETERS AND A PHYSICAL

281 MODEL FOR κ_0

282

283 Correlation of κ_0 with V_{S30} , deeper basin structure, and site response parameters

284

285 Often, when there is not enough data to measure κ_0 , existing empirical correlations are used to infer it.
286 Such correlations are made primarily with V_{S30} , such as those introduced by Silva et al. (1998) and
287 followed by Chandler et al. (2006), Drouet et al. (2010), Edwards et al. (2011), and Van Houtte et al.
288 (2011); see Ktenidou et al. (2014) for a discussion. Van Houtte et al. (2011) also proposed correlations
289 with the resonant frequency. V_{S30} is the main parameter used until recently for site classification,
290 though recent trends in site characterization go beneath the upper 30 m to include an index of the
291 depth of the entire soil column (e.g., Luzi et al., 2011; Pitilakis et al., 2011). This is usually achieved
292 through the fundamental frequency (or period) or the depth to bedrock, which may be defined in
293 different ways. In this section we make use of the extensive geological, geophysical, and geotechnical
294 studies already conducted at EUROSEISTEST (Raptakis et al., 2000; Manakou et al., 2010, among
295 others) and use the information available in order to correlate κ_0 with the main parameters used in site
296 characterization and response.

297

298 We first investigate the relation between κ_0 and V_{S30} , using κ_0 results from both approaches. For
299 downhole stations we use the value of V_s over the 30 m beneath the depth where the instrument is
300 installed. These V_{S30} values are computed from V_s profiles available at <http://euroseisdb.civil.auth.gr>.
301 For BUT and SCT, information is inadequate, so we infer V_{S30} by correlating with neighbouring
302 stations. For TST196, the V_{S30} was given by Raptakis and Makra (personal communication). In
303 Figure 10 we see a positive correlation with a coefficient of 40%. If we did not include downhole data,
304 the correlation would decrease to 25%. Most existing correlations with V_{S30} have even lower
305 coefficients. Van Houtte et al. (2011) found less than 15% for their Japanese surface data. This would
306 have been as high as 31% if they had also included downhole data in their correlation. Given the lack
307 of hard rock surface stations, we propose that downhole data could provide valuable information for κ_0
308 at higher V_s values.

309

310 Despite the correlation, it is evident that for soil sites with V_{S30} from 190 to 300 m/s there is a large
311 scatter in κ_0 values. This means that sites belonging to the same site class (here, class C according to
312 EC8) exhibit very different responses in terms of attenuation, which would render it difficult to
313 propose typical values for the class. We now look at the correlation of κ_0 with the other two site
314 classification parameters, f_{res} and $H_{bedrock}$ (by bedrock we mean formations G/G* of Figure 2) in Figure
315 11. The correlation coefficients are again of the order of 30-40%. This indicates that κ_0 is also
316 correlated with the deeper structure to a similar degree. We expected that κ_0 should correlate not only
317 with the first 30 m but also with the deeper structure of the basin, since it is considered to relate to
318 several hundreds of meters beneath a site. We then propose that correlations with indices of deeper
319 geology can be used to complement the classic correlations with V_{S30} .

320

321 The existing empirical correlations between κ_0 and V_{S30} have been made mainly in the context of hard
322 rock-to-rock GMPE adjustments, so the data come mainly from class A or B sites (EC8). In this study,
323 sites range from very soft to very hard. Almost no data come from site class C in existing correlations,
324 thus our data enriches them. Also, data from very hard sites ($V_{S30} > 1500$ m/s) is sparse and very
325 scattered, so it is important to compare our results for hard rock. In Figure 13 we plot existing
326 correlations within their range of applicability. The legend shows the method used to compute κ_0 (see
327 Ktenidou et al., 2014 for the taxonomy) and the region the data came from. Extrapolating available
328 correlations to lower V_{S30} values provides an upper bound if we use Silva et al. (1998) and Chandler
329 (2005), and a lower bound if we use Edwards et al. (2011). For stiff soil and soft rock sites (B class
330 and A/B interface), our results lie between available correlations. For hard rock (above 1500 m/s)
331 however, most existing correlations predict significantly lower κ_0 values. κ_0 values for very hard rock
332 are few in literature and it is important to understand their possible dependence on region and
333 measurement approach in order to improve empirical correlations and use them successfully for
334 extrapolating to high Vs values. Though there is still a strong need for more data on hard rock, in the
335 next section we propose another possible interpretation.

336

337 A possible background model for κ_0 -Vs dependence

338

339 As seen in Figure 14a, there is very little data available for high V_{S30} , and the functional forms
340 proposed in literature are different and poorly constrained near their upper V_{S30} limit. However, for
341 rock-to-hard rock adjustments, this range of V_{S30} values interests us the most. For very hard rock, the
342 question arises: what is the minimum value of κ_0 ? Some of the possible reasons for this scatter in
343 existing κ_0 - V_{S30} data are differences in the method of measurement, the range of frequencies used in it,
344 and the region (Ktenidou et al., 2014), as well as possible differences in the hardness of rock
345 (Rebollar, 1990) and the degree of fracturing and erosion (Fernandez et al., 2010). In this study we
346 have been consistent in terms of measurement method, frequency range, type of rock, and region.

347

348 For the sites in our region, we have shown (Figure 10) that it is possible to describe results using a
349 functional form similar to existing correlations, which predicts continuous decrease of κ_0 as the rock
350 hardens. However, we also observe that the downward trend is mainly due to site classes B and C. If
351 we focus on results from soft to hard rock alone, our data show no significant decrease of κ_0 beyond
352 $V_{S30}=550$ m/s (red points in Figure 14). So an alternative interpretation to the classic functional form
353 would be that κ_0 first decreases as rock hardens, but then reaches an asymptotic value (this is
354 illustrated using the shaded red area). In the same figure we highlight the results of another study,
355 which is again consistent in terms of method and frequency range. The green points show the results
356 of Ktenidou and Van Houtte (2012), who studied Swiss rock data. In that case too, on first inspection
357 we find an overall downward trend of κ_0 going from soft to hard rock. However, on closer inspection,
358 we note that κ_0 tends to stabilise for V_{S30} above 1600 m/s. We note here that this result comes from
359 measurement with the AS and TF method, and that other methods may give different values, possibly
360 lower.

361

362 The asymptotic values, shown in Figure 14 with dashed lines, are about 24 ms for Volvi and 17 ms for
363 Switzerland. The high- V_{S30} asymptotic κ_0 values might be a regional characteristic. Figure 15 shows a
364 tentative physical model describing this. At rock level, the asymptotic, high-Vs κ_0 value is determined

365 by regional attenuation (Q) along the path from the source to the upper crust. Any possible source
366 components -which in this study were not resolved-, may also affect this asymptotic value. As
367 sedimentary layers are added to the rock base, V_s gradually decreases, and κ_0 increases due to this
368 additional ‘deeper site’ attenuation. Finally, adding near-surface soil layers to the profile, the
369 additional ‘shallow local’ attenuation leads to the final value of κ_0 measured at the surface. The
370 attenuation in the uppermost layers is liable to increase under high-level excitations inciting non-linear
371 behaviour. This can be viewed in geotechnical engineering terms as the increase of hysteretic damping
372 ($\xi=(2Q)^{-1}$) with shear strain. This division of κ_0 into source/path and local site components is
373 schematically illustrated in Figure 15, along with its stabilisation around an asymptotic value that may
374 vary with region. We sketch various functional forms of decrease of κ_0 with V_s , to indicate different
375 possibilities.

376

377 This division into components could be a particularly useful way of looking at κ_0 in cases where a
378 reference rock level is sought. For instance, in cases where site-specific analyses are required to
379 predict ground motion, a reference input motion must be defined for the site response analysis and this
380 must be inserted at some reference rock level. It is important first to describe the reference rock
381 accurately in terms of V_s and κ , so as to adjust the chosen GMPEs to the region. Then it is important
382 to describe the overlying local geological structure in geotechnical terms such as V_s and ξ . For the top
383 layers these properties may also depend on the level of excitation, through G - γ - D degradation curves.
384 The relation between κ_0 and ξ for the top layers has not been fully investigated. Fernández-Heredia et
385 al. (2012) suggested a loose correlation between ξ and κ_0 . A successful separation of the reference
386 rock and overlying geology would help avoid any double counting of attenuation in the subsequent
387 response analysis. The asymptotic, regional value of κ_0 that we propose could characterize precisely
388 this ‘reference rock’ limit between the two. Establishing such a link between the seismological and
389 geotechnical aspects of attenuation may be a key decision to moving forward. In the next and final
390 section we make a first step towards this direction of correlating κ_0 and damping.

391

392 Correlation with damping and scattering

393

394 Hough and Anderson (1988) proposed that κ_0 could be integrated along the ray path in an analogy to
395 t^* based on Q and V_s in the shallow crust layers, and under the conditions described by Anderson
396 (1991) this can be written as a sum over each layer:

$$397 \quad t^* = \int_{path} \frac{dr}{V_s(z)Q(z)} = \sum \frac{H}{V_s Q} = \kappa_0 \quad (4)$$

398 From a geotechnical engineering point of view, Q in the surface layers is related to soil damping. Silva
399 (1997) proposed that, in a relationship such as equation 4, κ_0 can be linked to damping in the shallow
400 crust if we consider:

$$401 \quad Q = \frac{1}{2\xi} \quad (5)$$

402 where ξ is the decimal damping ratio over depth H . Similarly, Fernandez-Heredia et al. (2012) derived
403 the same relationship theoretically for a soil layer over halfspace, considering it as a damped linear
404 system:

$$405 \quad \xi = \frac{V_s}{2H} \kappa_0 \quad (6)$$

406 These authors assume that Q corresponds only to intrinsic (frequency-independent) attenuation and
407 does not include scattering (frequency-dependent) attenuation.

408

409 Since we know the soil profile and have available measured values of soil damping (i.e., shallow Q)
410 for EUROSEISTEST, we can examine the relation between damping and κ_0 in our data. We focus on
411 the downhole arrays TST and PRO (see Figure 3) and use expression 4 to compute t^* . Then we can
412 predict κ_0 at the surface of the boreholes (κ_0^{SUR}) based on the measured downhole value of κ_0 (κ_0^{DH})
413 and the borehole-to-surface t^* based on the known V_s , H , and ξ (or Q) of each layer. By comparing
414 predicted and measured surface κ_0 values we will try to better understand κ_0 . The expression we use is
415 the following:

$$416 \quad \kappa_0^{SUR} = \kappa_0^{DH} + t^* = \kappa_0^{DH} + \sum \frac{H}{V_s Q} = \kappa_0^{DH} + \sum \frac{2H\xi}{V_s} \quad (7)$$

417

418 At EUROSEISTEST, soil damping values are available from Pitilakis et al. (1999) for formations A
419 through G within the TST borehole, based on cyclic triaxial and resonant column tests. The small-
420 strain ξ ranges from 3.3% down to 0.3% for formations A to G*, corresponding -based on equation 5-
421 to Q values from 15 up to 200 (see table in Figure 3). The accuracy of ξ measurement by dynamic
422 laboratory testing is not always considered dependable. However, these lab results are in good
423 agreement with in situ measurements. Jongmans et al. (1999) performed analysis of attenuation of
424 surface waves at EUROSEISTEST, assuming frequency-independent Q. They found Q values down to
425 40 m depth (formations A to C) that range from 15 to 30 (see table in Figure 3). These authors stress
426 the consistency in the results of the two approaches. The uncertainty in the lab Q values is unknown.
427 However, the scatter in the in situ Q values can be estimated because Jongmans et al. (1999)
428 performed attenuation analysis along various profiles in the basin. Combining these profiles, we find
429 that the scatter around the mean Q for the top three layers ranges between 30%-35%. We also note
430 here that the Vs values that Jongmans et al. (1999) found for the various formations in Volvi are also
431 in good agreement with the model we are using here.

432

433 At downhole stations PRO33 and TST200, measured κ_0^{DH} values using the AS approach are 19 ± 4 ms
434 and 21 ± 8 ms (see points lying on the diagonals in Figure 16). Assuming that Qs and Vs are constant
435 and frequency-independent in each overlying layer, we use equation 7 and, by adding travel times to
436 the downhole measurements, we predict mean κ_0^{SUR} values at surface stations PRO0 and TST0 equal
437 to 20 and 36 ms (see the black arrows along the diagonal in the figure). But the measured values are
438 24 ± 7 and 61 ± 11 s. This means that there is a discrepancy between t^* based on the damping and the
439 measured $\kappa_0^{\text{SUR}} - \kappa_0^{\text{DH}}$; we will call this discrepancy $\Delta\kappa_0$ in the figure. For PRO0, $\Delta\kappa_0 = 24 - 20 = 4$ ms,
440 which lies within the standard deviation on the measured κ_0 . For TST0, however, there is a large
441 discrepancy of $\Delta\kappa_0 = 61 - 36 = 25$ ms, significantly larger than the measurement uncertainty. In Figure 16
442 we only show predicted vs. measured κ_0 values for stations with more than 10 records for PRO
443 (above) and TST (below). Starting from the deepest downhole station, as $t^* = 0$, the starting points lie
444 on the diagonal. Moving towards the surface, the points should move along the diagonal if κ_0 were

445 accounted for entirely by t^* (following the arrow). But they move away from the diagonal towards the
446 right, indicating measured κ_0 is larger than predicted. In the TST panel below, we also illustrate the
447 uncertainty in the damping values. As stated previously, the in situ Qs values have a scatter up to 35%
448 around the mean. We modify all Qs values over the entire TST profile by 50% (more than the actual
449 uncertainty), increasing and decreasing them, and recompute the predicted κ_0^{SUR} . These predictions are
450 shown by the red envelopes, and the shaded red area between them represents the expected variability
451 in predicted κ_0 due to Q uncertainty. Even for such systematic errors in all Qs, the predicted values
452 cannot get near the measured ones, indicating there must be another reason for this discrepancy.

453

454 For PRO, $\Delta\kappa_0$ is within the epistemic uncertainty of the κ measurements and the measured κ_0^{SUR} is can
455 be accounted for by our geotechnical model and its uncertainty. However, at TST, $\Delta\kappa_0$ is significant.
456 Our knowledge of the soil profile is well constrained between different studies and cannot lead to such
457 a global underprediction of κ_0 . We also note here that all records have peak amplitudes under 0.1g
458 (and most under 0.01g), so non-linear behaviour is not a probable reason behind this observed increase
459 in attenuation. Hence we consider an alternative interpretation for the observed $\Delta\kappa_0$. According to
460 Figure 3, the soil profile at PRO is rather simple, with a layer of weathered rock overlying healthy
461 rock. At TST, on the other hand, the soil profile is very complex, especially near the surface, due to
462 numerous thin deposit layers. Raptakis et al. (1998) show that the borehole logging at TST resulted in
463 24 geological units, which were later grouped in order to produce the simpler, homogenized
464 geotechnical model of Figure 3. Moreover, the near-surface stratigraphy revealed by CPT and SPT
465 testing in the TST borehole is even more complex, given that more than 30 units were identified
466 within the first 25 m (Raptakis et al., 1998; Manakou, 2007). We believe that this important small-
467 scale inhomogeneity of the profile may cause additional high-frequency attenuation through
468 scattering. High-frequency perturbations in Vs and Q values could, at least partly, explain the
469 discrepancy between the observed and predicted κ_0 at the surface. It would mean that the measured
470 κ_0^{SUR} at TST0 is the sum of intrinsic material attenuation and scattering, and that the former is
471 accounted in the predicted κ_0 while the latter is not.

472

473 The possibility that κ_0 comprises a component due to scattering is usually not considered. However,
474 Faccioli et al. (1989) studied self-similar random media numerically, where fluctuations in the Vs soil
475 profile were introduced stochastically. They found that such fluctuations introduce additional
476 constant-Q high-frequency attenuation that corresponds to κ . We believe that this may be one
477 interpretation for the observed discrepancy in $\Delta\kappa_0$. We find this more probable than the possibility that
478 the available estimates of both Vs and Q are gravely underpredicted (since the near-surface Q values
479 are consistent between laboratory and geophysical tests), or that the measured κ_0 values are gravely
480 overpredicted (since they are consistent between two different methods and also with regional
481 attenuation). Furthermore, the methods used to measure Q may capture for the most part its intrinsic
482 component rather than its scattering component. Lab tests (Pitilakis et al., 1999) would be expected to
483 measure the behaviour of a small-scale, relatively homogeneous sample, not accounting for additional
484 damping from spatial variability of material properties. In situ tests (Jongmans et al., 1999) were made
485 using surface waves, which are less scattering than S waves, and at frequencies lower than those we
486 used for κ (up to 10 Hz, while we went up to 30 Hz), where again the scattering effect is expected to be
487 lower. Our interpretation may also account for some of the scatter in correlations of κ_0 with indices
488 such as V_{S30} and bedrock depth. An index that averages over 30 or more meters of the profile will
489 correlate with the component of κ_0 that is due to intrinsic damping, but not with the component due to
490 small-scale fluctuations. It is possible that another index could be found, perhaps a descriptor of the
491 profile's heterogeneity, which would correlate with the scattering part of κ_0 .

492

493 If this interpretation stands, it would entail that knowledge of ξ (or Q) for the surface layers may help
494 compute a lower bound for κ_0 , which however may be higher if there is significant small-scale
495 variability causing scattering in the profile. Based on the above considerations, in Figure 17 we
496 quantify our model for the case of TST, quantifying the components of κ_0 . We start from the rock and
497 borehole data which give us the asymptotic value (24 ms), which is tied to possible source effects and
498 the regional crustal attenuation which we estimated at $Q_s=590$ for high frequencies. We then add the
499 contribution of soil damping in the near-surface layers, getting at 36 ms. Since there is no non-
500 linearity effect, the remaining 25 ms of measured attenuation are possibly due to scattering. Once

501 more we note that our results re based on the AS and TF methods, and that values may be lower for
502 other measurement methods, such as the broadband method (Ktenidou et al., 2014).

503

504 CONCLUSIONS

505

506 We use the surface and downhole stations of the EUROSEISTEST array to compute κ_0 at 21 locations
507 in and around the basin. We follow two approaches that belong to the high-frequency family of κ
508 estimation approaches: κ_{AS} and κ_{TF} . The agreement between the two approaches is good in terms of
509 both site-specific (κ_0) and regional attenuation. The regional component is also verified against
510 independent Q studies. The difference between the two approaches provides an estimate of the
511 epistemic uncertainty of κ_0 . Individual site-specific κ_0 values range from 0.018 s to 0.070 s, depending
512 on the type of site. κ_0 correlates with V_{S30} across our sites, which range from EC8 class A through
513 C/D. It also correlates with the resonant frequency and the depth to bedrock, indicating that the origins
514 of κ_0 are deeper, and that the first 30 m do not suffice to capture it. This is important because when it
515 cannot be measured, κ_0 is usually inferred purely from empirical correlations with V_{S30} . We suggest
516 that these may be complemented with correlations with depth of bedrock or resonant frequency. We
517 also put forward a new idea: although κ_0 decreases for harder sites, we observe that its value stabilises
518 above a certain value of V_{S30} . We suggest a physical model in which the asymptotic minimum value of
519 κ_0 is regional (and may be estimated from borehole recordings), and the additional attenuation from
520 surface layers is site-specific. We then quantify the effect of material damping (i.e., $t^*=H/QVs$) on
521 local attenuation using borehole data, and find that it may not suffice to predict the total measured
522 attenuation. Even considering epistemic uncertainty in the measurement of κ_0 and in the profile's Q
523 and Vs, the measured κ_0 significantly exceeds the sum of the regional (borehole) and local site
524 (damping) components. We show that the uncertainty in the damping does not justify this discrepancy,
525 because our values are constrained from both lab and in situ tests. Non-linear soil behaviour is also not
526 a possibility due to the low amplitude of our records. We then propose that the additional attenuation
527 may be due to scattering from the numerous thin near-surface layers. In the presence of such small-
528 scale variability in the profile, it is possible that geotechnical and geophysical measurements of Q (or

529 ξ) in the layers may not suffice to estimate the overall κ_0 of a site. This may be because Q
530 measurements tend to capture the intrinsic material damping more than the scattering attenuation.
531 Starting from regional or borehole values of κ_0 , knowledge of the damping can help derive a lower
532 bound value for the total site-specific κ_0 . But for a more precise estimate of the total κ_0 , seismological
533 data are needed, preferably from a combination of local and regional stations, so as to measure and
534 decouple total site and path attenuation.

535

536

537 ACKNOWLEDGEMENTS

538

539 Accelerometric, geophysical and geotechnical data for the EUROSEISTEST array can be freely
540 downloaded from <http://euroseisdb.civil.auth.gr> (last accessed June 2013). The research was funded by
541 French national project SIGMA. Signal processing benefited from SAC2008
542 (<http://www.iris.edu/software/sac>; Goldstein et al., 2003) and some figures were made using Generic
543 Mapping Tools v. 3.4 (www.soest.hawaii.edu/gmt; Wessel and Smith, 1998). Many thanks go to N.
544 Theodulidis and E. Chaljub for preparing an initial version of the dataset. We thank R. Archuleta, S.
545 Arnaouti, P.-Y. Bard, R. Castro, S. Day, H. Kawase, E. Larose, M. Manakou, R. Paolucci, Ch.
546 Papaioannou, K. Pitilakis, D. Raptakis, and Z. Roumelioti for discussions.

547

548

549 REFERENCES

550

- 551 Anderson, J.G. and S.E. Hough (1984). A model for the shape of the Fourier amplitude spectrum of
552 acceleration at high frequencies, *Bull. Seism. Soc. Am.* **74**, 1969-1993.
- 553 Anderson, J.G. (1991). A preliminary descriptive model for the distance dependence of the spectral
554 decay parameter in southern California, *Bull. Seismol. Soc. Am.* **81**, 2186–2193.
- 555 Anderson, J.G., Y. Lee, Y. Zeng, and S. Day (1996). Control of strong motion by the upper 30 meters,
556 *Bull. Seismol. Soc. Am.* **86**, 1749–1759.

557 Biro, Y., and P. Renault (2012). Importance and Impact of Host-to-Target Conversions for Ground
558 Motion Prediction Equations in PSHA. Proc. 15th World Conference of Earthquake
559 Engineering, Lisbon, Portugal, 24-28 Sep., 10 pp.

560 Boore, D.M. (2003), Simulation of ground motion using the stochastic method, *Pure Appl. Geoph.*
561 **160**, 635-676.

562 Brune, J. (1970). Tectonic stress and the spectra of seismic shear waves, *J. Geophys. Res.* **75**, 4997–
563 5009.

564 CEN (2003). Eurocode 8: Design of structures for earthquake resistance. Part 1: General rules, seismic
565 actions and rules for buildings, (EN 1998-1: 2004). Brussels, Belgium.

566 Campbell, K.W. (2009). Estimates of Shear-Wave Q and κ_0 for Unconsolidated and Semiconsolidated
567 Sediments in Eastern North America, *Bull. Seismol. Soc. Am.* **99**, 2365-2392.

568 Castro R., F. Pacor, A. Sala, C. Petrongaro (1996). S wave attenuation and site effects in the region of
569 Friuli, Italy, *J. Geophys. Res.* **101**, 22355-22369.

570 Chandler A.M., N.T.K. Lamb, H.H. Tsang (2006). Near-surface attenuation modelling based on rock
571 shear-wave velocity profile, *Soil Dyn. Earthq. Eng.* **26**, 1004–1014.

572 Douglas, J., P. Gehl, L. F. Bonilla and C. Gélis (2010). A κ Model for Mainland France, *Pure Appl.*
573 *Geophys.* **167**, 1303-1315.

574 Drouet S., F. Cotton, P. Gueguen (2010). V_{s30} , κ , regional attenuation and Mw from accelerograms:
575 application to magnitude 3–5 French earthquakes, *Geophys. J. Int.* **182**, 880-898.

576 Drouet S, S. Chevrot, F. Cotton, and A. Souriau (2008a). Simultaneous inversion of source spectra,
577 attenuation parameters and site responses. Application to the data of the French Accelerometric
578 Network, *Bull. Seism. Soc. Am.* **98**, 198-219.

579 Drouet S., N. Theodulidis and A. Savvaidis (2008b). Site effects from parameterised generalised
580 inversions. ESC 31st General Assembly, Hersonissos, Crete, Greece, 8-12 Sept.

581 Edwards B., D. Fah and D. Giardini (2011). Attenuation of seismic shear wave energy in Switzerland.
582 *Geophys. J. Int.* **185**, 967–984.

583 Gentili S. and G. Franceschina (2011). High frequency attenuation of shear waves in the southeastern
584 Alps and northern Dinarides, *Geophys. J. Int.* **185**, 1393–1416.

585 Graves, R. W. and A. Pitarka (2010). Broadband ground-motion simulation using a hybrid approach,
586 *Bull. Seismol. Soc. Am.* **100**, 2095–2123.

587 Faccioli, E., A. Tagliani, and R. Paolucci (1989). Effects of wave propagation in random earth media
588 on the seismic radiation spectrum, in *Structural Dynamics and Soil-structure Interaction*, A.S.
589 Cakmac and I. Herrera, (Editors), Computation Mech. Pub., Southampton, 61-75.

590 Fernández, A. I., R. R. Castro, and C. I. Huerta (2010). The spectral decay parameter kappa in
591 Northeastern Sonora, Mexico, *Bull. Seismol. Soc. Am.* **100**, 196–206.

592 Fernández-Heredia, A.I., C.I. Huerta-Lopez, R.R. Castro-Escamilla, and J. Romo-Jones. (2012). Soil
593 damping and site dominant vibration period determination, by means of random decrement
594 method and its relationship with the site-specific spectral decay parameter kappa. *Soil Dyn.*
595 *Earthq. Eng* **43**, 237-246.

596 Goldstein, P., D. Dodge, M. Firpo, and L. Minner (2003). SAC2000: Signal processing and analysis
597 tools for seismologists and engineers, *The IASPEI International Handbook of Earthquake and*
598 *Engineering Seismology*, W.H.K. Lee, H. Kanamori, P.C. Jennings, C. Kisslinger (Editors),
599 Academic Press, London.

600 Hanks, T. C. (1982). f_{max} , *Bull. Seismol. Soc. Am.* **72**, 1867-1879.

601 Hatzidimitriou, P., C. Papazachos, A. Kiratzi, and N. Theodulidis (1993). Estimation of attenuation
602 structure and local earthquake magnitude based on acceleration records in Greece, *Tectonophysics*
603 **217**, 243–253.

604 Hatzidimitriou, P. (1995). S-wave attenuation in the crust in Northern Greece, *Bull. Seism. Soc. Am.*
605 **85**, 1381-1387.

606 Hough, S. E., and J. G. Anderson (1988). High-frequency spectra observed at Anza, California:
607 Implications for Q structure, *Bull. Seismol. Soc. Am.* **78**, 692–707.

608 Hough, S.E., J.G. Anderson, J. Brune, F. Vernon, J. Berger, J. Fletcher, L. Haar, T. Hanks, and L.
609 Baker (1988). Attenuation near Anza, California, *Bull. Seism. Soc. Am.* **78**, 672-691.

610 Humphrey, J.R., Jr. and J.G. Anderson (1992). Shear wave attenuation and site response in Guerrero,

611 Mexico, *Bull. Seism. Soc. Am.* **81**, 1622-1645.

612 Jongmans, D., K. Pitilakis, D. Demanet, D. Raptakis, J. Riepl, C. Horrent, G. Tsokas, K. Lontzetidis,
613 and P.-Y. Bard (1999). EURO-SEISTEST: Determination of the Geological Structure of the
614 Volvi Basin and Validation of the Basin Response, *Bull. Seism. Soc. Am.* **88**, 473-487.

615 Konno, K. and Ohmachi, T. (1998). Ground-motion characteristics estimated from spectral ratio
616 between horizontal and vertical components of microtremor, *Bull. Seismol. Soc. Am.* **88**, 228-241.

617 Kramer, S.L. (1996). Geotechnical earthquake engineering. Prentice-Hall, Upper Saddle River, New
618 Jersey, 653 pp.

619 Ktenidou O.-J., Van Houtte, C. (2012). Empirical estimation of kappa from rock velocity profiles at
620 the Swiss NPP sites (19.02.2012). Report TP2-TB-1090, Pegasos Refinement Project.

621 Ktenidou O.-J., C. Gelis, F. Bonilla (2013). ‘A study on the variability of kappa in a borehole.
622 Implications on the computation method used’. *Bull. Seismol. Soc. Am.* **103**, 1048-1068.

623 Ktenidou O.-J., F. Cotton, N. Abrahamson, J.G. Anderson (2014). ‘Taxonomy of κ (kappa): a review
624 of definitions and estimation methods targeted to applications’. *Seismol. Res. Letts* 85(1) doi:
625 10.1785/0220130027.

626 Laurendeau A., F. Cotton, O.-J. Ktenidou, L-F. Bonilla, and F. Hollender (2013). Rock and stiff-soil
627 site amplification: Dependencies on Vs30 and kappa (κ_0), *Bull. Seismol. Soc. Am.* **103**, 3131-
628 3148.

629 Luzi, L., R. Puglia, F. Pacor, M.R. Gallipoli, D. Bindi, M. Mucciarelli (2011). Proposal for a soil
630 classification based on parameters alternative or complementary to Vs30, *Bull. Earthq. Eng.* **9**,
631 1877-1898.

632 Manakou, M. (2007). Contribution to the determination of a 3D soil model for site response analysis.
633 The case of the Mygdonian basin. PhD Thesis (in Greek with English abstract), Dept. of Civil
634 Engineering, Aristotle University of Thessaloniki. Available in pdf format at:
635 [/http://invenio.lib.auth.gr/](http://invenio.lib.auth.gr/).

636 Manakou M.V., D.G. Raptakis, F.J. Chavez-Garcia, P.I. Apostolidis, K.D. Pitilakis (2010). 3D soil
637 structure of the Mygdonian basin for site response analysis, *Soil Dyn. Earthq. Eng.* **30**, 1198–
638 1211.

639 Nava, F.A., García R., Castro R.R., Suárez C., Márquez B., Núñez-Cornú F., Saavedra G., Toscano
640 R., (1999). S wave attenuation in the coastal region of Jalisco-Colima, Mexico, *Phys. Earth*
641 *Planet. Inter.* **115**, 247–257.

642 Papaioannou Ch. (2007). A preliminary study for the distance dependence of the spectral decay
643 parameter κ for the Euroseisrisk strong motion array. Proc. 4ICEGE, Thessaloniki June 25-28,
644 Paper 1524.

645 Parolai S. and D. Bindi (2004). Influence of Soil-Layer Properties on κ Evaluation, *Bull. Seism. Soc.*
646 *Am.* **94**, 349-356.

647 Pitilakis, K., D. Raptakis, K. Lontzetidis, Th. Tika-Vassilikou & D. Jongmans (1999). Geotechnical &
648 Geophysical description of EURO-SEISTEST, using field, laboratory tests and moderate strong-
649 motion recordings, *J. Earthq. Eng.* 3, 381-409.

650 Pitilakis, K., Anastasiadis, A., & Riga, E. (2011a). New soil classification system and spectral
651 amplification factors for EC8, in Proceedings of ISSMGE - ERTC 12 Workshop on Evaluation of
652 Geotechnical Aspects of EC8, XV European Conference on Soil Mechanics and Geotechnical
653 Engineering, M. Maugeri (Editor), Athens, 11 September 2011, Part 1, Ch. 6.

654 Pitilakis K., Z. Roumelioti, D. Raptakis, M. Manakou, K. Liakakis, A. Anastasiadis, and D. Pitilakis
655 (2013). The EUROSEISTEST Strong-Motion Database and Web Portal, *Seismol. Res. Letts* **84**,
656 796-804.

657 Polatidis, A., A. Kiratzi, P. Hatzidimitrioua, and B. Margaris (2003). Attenuation of shear-waves in
658 the back-arc region of the Hellenic arc for frequencies from 0.6 to 16 Hz, *Tectonophysics* **367**,
659 29–40.

660 Raptakis D., F.J. Chavez-Garcia, K. Makra, K. Pitilakis (2000). Site effects at Euroseistest—I.
661 Determination of the valley structure and confrontation of observations with 1D analysis. *Soil*
662 *Dyn. Earthq. Eng.* **19**, 1-22.

663 Rebollar, C. J. (1990). Estimates of shallow attenuation of the San Miguel fault, Baja California, *Bull.*
664 *Seismol. Soc. Am.* **80**, 43–46.

665 Silva, W., Darragh, R., Gregor, N., Martin, G., Abrahamson, N. and Kircher, C. (1998). Reassessment
666 of site coefficients and near-fault factors for building code provisions, Technical Report Program

667 Element II: 98-HQGR-1010, Pacific Engineering and Analysis, El Cerrito, USA.

668 Silva, W.J. (1997). "Characteristics of vertical strong ground motions for applications to engineering
669 design." Proc. Of the FHWA/NCEER Workshop on the National Representation of Seismic
670 Ground Motion for New and Existing Highway Facilities, I.M. Friedland, M.S Power and R. L.
671 Mayes eds., Technical Report NCEER-97-0010.

672 Tsai, C.-C. P., and K.-C. Chen (2000). A model for the high-cut process of strong motion
673 accelerations in terms of distance, magnitude, and site condition: an example from the SMART 1
674 array, Lotung, Taiwan, *Bull. Seism. Soc. Am.* **90**, 1535-1542.

675 Van Houtte C., Drouet C. and F. Cotton (2011). Analysis of the origins of κ (Kappa) to compute hard
676 rock to rock adjustment factors for GMPEs, *Bull. Seism. Soc. Am.* **101**, 2926-2941.

677 Wessel, P., and W. H. F. Smith (1998). New, improved version of the Generic Mapping Tools
678 Released, *EOS Trans. AGU* **79**, 579.

679

680

681 AUTHORS' AFFILIATIONS, ADDRESSES

682

683 Olga-Joan Ktenidou:

684 ISTERre, Université de Grenoble 1, CNRS, F-38041 Grenoble, France

685 email: olga.ktenidou@ujf-grenoble.fr

686

687 Stephane Drouet :

688 Observatório Nacional, R. Gen. José Cristino, 77 - São Cristóvão, Rio de Janeiro, Brazil

689

690 Fabrice Cotton:

691 ISTERre, Université de Grenoble 1, CNRS, F-38041 Grenoble, France

692

693 Norman A. Abrahamson :

694 University of California, Berkeley, Department of Civil and Environmental Engineering, 447 Davis

695 Hall, Berkeley, California 94720, U.S.A.

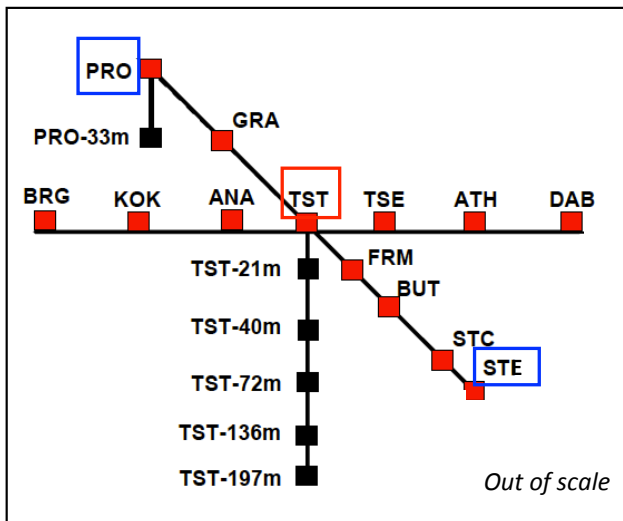
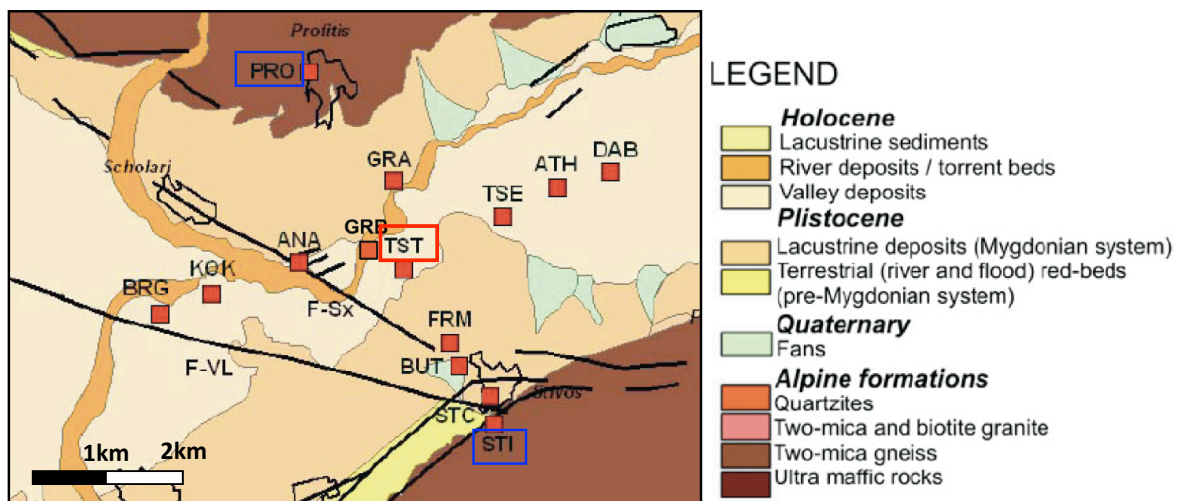


Figure 1. Layout of the 14 surface and 6 downhole accelerometers of the EUROSEISTEST array in plan (top) and cross-section (bottom). Blue marks the edges of the Profitis-Stivos cross-section, red marks TST borehole (adapted from Manakou et al., 2010).

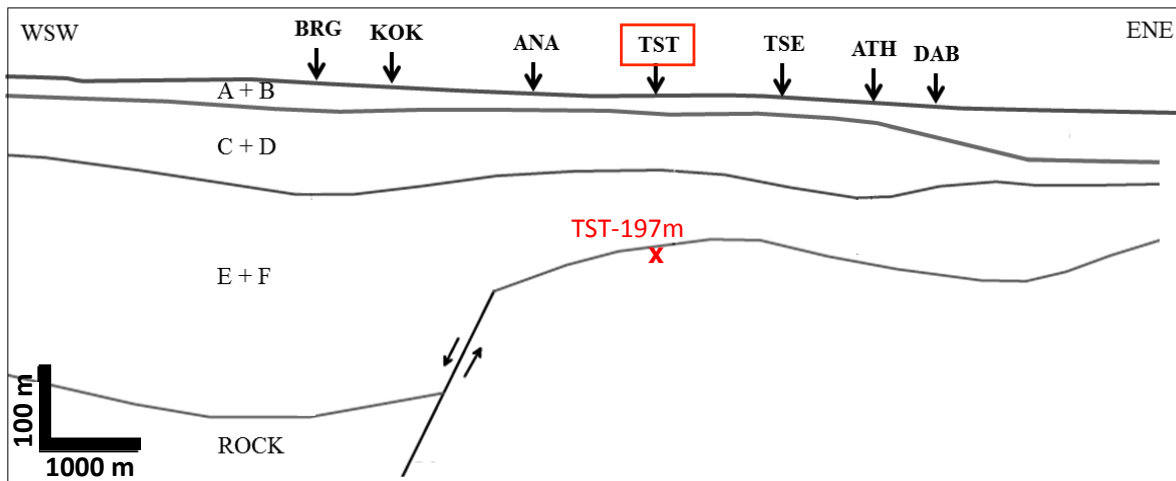
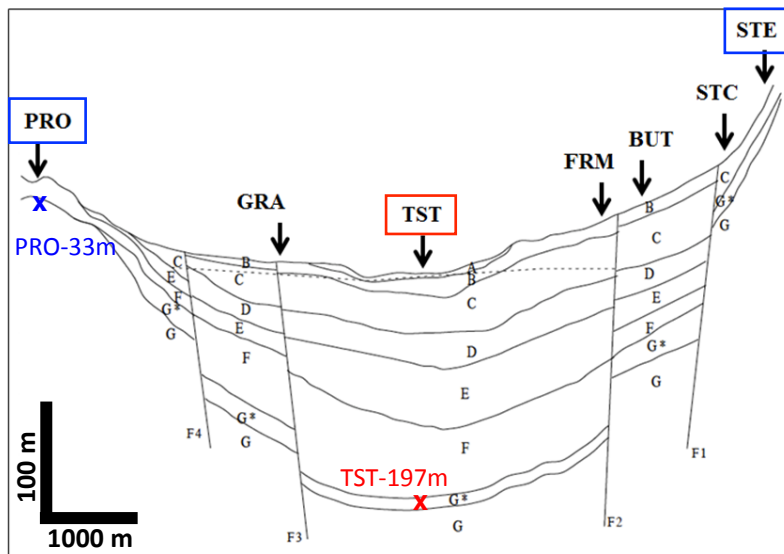


Figure 2. Geological cross-sections along the Profitis-Stivos axis (Raptakis et al., 2000, top) and in the perpendicular axis (Manakou et al., 2010, bottom). Location of surface and downhole sensors of TST borehole are marked in red.

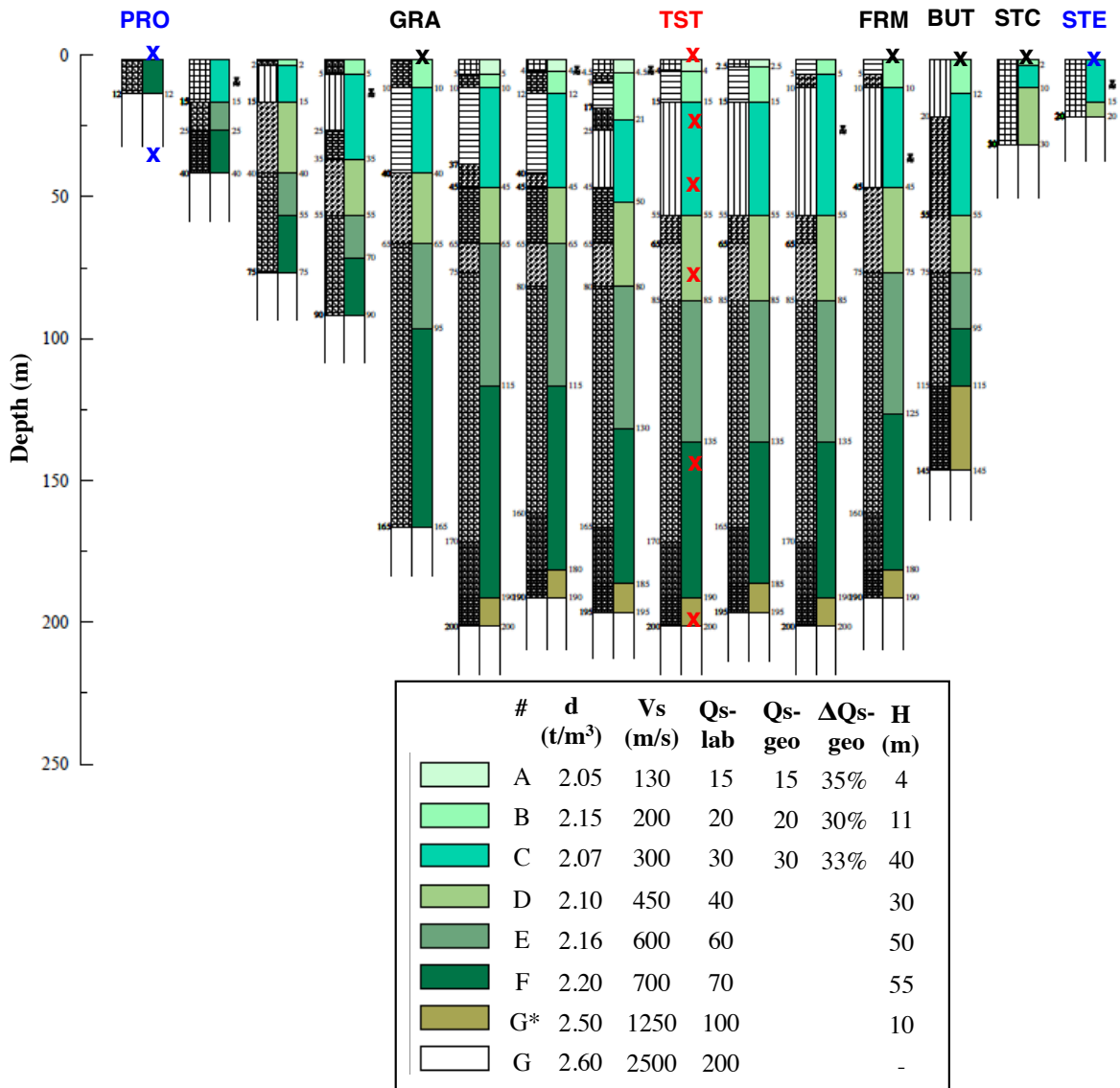


Figure 3. Indicative geotechnical and Vs profiles across the Profitis-Stivos section (adapted from Pitilakis et al., 1999). Crosses indicate the location of surface and downhole sensors. The table shows density, mean Vs, Qs from laboratory testing, and layer thickness at TST from Pitilakis et al. (1999), along with average Qs values and their scatter (ΔQs) from Jongmans et al. (1999).

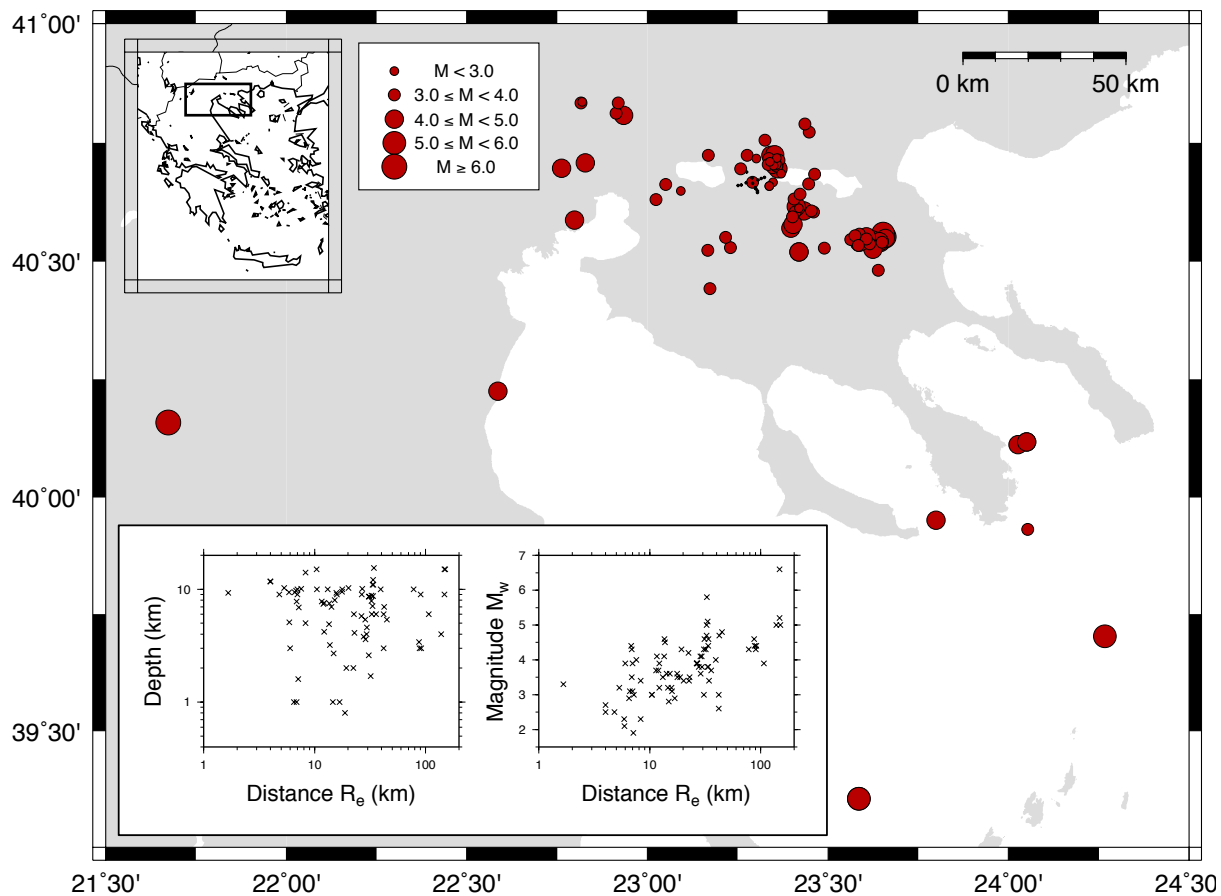


Figure 4. Epicentral distribution of events (red circles) and location of array (black dots near N40.45, E23.15). Also shown in inset: moment magnitude and depth of events versus epicentral distance (using TST as reference).

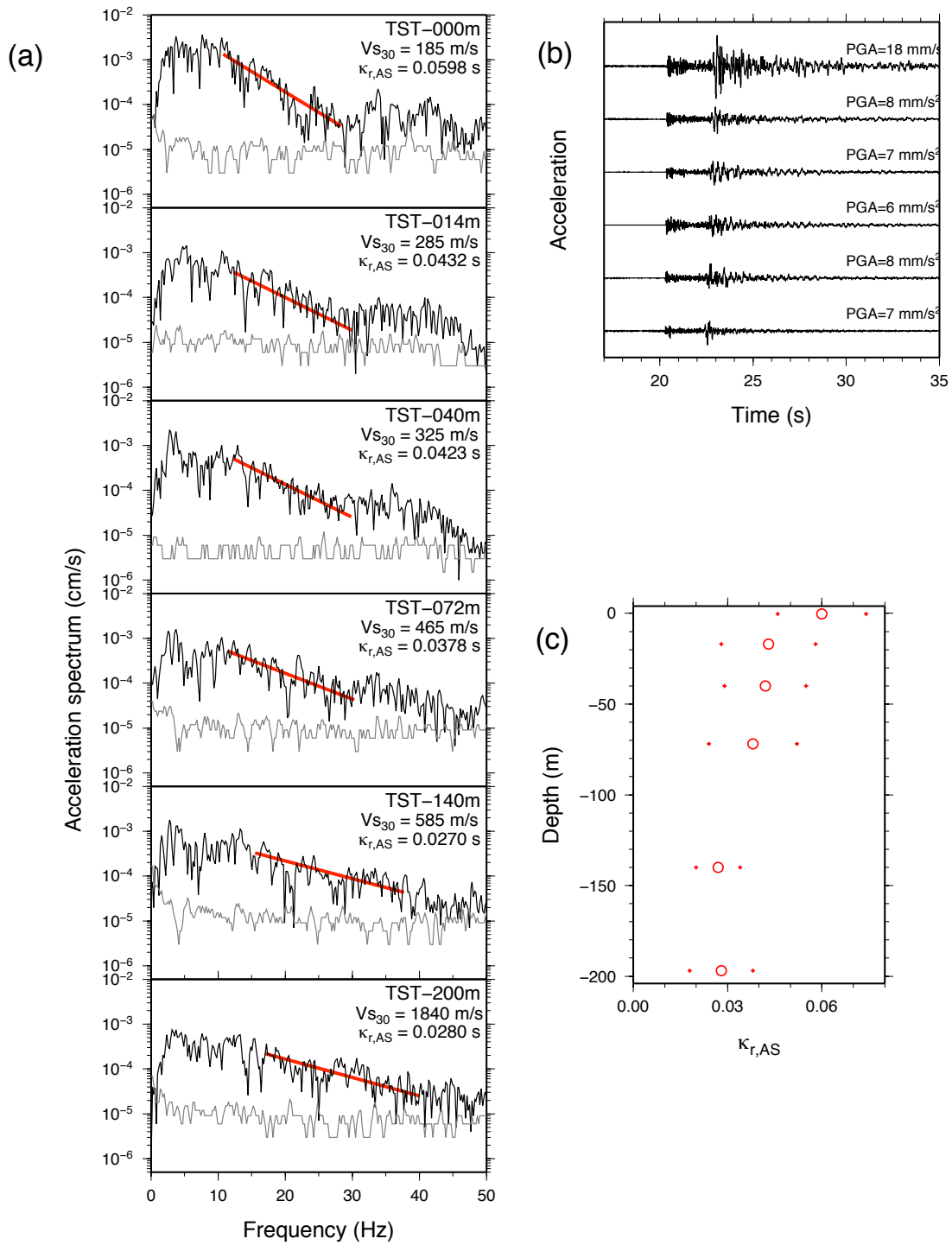


Figure 5. a. Example of the picking of f_1 and f_2 and $\kappa_{r,AS}$ measurement for a simultaneous earthquake (M3.9) recorded at all stations of the downhole array at TST. Noise spectrum plotted in grey, S-window in black, κ fit in red. b. The time histories of the records. c. The distribution of measured $\kappa_{r,AS}$ with sensor depth plotted with their uncertainties.

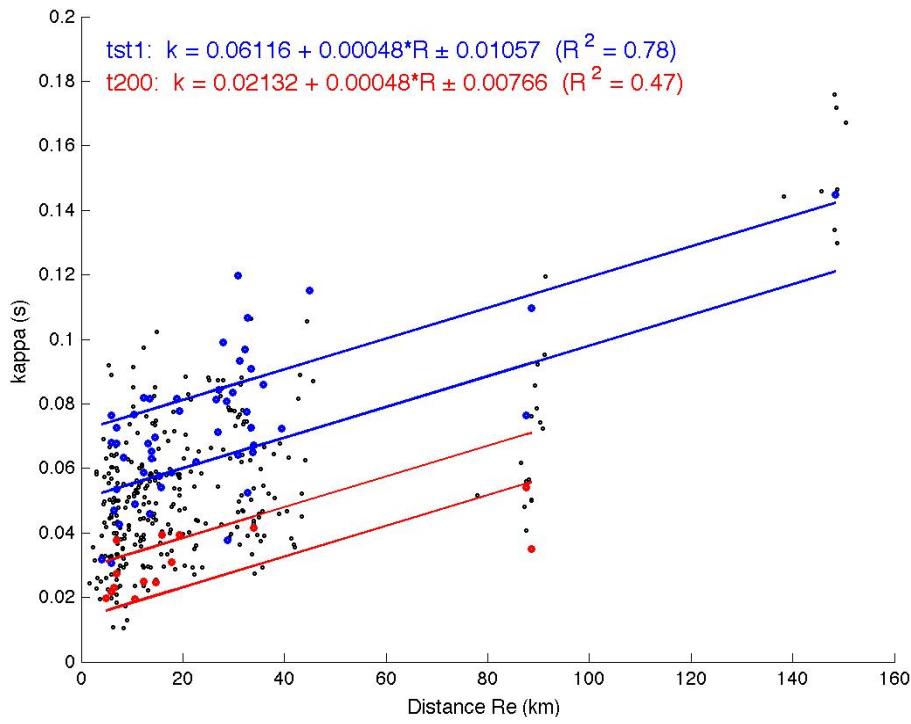


Figure 6. Distribution of individual $\kappa_{r,AS}$ values (black) and regression with distance for the surface (blue) and deepest sensor (red) of the TST borehole. Lines plotted for ± 1 standard deviation.

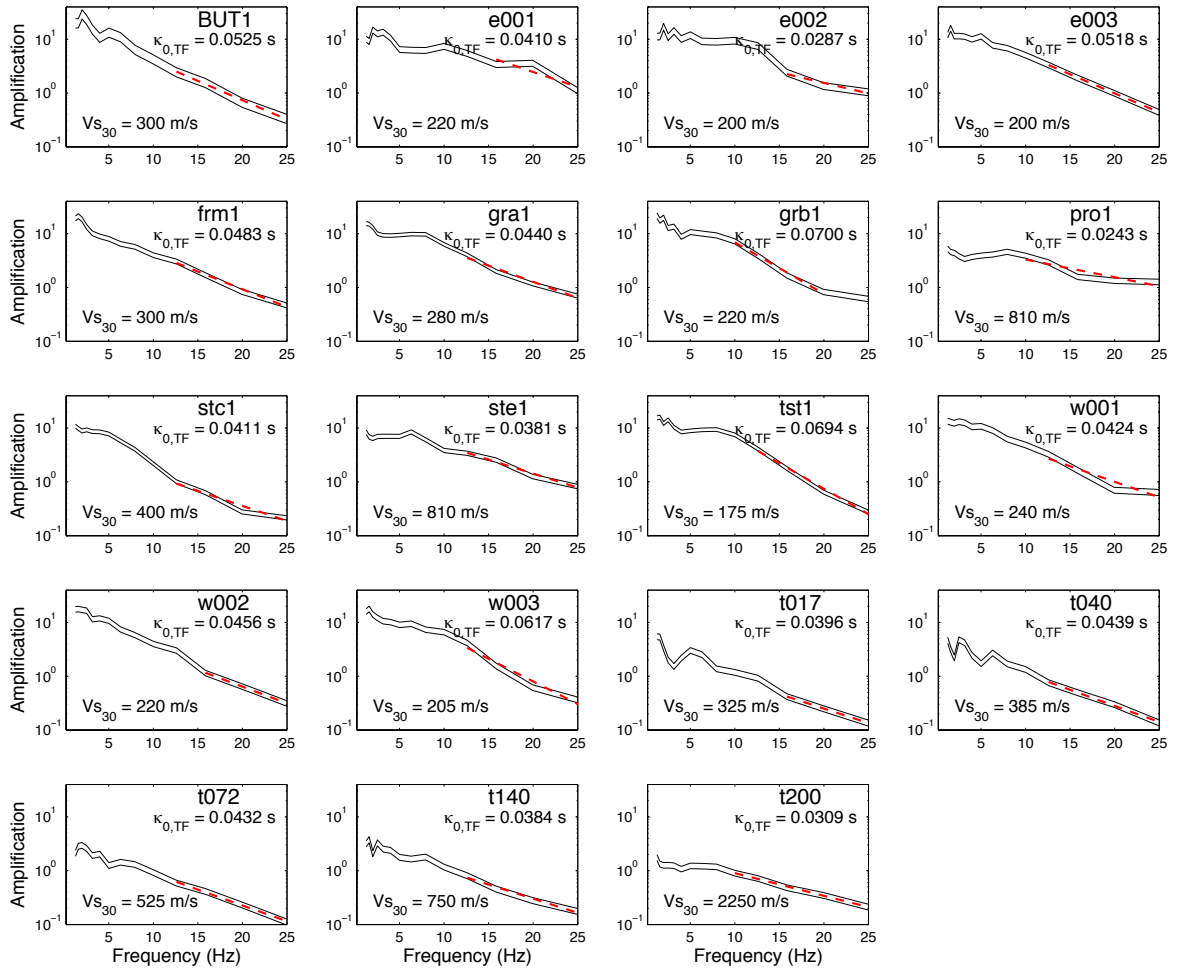


Figure 7. Site functions for all stations of the array (in black) and estimation of $\kappa_{0,TF}$ from their high-frequency part (in red).

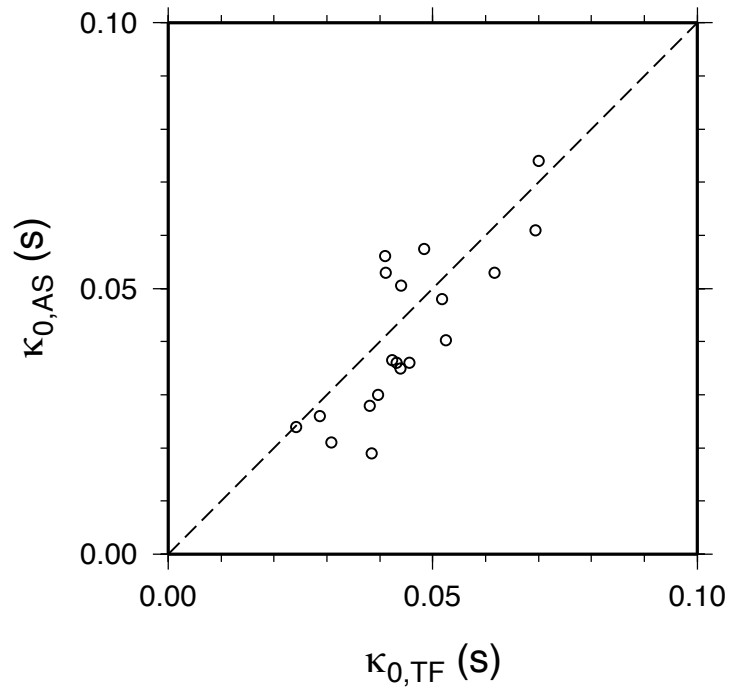


Figure 8. Correlation of κ_0 values using the two high-frequency approaches: the transfer function (TF) and the traditional approach (AS).

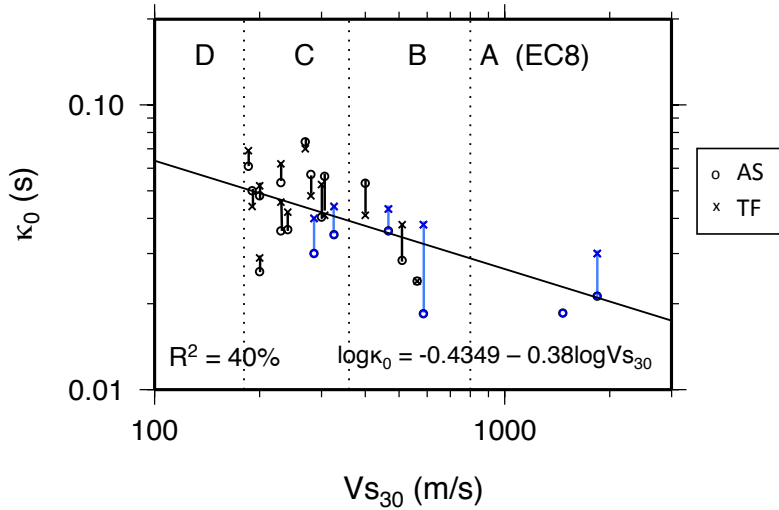


Figure 10. Correlation of κ_0 values with V_{s30} based on the two approaches (circles denote AS and crosses denote TF). Dotted lines indicate limits between EC8 site classes A through D. Downhole values are shown in blue and surface values in black. For each station, the vertical lines connect the results derived from the two approaches and are used to illustrate the epistemic uncertainty of κ_0 per site due to the method of measurement.

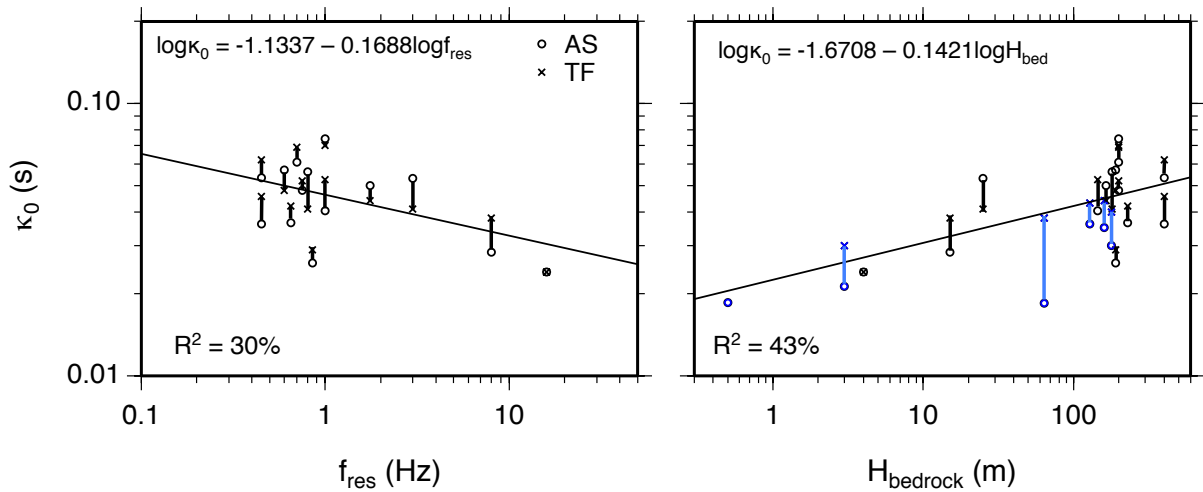


Figure 11. Correlation of κ_0 values with resonant frequency (left) and depth to bedrock (right). Circles denote AS and crosses denote TF method. Correlation coefficients are also shown. Blue indicates downhole stations. For each station, the vertical lines connect the results derived from the two approaches and are used to illustrate the epistemic uncertainty of κ_0 per site due to the method of measurement.

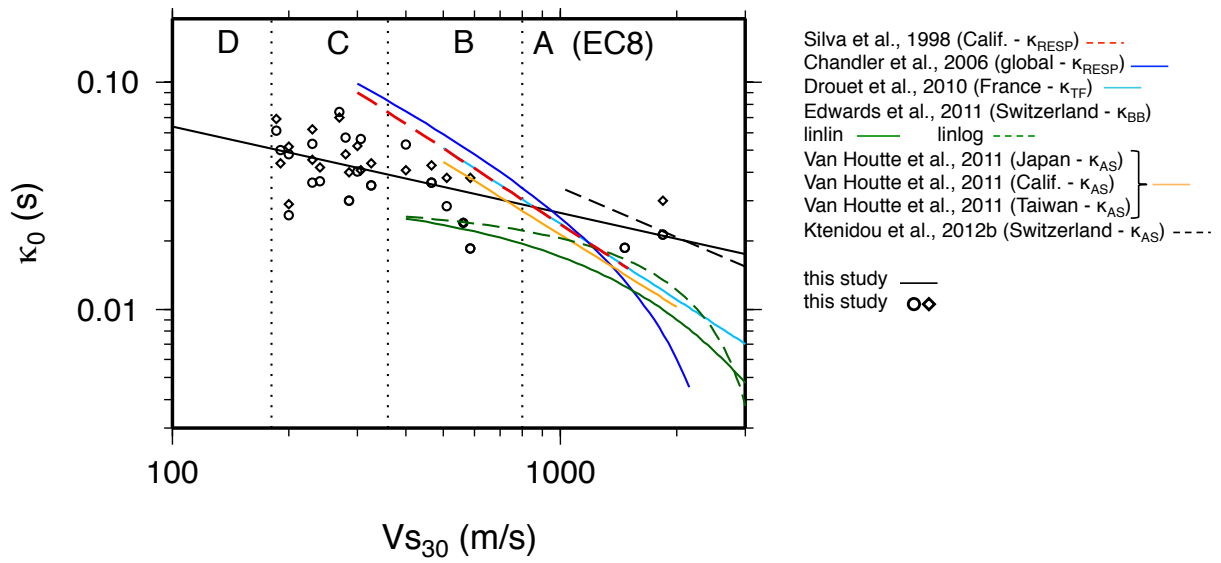


Figure 13. Correlations of κ_0 with V_{s30} : comparison of the results of this study with existing empirical correlations.

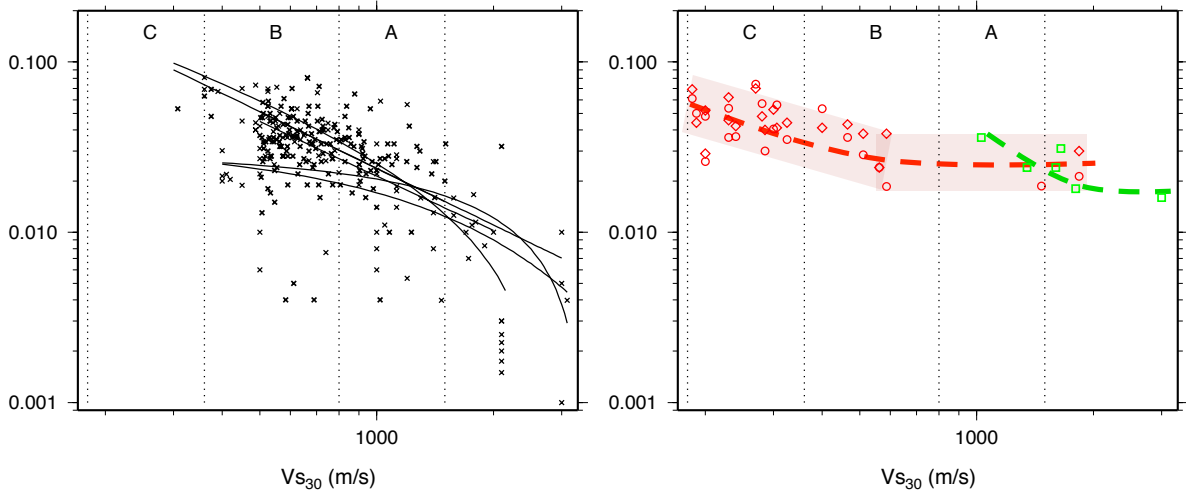


Figure 14. Left: Existing data and correlations, all showing a downward tendency for hard rock. Right: The alternative asymptotic functional form for correlations of κ_0 with V_{s30} , based on data from Euroseistest (red) and Switzerland (green), following solely the AS or TF measurement method.

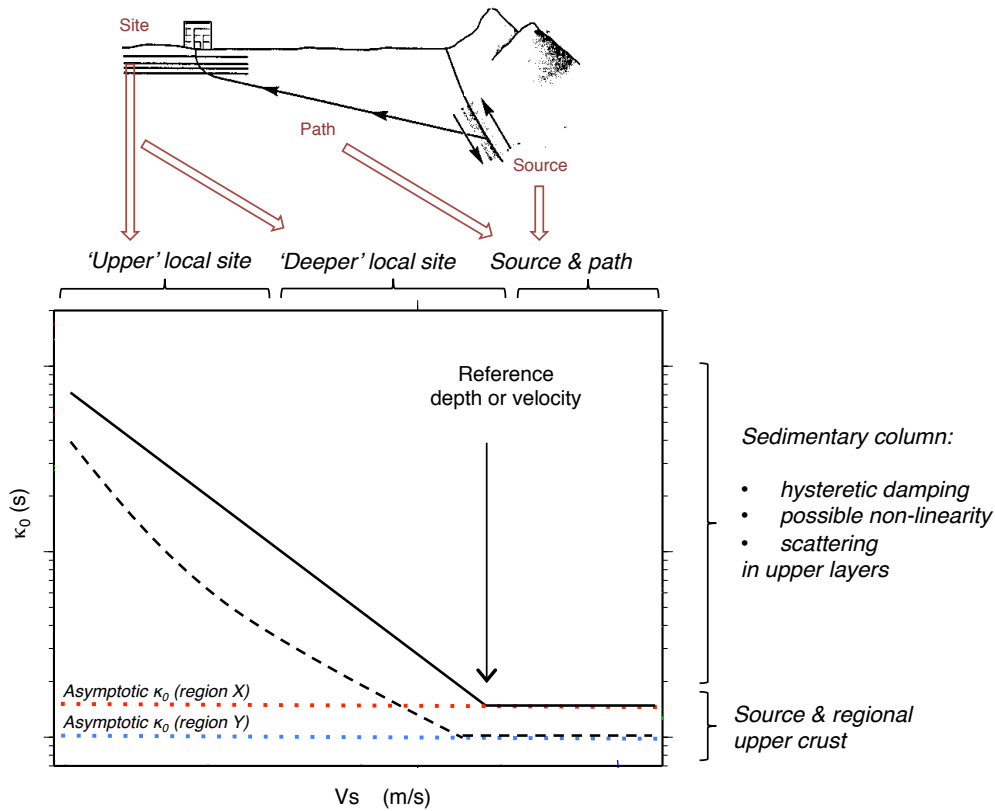


Figure 15. Example illustration of the possible regionalization of $\kappa_0 - V_{s30}$ correlation and description of the suggested underlying model. Regardless of the possible functional forms that the $\kappa_0 - V_{s30}$ relation may take depending on shallow and deeper local site properties (solid and dashed lines), we propose an asymptotic κ_0 value for very high V_s which will depend on the source and regional upper crust (dotted lines). The cartoon on top illustrates the contribution of source, path, deeper and shallower site components to κ_0 (adapted from Kramer, 1996).

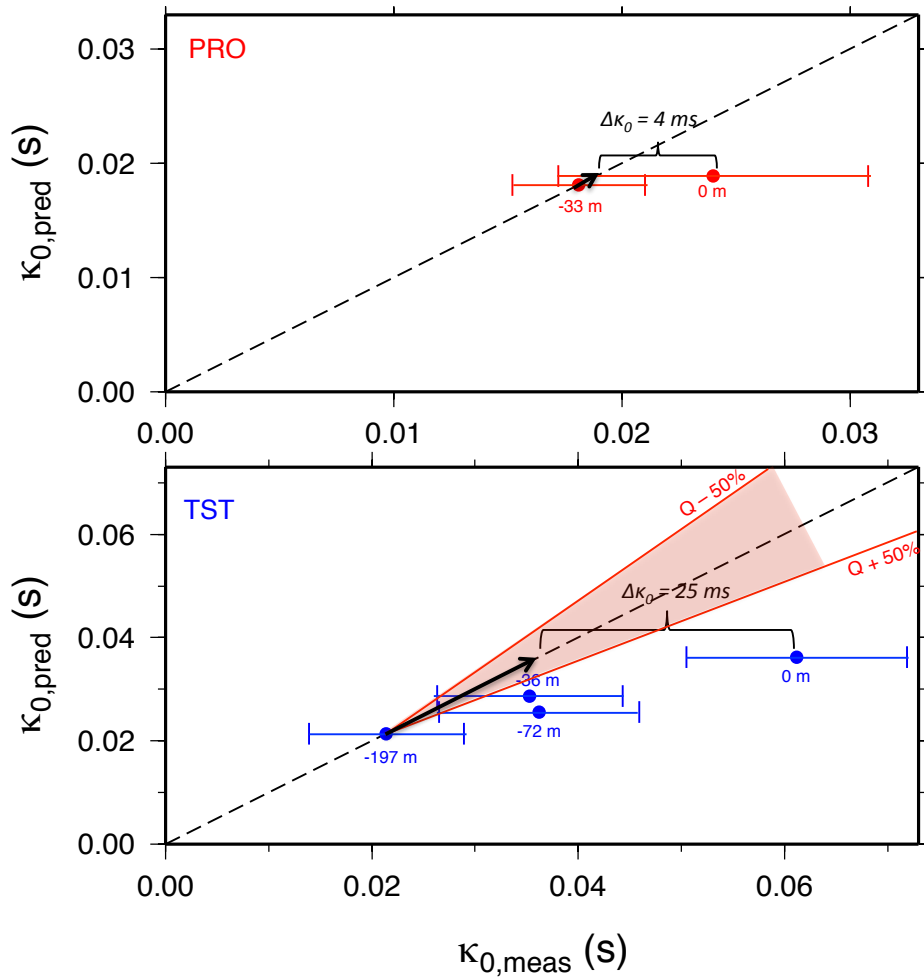


Figure 16. Predicted vs measured κ_0 values for each station in the PRO (above) and TST (below) boreholes (for TST we only show stations with more than 10 records). For the deepest downhole station the data points start on the diagonal. Nearing the surface, they move away from it, as measured κ_0 becomes larger than predicted. The error bars show uncertainty in κ_0 measurement. The light circles mark the final predicted κ_0 at the surface. $\Delta\kappa_0$ is measured between the measured and predicted surface κ_0 values. The shaded red area represents the epistemic uncertainty in predicted κ_0 due to Q uncertainty, computed for a 50% shift in Q over the entire profile.

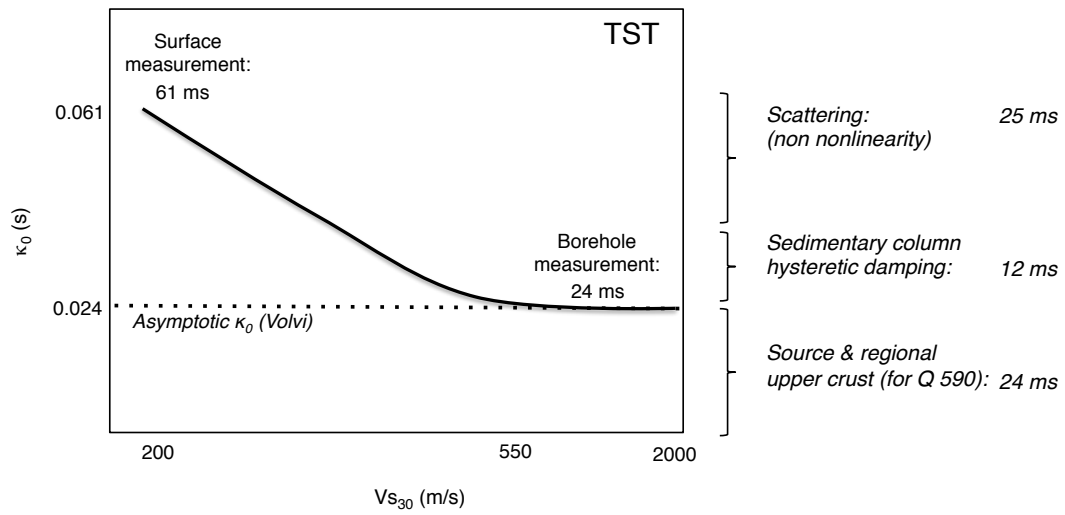


Figure 17. Schematic illustration of the contribution of the different attenuation components to the final measured κ_0 at the surface of TST site, according to the asymptotic κ_0 - V_{s30} model.

4. MEASURING KAPPA FOR LOW-SEISMICITY REGIONS

4.1 κ_0 estimates for hard rock SED stations in Switzerland using a high-frequency approach

Different groups of approaches have been identified for the measurement of κ_0 . The high-frequency group is based on the initial definition and measures kappa on the high-frequency decay of the data. Within the PEGASOS Refinement Project, κ_0 values were computed for the 6 hardest rock stations of the Swiss Seismological Service (SED), with V_{s30} values between 1000-3000 m/s. The task was performed using both groups of approaches. In this study we present results for the high-frequency approach. We use 1550 records of events with magnitudes 2.0-5.5 at distances out to 200 km. We are interested not only in the mean values of κ_0 at each station but also in their variability. Thus we follow 14 different 'scenarios', which are sub-scenarios of the same approach. Each one consists of different criteria in terms of frequency bands, event magnitudes, constraints on regional Q, etc., which are applied before treating individual kappa measurements and deriving overall site values. Thus we quantify the epistemic uncertainty stemming from the different choices made within a single approach. The between-scenario uncertainty can be larger than the within-scenario uncertainty, meaning that κ_0 depends on the choices we make in the computation process. The trade-off with Q is a determining factor in this process. For a single station, our κ_0 values can vary by a factor of 4. We find generally higher Q values than the current regional estimates. The overall scatter of the results across all stations is large, but we can see that κ_0 scales with V_{s30} , i.e. harder rock formations have lower κ_0 . However, when comparing our κ_0 results with predictions based on existing κ_0 - V_{s30} correlations we find they are generally higher. This supports previous notions that such correlations should be used separately according to regions and measurement methods and that site- or region-specific estimation of κ_0 may be preferable.

This chapter reports the work shown in publication A3, which is currently being expanded within publication J5 (see Annex). More results will be reported in the final deliverable when the work is finalised.

Kappa₀ (κ_0) estimates for hard rock SED stations in Switzerland using a high-frequency approach

Olga-Joan KTENIDOU, Chris VAN HOUTTE, Fabrice COTTON, Norman ABRAHAMSON³

AGU Fall Meeting, 13 Dec. 2013

Scope & Goals

At high frequencies the acceleration FAS decays rapidly. This attenuation is typically modeled by kappa, the S-wave spectral decay parameter introduced by Anderson and Hough (1984). Its site-specific, zero-distance component (kappa₀), is crucial in the creation and adjustment of GMPEs and in the simulation of ground motion for describing high-frequency ground motion. Different groups of approaches have been identified for the measurement of kappa₀ (Ktenidou et al., 2013): the high-frequency group is based on the initial definition and measures kappa on the high-frequency decay of the data, while the broadband group of approaches using the entire frequency band of the data to invert kappa, source and path parameters.

Within the PEGASOS Refinement Project, kappa₀ values were recently computed for the 9 hardest rock stations of the Swiss Seismological Service (SED), with Vs30 values between 1000-3000 m/s.

We aim to:

- compute site-specific κ (κ_0) for 6 of the hardest Swiss rock sites,
- evaluate the epistemic uncertainty in the results,
- understand the importance of the trade-off between κ_0 and whole-path regional attenuation (Q),
- compare with empirical Vs30 correlation predictions.

Study area & Dataset

We select 6 of the hardest rock stations in Switzerland (4 sites in the central part and 2 in the northern part), with Vs30 values ranging between 1000 and 3000 m/s. Our dataset comprises 1558 two-component records with magnitudes from 2 to 5.5, with half the data below M3.0 and 75% of the data below M2.5 (Figures 1,2). The stations are STS-2 velocimeters of the SED broadband network.

κ estimation method

Backbone method

Following its original definition by Anderson & Hough (1984), various methods are used to compute κ , including high-frequency and broadband approaches (Ktenidou et al., 2014). We follow a high-frequency approach based on the original definition (Ktenidou et al., 2013).

For each record we measure an individual value of κ_r on the S-wave acceleration Fourier spectrum. We work in a frequency band (df) that must be between the possible corner frequency, f_c (assuming stress parameter, $\Delta\sigma$, of 1-5 bars, Edwards and Faeh, 2013) and the highest usable frequency of the instrument response, which is 30 Hz, the corner of the anti-alias filter (Figure 3; see also Laurendeau et al. 2013).

κ_r (Figure 4) comprises site (κ_0) and regional (Q) attenuation. To get κ_0 we must separate the contribution of Q and extrapolate κ_r to zero distance. We work out to 200 km where data is ample. Based on the binning of κ_r with distance we assume a simple linear model (Figure 5), implying a frequency-independent Q over the df range. We assume the underlying Q structure is similar for all regions, so the linear model will have the same slope (b) for all stations.

Investigation of uncertainty

To decide which of the individual κ_r values will be accepted and used to regress κ_0 , we need a set of quality criteria for κ_r . The main considerations are:

- do we define a minimum spectral range (e.g., $df > 8$ Hz)?
- do we accept negative κ_r values as physically meaningful?
- do we set a threshold for the difference in the 2 horizontal components (e.g. $\Delta\kappa_r < 50\%$)
- do we remove small magnitude events (e.g. $M < 2.5$ or 3) to avoid the trade-off of κ_r with the source f_c if $\Delta\sigma > 5$ bars?

We are interested not only in the mean values of κ_0 at each station but also in their variability. In order to account for epistemic uncertainty we create several possible sets of criteria and investigate the effects that these choices may have on κ_0 (Table 2).

After selecting the data, we select two ways to regress with distance based on Q constraints:

- allowing the data to determine Q, and
- fixing Q to 1200: the value of the Swiss stochastic model (Edwards and Faeh, 2013).

Thus we follow 14 different ‘scenarios’, which are sub-scenarios of the same approach. This will allow us to evaluate the epistemic uncertainty stemming from the different choices made within a single approach, including the constraints of Q and its trade-off with κ .

Sensitivity and trade-offs

We have 14 combinations of κ_r criteria and Q constraints. Figure 6 shows results for one of the combinations. κ_0 values for the 6 sites correlate with V_{s30} . The large standard deviation means that without such a large dataset we cannot be confident of the mean.

Figure 7 shows the final values of κ_0 and Q for each combination (7 criteria sets and 2 Q constraints: free, or data-driven, and fixed to 1200). The data-driven analysis indicates that Q values between 15-30 Hz range from 1600-2400, with an average of 1900. This is higher than the currently used value of 1200, but in agreement with some other independent estimates.

The constraint on Q significantly affects κ_0 . Fixing Q to 1200 biases residuals with distances (Figure 9) and systematically underpredicts κ_0 . The range of κ_0 values generated from the two Q assumptions for the 7 criteria sets have little overlap. Figure 8 compares the range of κ_0 with existing estimates for the same stations, derived from broadband methods. The data-driven Q case yields κ_0 that mostly define an upper bound for existing values. The fixed Q case yields κ_0 that mostly define a lower bound. Together the 14 cases cover most of the range of existing κ_0 values.

Finally, we compare our results to existing κ_0 - V_{s30} data (Figure 10). Our range of values agrees more with κ_0 values derived from similar high-frequency methods (κ_{AS}), but correlations derived from other approaches may underpredict it.

Conclusions

We computed hard rock κ_0 with a high-frequency method. The large scatter in the computed values means that we need a large dataset for a reliable mean. We use various sets of criteria to capture epistemic uncertainty. We have 7 sets of criteria to assess κ_r quality. For a single station, our κ_0 values can vary by a factor of 2. We then consider 2 cases for constraining Q, and then the κ_0 per site varies up to 4. The data indicates higher Q values than currently used in the Swiss stochastic model: 1900 as opposed to 1200 (for frequency-independent Q at 15-30 Hz). There is significant trade-off between κ_0 and Q, and decision as to the Q constraint is important. The overall scatter of the results across all stations is large, but we can see that κ_0 scales with V_{s30} , i.e. harder rock formations have lower κ_0 . However, when comparing our κ_0 results with predictions based on existing κ_0 -

Vs30 correlations we find they are generally higher. This supports the notion that such correlations should be used separately according to regions and measurement methods. Correlations overall should be used with caution, and site- or region-specific measurement of κ_0 is preferable.

References

- Anderson and Hough (1984). A model for the shape of the Fourier amplitude spectrum of acceleration at high frequencies, BSSA 74(5).
- Edwards et al. (2011). Attenuation of seismic shear wave energy in Switzerland, GJI 185.
- Edwards and Fäh (2013). A Stochastic Ground-Motion Model for Switzerland, BSSA 103(1).
- Ktenidou et al. (2013). A study on the variability of kappa in a borehole: Implications of the computation method. BSSA 103(2a).
- Ktenidou et al. (2014). Taxonomy of kappa: a review of definitions and estimation methods targeted to applications, SRL 85(1).
- Laurendeau et al. (2013). Rock and stiff soil site Amplification: Dependency on Vs30 and kappa (κ_0), BSSA 103(6).
- PEGASOS Refinement Project (2012). Overview of available κ estimates for Switzerland as constraints for NPP specific κ values, PMT-TN-1221 Internal Report.

Acknowledgements

Data was provided by SED and is available at <http://www.seismo.ethz.ch/sed>. This research was funded by the Swiss Pegasos Refinement Project and the French Sigma Project. We thank Philippe Renault, PRP experts, Stella Arnaouti, and Mickael Langlais for discussions. A big thank you to the people who gave the scientific world SAC2008 (<http://www.iris.edu/software/sac>; Goldstein et al., 2003) and GMT v.3.4 (www.soest.hawaii.edu/gmt; Wessel & Smith, 1998).

Table 1. Station data.

Station	Vs30 (m/s)	Number of records
SULZ	1030	232
BALT	1350	243
HASI	1600	291
BNAP	1650	334
PLOS	1810	188
LLS	3000	270

Table 2. Sets of quality criteria for treating κr values

Criteria set #	Criteria	Approx. % of data
1	No criteria	100%
2	$df > 8$ Hz	98%
3	$df > 8$ Hz, $\kappa r > 0$	95%
4	$df > 8$ Hz, $\kappa r > 0$, $\Delta \kappa r < 50\%$	78%
5	$df > 8$ Hz, $\kappa r > 0$, $\Delta \kappa r < 50\%$, $M > 2.5$	45%
6	$df > 8$ Hz, $M > 3.0$	55%
7	$df > 8$ Hz, $M > 2.5$	24%

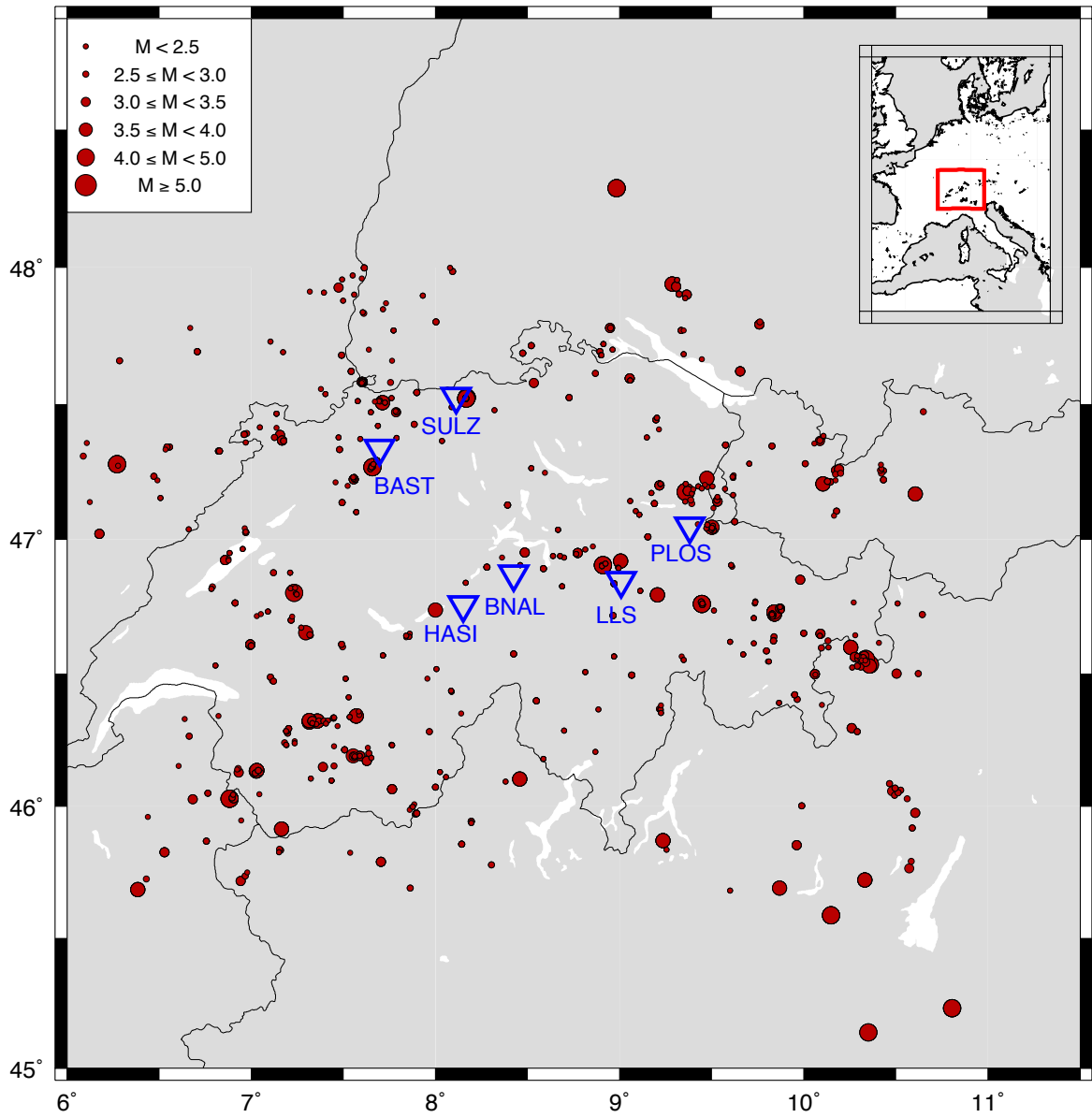


Figure 1. Station and epicentral distribution.

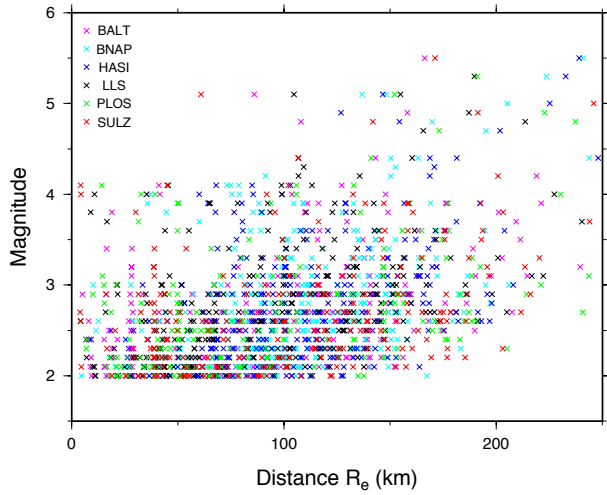


Figure 2. Magnitude-distance distribution.

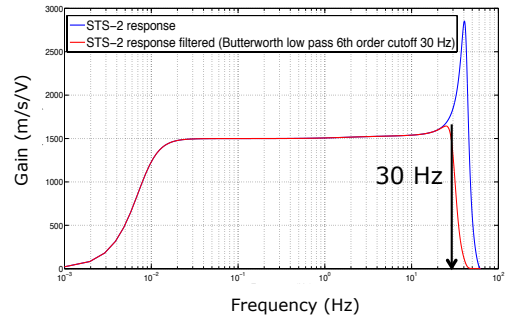


Figure 3. Instrument response and filter.

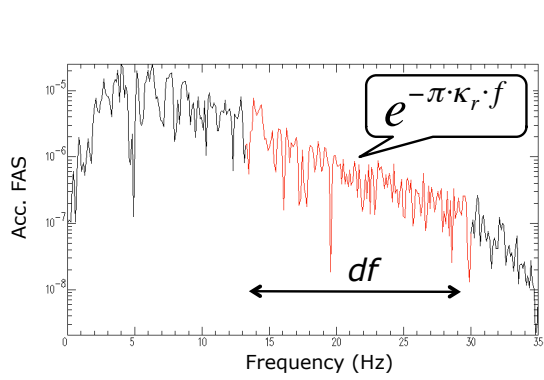


Figure 4. Example of individual κ_r estimation

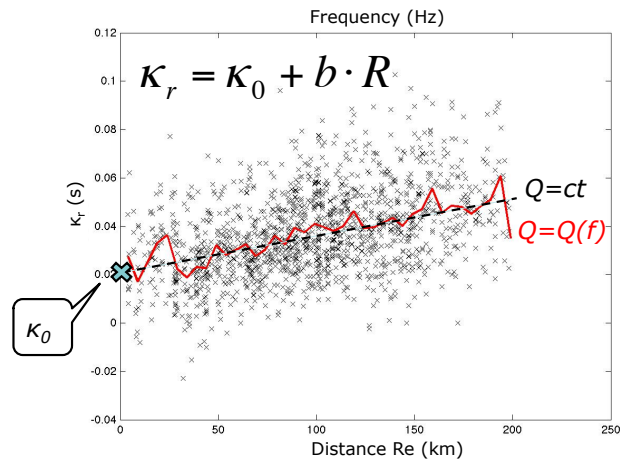


Figure 5. Distribution of κ_r with distance (red line: mean of 5-km bins).

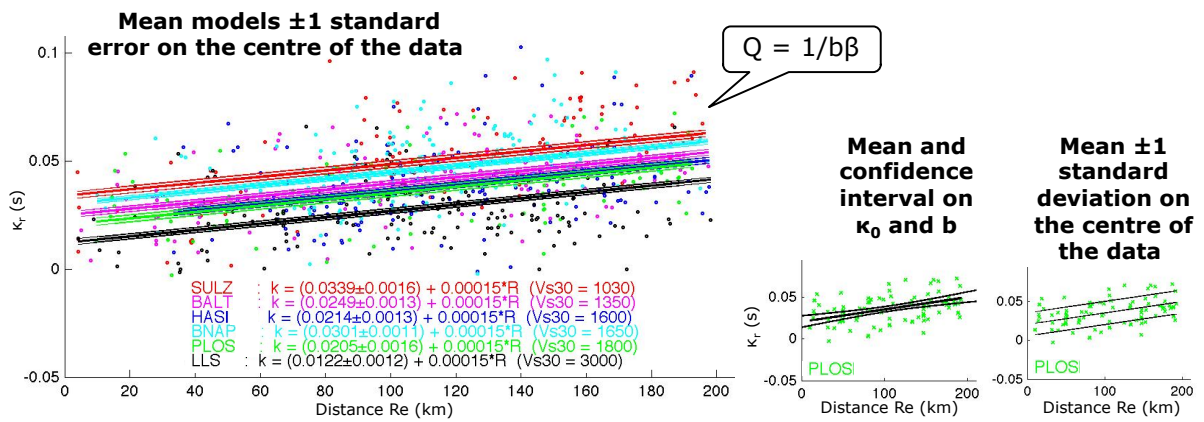


Figure 6. Example of mean κ models ± 1 standard error on κ_0 (left), 95% confidence interval (centre), and standard deviation (right).

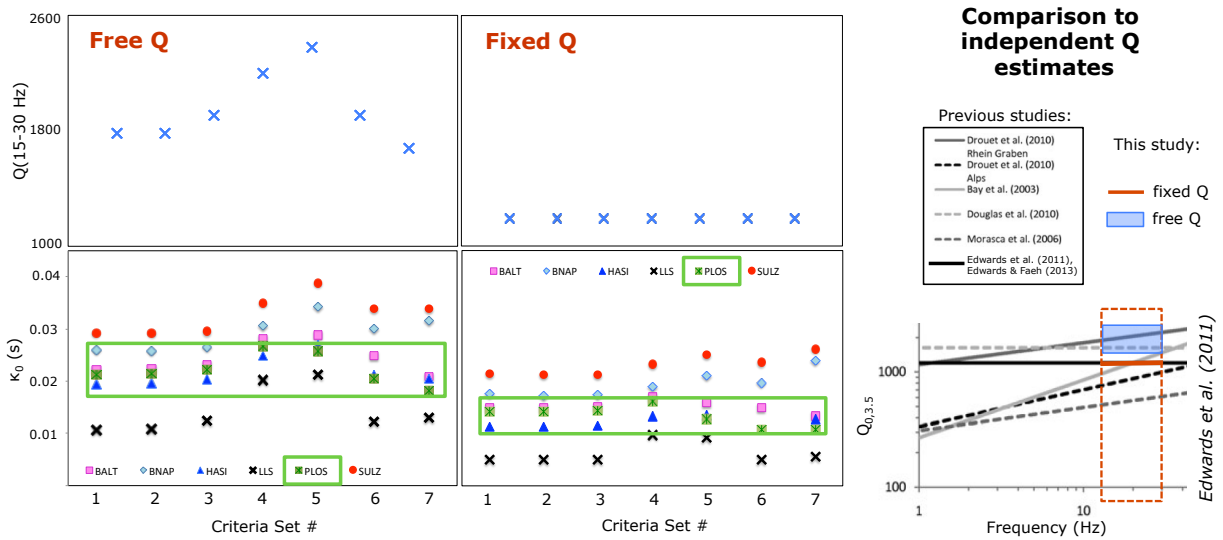


Figure 7. Values of κ_0 and Q for the 7 criteria sets (left). Comparison with existing Q models (right).

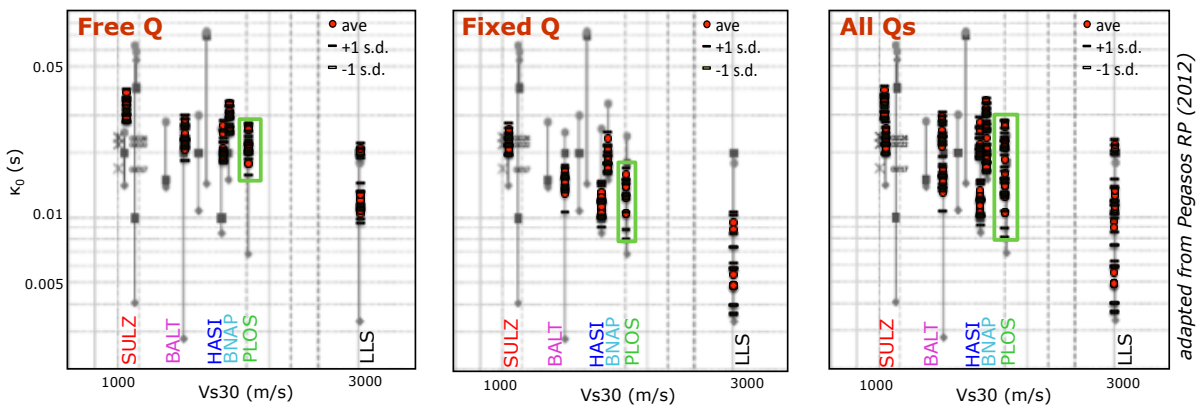


Figure 8. Comparison of κ_0 range for the 7 criteria sets with independent estimates for the same stations.

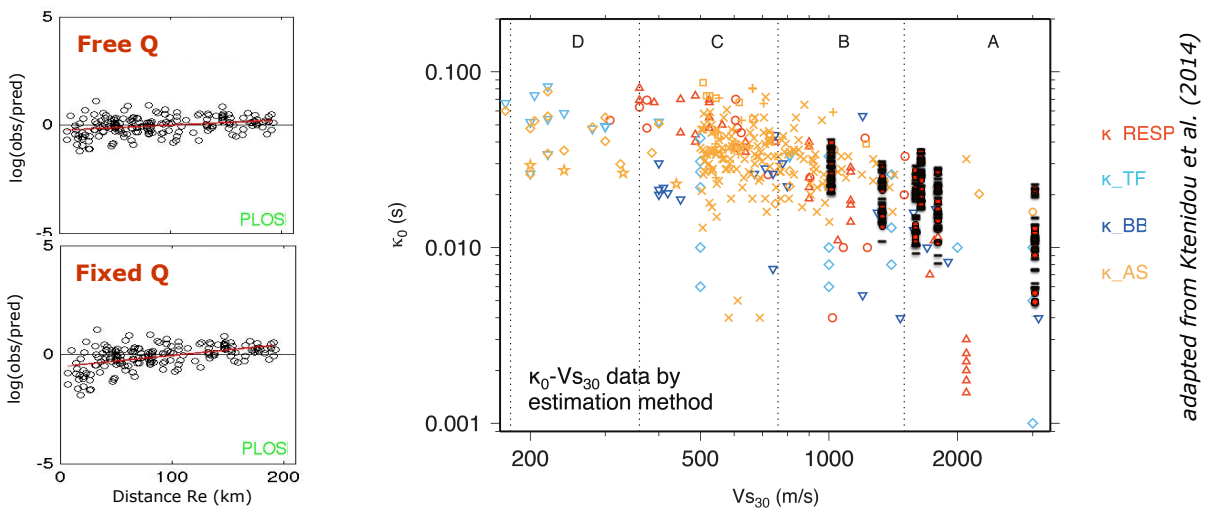


Figure 9. Example κ_r residuals with distance.

Figure 10. Comparison of results with existing κ_0 - Vs_{30} data.

Kappa₀ (κ₀) estimates for hard rock SED stations in Switzerland using a high-frequency approach

Olga-Joan KTENIDOU¹, Chris VAN HOUTTE², Fabrice COTTON¹, Norman ABRAHAMSON³

1. ISTerre, Université Joseph Fourier, CNRS, Grenoble, France & PEER, University of California, Berkeley
olga.ktenidou@ujf-grenoble.fr

2. Department of Civil Engineering, University of Auckland, New Zealand

3. Department of Civil & Environmental Engineering, University of California, Berkeley



Scope & Goals

- We use data from broadband stations of the Swiss Seismological Service to study κ, the high-frequency decay parameter of Anderson & Hough (1984). We aim to:
- compute site-specific κ (κ₀) for 6 of the hardest Swiss rock sites,
 - evaluate the epistemic uncertainty in the results,
 - understand the importance of the trade-off between κ₀ and whole-path regional attenuation (Q),
 - compare with empirical Vs₃₀ correlation predictions.

Study area & Dataset

We select 6 of the hardest rock stations in Switzerland (4 sites in the central part and 2 in the northern part), with Vs₃₀ values ranging between 1000 and 3000 m/s. Our dataset comprises 1558 two-component records with magnitudes from 2 to 5.5, with half the data below M3.0 and 75% of the data below M2.5 (Fig. 1). The stations are STS-2 velocimeters of the SED broadband network.

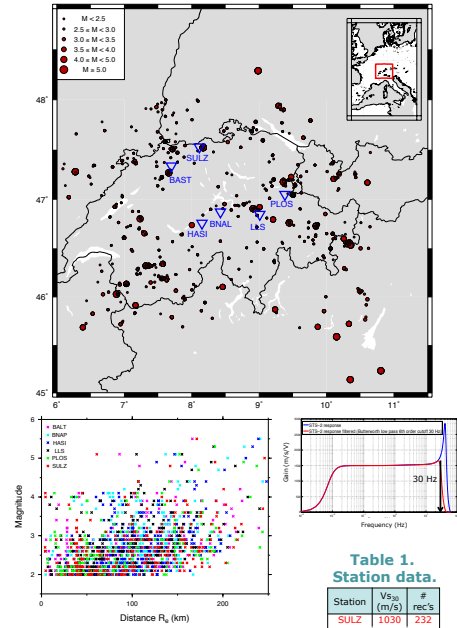


Table 1. Station data.

Station	Vs ₃₀ (m/s)	# rec's
SULZ	1030	232
BALT	1350	243
HASI	1600	291
BNAP	1650	334
PLDS	1810	188
LLS	3000	270

Figure 1. Station and epicentral distribution; distance-magnitude distribution; instrument response before and after LP filtering at 30 Hz.

κ estimation method

Backbone method
 Following its original definition by Anderson & Hough (1984), various methods are used to compute κ, including high-frequency and broadband approaches (Ktenidou et al., 2014). We follow a high-frequency approach based on the original definition (Ktenidou et al., 2013, Figure 2). For each record we measure an individual value of κ₀ on the S-wave acceleration Fourier spectrum. We work in a frequency band (df) that must be between the possible corner frequency, f_c (assuming stress parameter, Δσ, of 1-5 bars, Edwards and Faeh, 2013) and the highest usable frequency of the instrument response (30 Hz, the corner of the anti-alias filter, Fig. 1, see also: Laurendeau et al. 2013). κ₀ comprises site (κ₀) and regional (Q) attenuation. To get κ₀ we must separate the contribution of Q and extrapolate κ₀ to zero distance. We work out to 200 km where data is ample. Based on the binning of κ₀ with distance we assume a simple linear model (implying a frequency-independent Q over the df range). We assume the underlying Q structure is similar for all regions, so the linear model will have the same slope (b) for all stations.

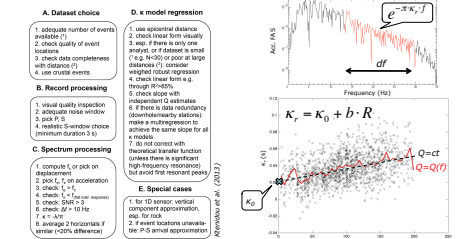


Figure 2. Outline of high-frequency κ approach, example of individual κ estimation, and distribution of κ₀ with distance (red line: mean of 5-km bins).

Investigation of uncertainty
 To decide which of the individual κ₀ values will be accepted and used to regress κ₀, we need a set of quality criteria for κ₀. The main considerations are:

- do we define a minimum spectral range (e.g., df>8 Hz)?
- do we accept negative κ₀ values as physically meaningful?
- do we set a threshold for the difference in the 2 horizontal components (e.g. Δκ₀<50%)
- do we remove small magnitude events (e.g. M<2.5 or 3) to avoid the trade-off of κ₀ with the source f_c if Δσ>5 bars?

In order to account for epistemic uncertainty we create several possible sets of criteria and investigate the effects that these choices may have on κ₀ (Table 2).

Table 2. Sets of quality criteria for treating κ₀ values.

Criteria set #	Criteria	Approx % of data
1	No criteria	100%
2	df>8 Hz	98%
3	df>8 Hz, κ ₀ >0	95%
4	df>8 Hz, κ ₀ >0, Δκ ₀ <50%	78%
5	df>8 Hz, κ ₀ >0, Δκ ₀ <50%, M>2.5	45%
6	df>8 Hz, M>3.0	55%
7	df>8 Hz, M>2.5	24%

After selecting the data, we select two ways to regress with distance based on Q constraints:

- allowing the data to determine Q, and
- fixing Q to 1200: the value of the Swiss stochastic model (Edwards and Faeh, 2013).

This will allow us to evaluate the epistemic uncertainty in Q and its trade-off with κ.

Sensitivity and trade-offs

We have 14 combinations of κ₀ criteria and Q constraints. Figure 3 shows results for one of the combinations. κ₀ values for the 6 sites correlate with Vs₃₀. The large standard deviation means that without such a large dataset we cannot be confident of the mean.

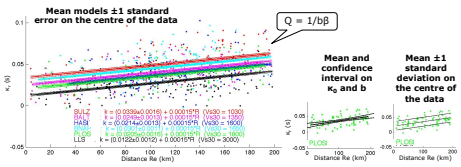


Figure 3. Example of mean κ models ±1 standard error on κ₀, 95% confidence interval and standard deviation.

Figure 4 shows the final values of κ₀ and Q for each combination (7 criteria sets and 2 Q constraints: free, or data-driven, and fixed to 1200). The data-driven analysis indicates that Q values between 15-30 Hz range from 1600-2400, with an average of 1900. This is higher than the currently used value of 1200, but in agreement with some other independent estimates.

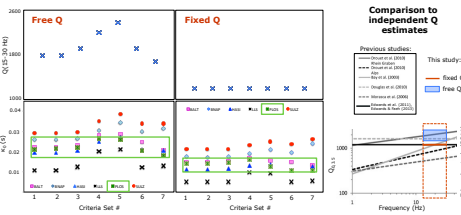


Figure 4. Values of κ₀ and Q for the 7 criteria sets (left). Comparison with existing Q models (right).

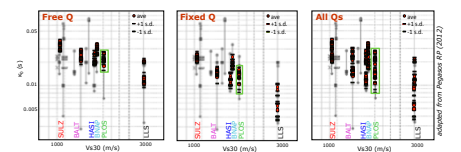


Figure 5. Comparison of κ₀ range for the 7 criteria sets with independent estimates for the same stations.

The constraint on Q significantly affects κ₀. Fixing Q to 1200 biases residuals with distances (Figure 6) and systematically underpredicts κ₀. The range of κ₀ values generated from the two Q assumptions for the 7 criteria sets have little overlap. Figure 5 compares the range of κ₀ with existing estimates for the same stations, derived from broadband methods. The data-driven Q case yields κ₀ that mostly define an upper bound for existing values. The fixed Q case yields κ₀ that mostly define a lower bound. Together the 14 cases cover most of the range of existing κ₀ values.

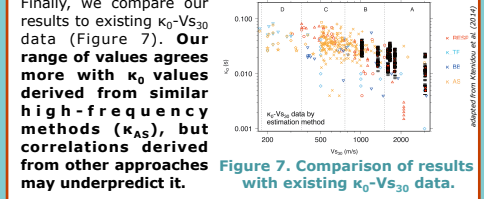


Figure 6. κ₀ residuals with distance.

Finally, we compare our results to existing κ₀-Vs₃₀ data (Figure 7). Our range of values agrees more with κ₀ values derived from high-frequency methods (κAS), but correlations derived from other approaches may underpredict it.

Conclusions

- We computed hard rock κ₀ with a high-frequency method.
- Large scatter → need large dataset for a reliable mean.
- Various sets of criteria to capture epistemic uncertainty.
- 7 sets of criteria for κ₀ quality → κ₀ per site varies up to 2.
- With 2 cases of Q constraint → κ₀ per site varies up to 4.
- Data indicates higher Q value than currently used: 1900 as opposed to 1200 (frequency-independent at 15-30 Hz).
- Significant trade-off between κ₀ and Q → the Q constraint is important!
- Empirical κ₀-Vs₃₀ correlations, even regional, may underpredict κ₀ if they are derived from different (e.g. broadband) methods → use correlations with caution!

References
 • Anderson and Hough (1984). A model for the shape of the Fourier amplitude spectrum of acceleration at high frequencies. BSSA 74(5).
 • Edwards et al. (2011). Attenuation of seismic shear wave energy in Switzerland, GJI 185.
 • Edwards and Fäh (2013). A Stochastic Ground-Motion Model for Switzerland, BSSA 103(1).
 • Ktenidou et al. (2013). A study on the variability of kappa in a borehole: Implications of the computation method. BSSA 103(2a).
 • Ktenidou et al. (2014). Taxonomy of kappa: a review of definitions and estimation methods targeted to applications. BSSA 103(1).
 • Laurendeau et al. (2013). Rock and stiff soil site Amplification: Dependency on Vs₃₀ and kappa (κ₀). BSSA 103(6).
 • PEGASOS Refinement Project (2012). Overview of available κ estimates for Switzerland as constraints for NPP specific κ values, PMT-TN-1221 Internal Report.

Acknowledgements
 Data was provided by SED and is available at <http://www.seismo.ethz.ch/seed>. This research was funded by the Swiss Pegasos Refinement Project and the French Sigma Project. We thank Philippe Renaud, PRP experts, Stélie Arnoult, and Mickael Langlais for discussions. A big thank you to the people who gave the scientific world SAC2008 (<http://www.ins.edu/software/sac>; Goldstein et al., 2003) and GMT v.3.4 (<http://www.soest.hawaii.edu/gmt>; Wessel & Smith, 1998).

4.2 Measuring κ in Arizona from the Transportable Array

We present a case where the seismicity and instrument characteristics render κ measurement a challenge. Our site is located in a low seismicity region (Southern Arizona). The available seismic records are few and often noisy. They come from distances between 10-300 km, which makes the trade-off between site and path attenuation significant. The event magnitudes (M1.2-M3.4) are rather low for the classic κ estimation method to be used. The stress drop values from different studies in the region vary greatly (1-50 bar), leading to large uncertainty in the source corner frequencies. Hence κ should be measured ideally above 10 Hz (above M3) or 20 Hz (below M2) to avoid trade-offs. Possible high-frequency resonances due to shallow soil layers may also interfere with the measurement. However, because our data come from the Transportable Array, the low sampling rate limits the maximum usable frequency to 16 Hz. This allows us very little bandwidth to resolve source, path, and site effects and constrain κ_0 . We use three measurement approaches (above the corner frequency, below it, and across the entire frequency range) to define upper and lower bounds for κ_0 in Southern Arizona, as well as estimates of regional Q and stress drop. The TA has greatly increased the available dataset for North America and, in certain low-seismicity regions, represents the majority of available seismic records at short distances. The severe obstacles faced in this study will be relevant in future κ studies in other regions with such band-limited data. We believe that an increase in the sampling rate of the TA would help avoid them.

This chapter reports the work shown in publication A4, which is currently being expanded within publication R2 (see Annex). More results will be reported in the final deliverable when the work is finalised.



Squeezing kappa out of the Transportable Array: when the going gets tough

O.-J. Ktenidou, T. Kishida, W. Silva,
R. Darragh, N. Abrahamson, F. Cotton

SSIM 2 May, 2014 1

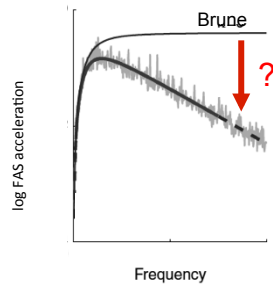
Overview

- Intro
- Goal
- Problem
- Solution
- Conclude + complain

SSIM 2 May, 2014 2

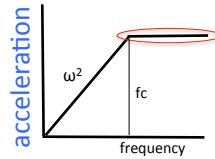
Intro

What is κ ?



How do we measure it?

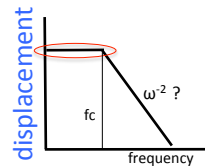
K_{AS}



large M
above f_c

Anderson & Hough (1984)

K_{DS}
(K_{mini})



small M
below f_c

Biasi & Smith (2001)

K_{AS_r}

K_{AS_0}

Anderson (1991)

$$K = K_0 + \kappa(R)$$

'site' 'régional'

K_{DS_r}

K_{DS_0}

Kramer (1996)

SSIM 2 May, 2014

5

K_{BB}

...from broadband inversions

Anderson & Humphrey (1991), Silva et al. (1996), ...

Fourier Amplitude (cm/s)

Frequency (hz)

$M=1.63, D=44.7\text{km}$

Fit the entire spectrum to the PSSM

Get a set of parameters:

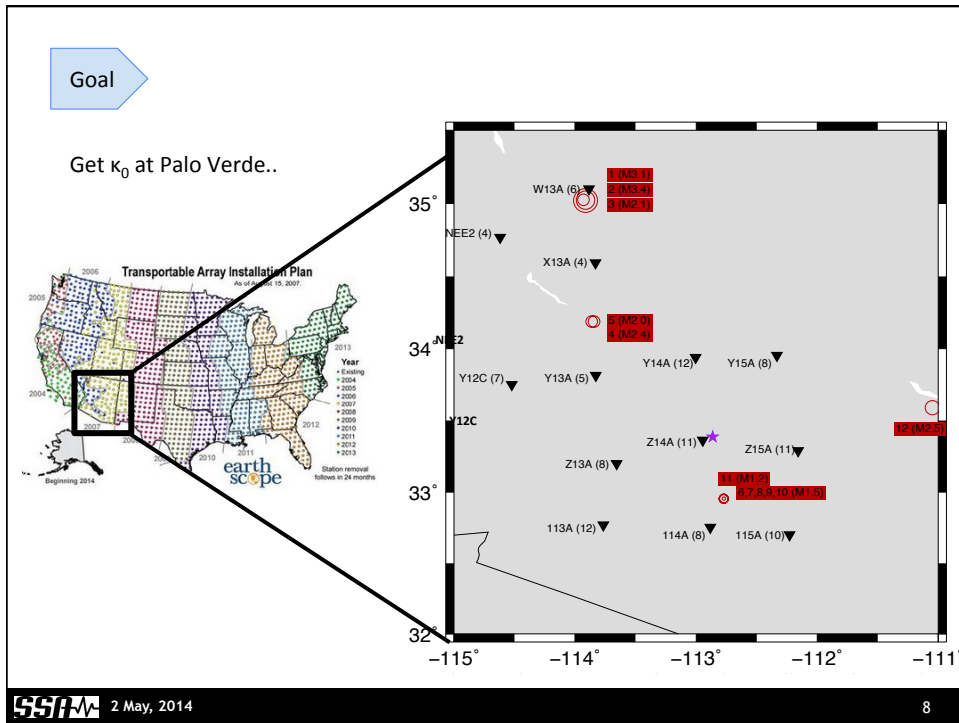
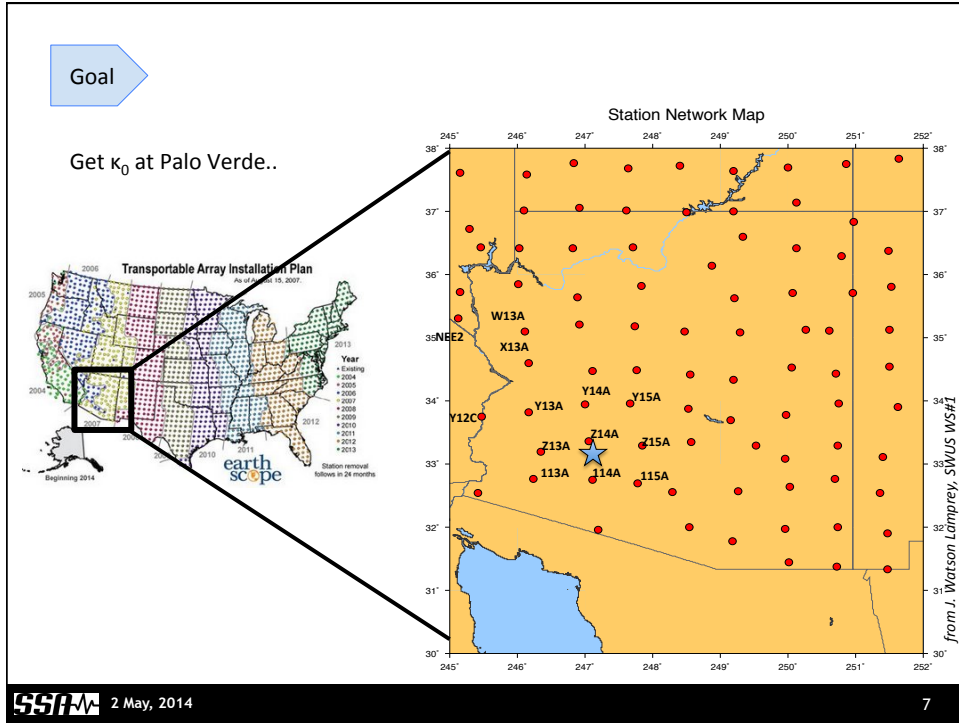
$\Delta\sigma, \kappa, Q(f)=Q_0 f^n$

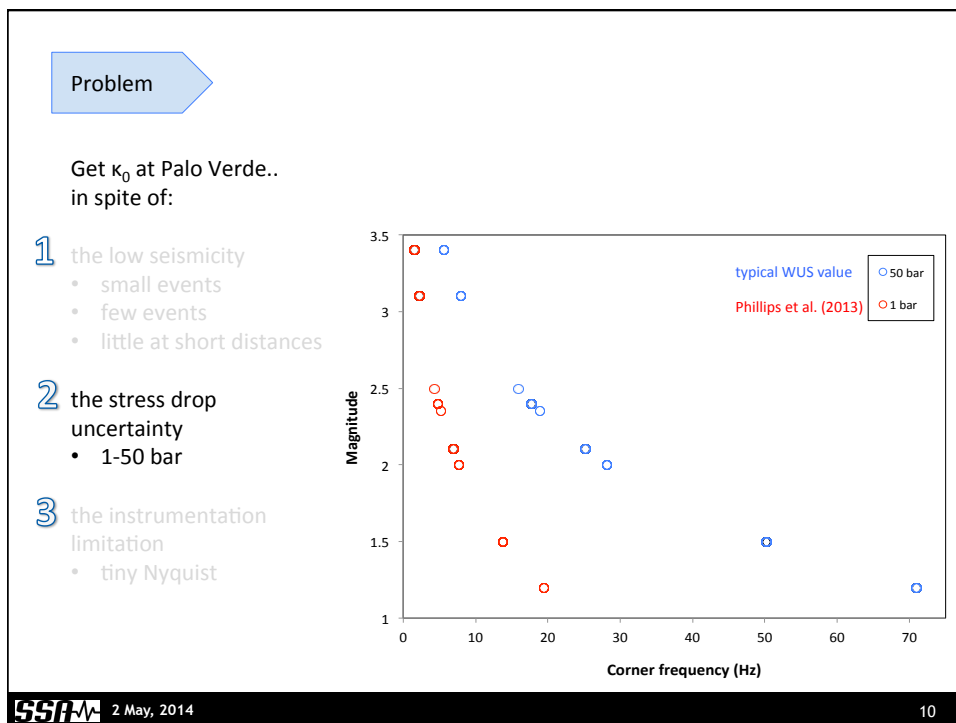
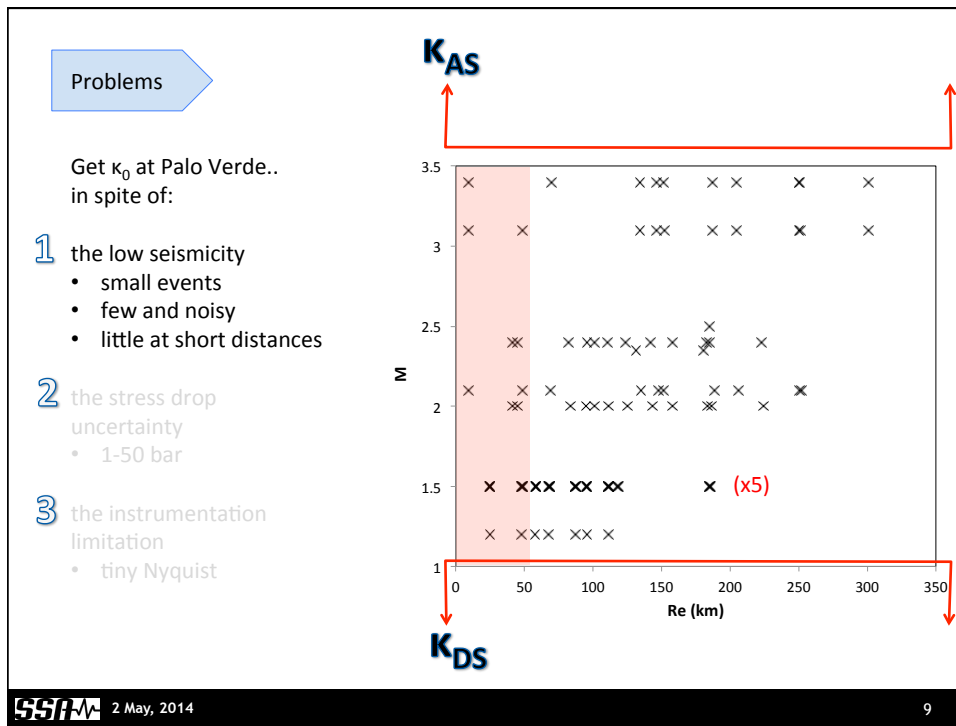
and amplification!

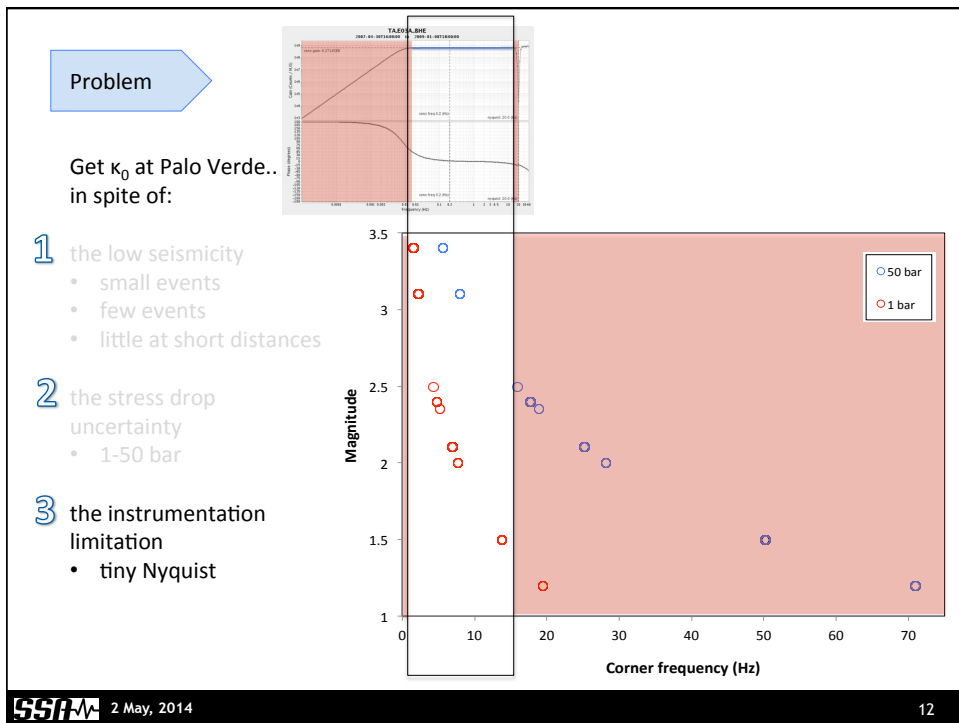
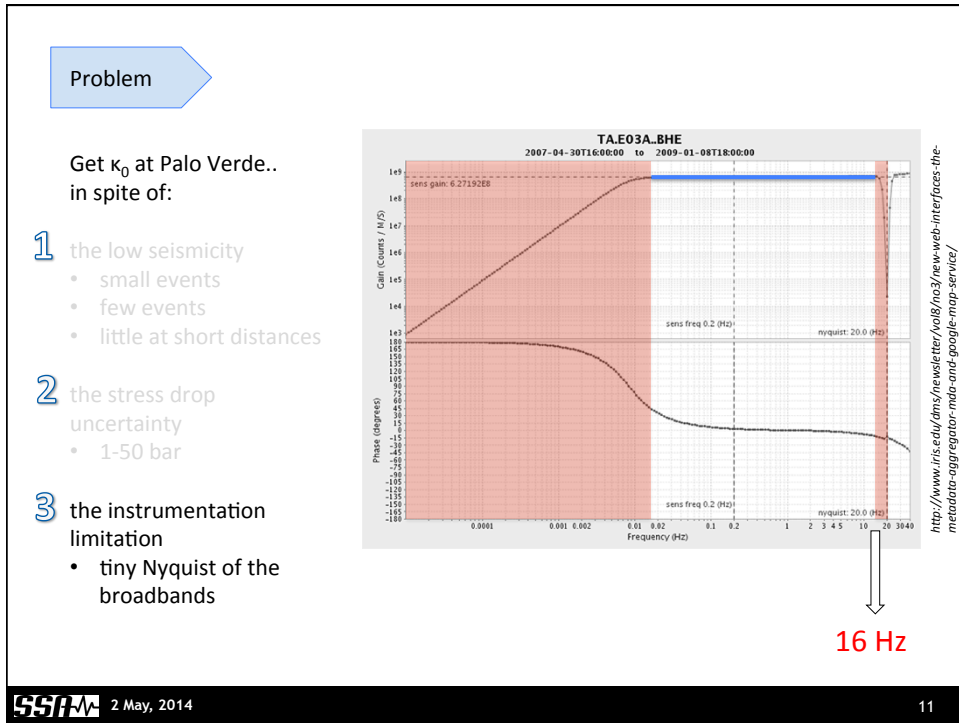
SSIM 2 May, 2014

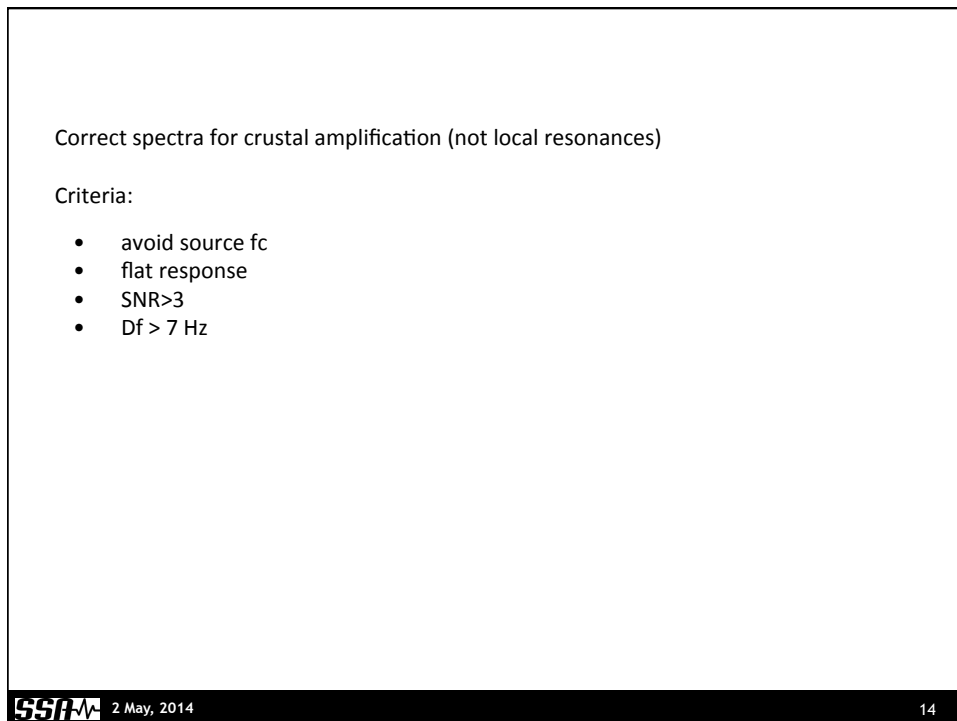
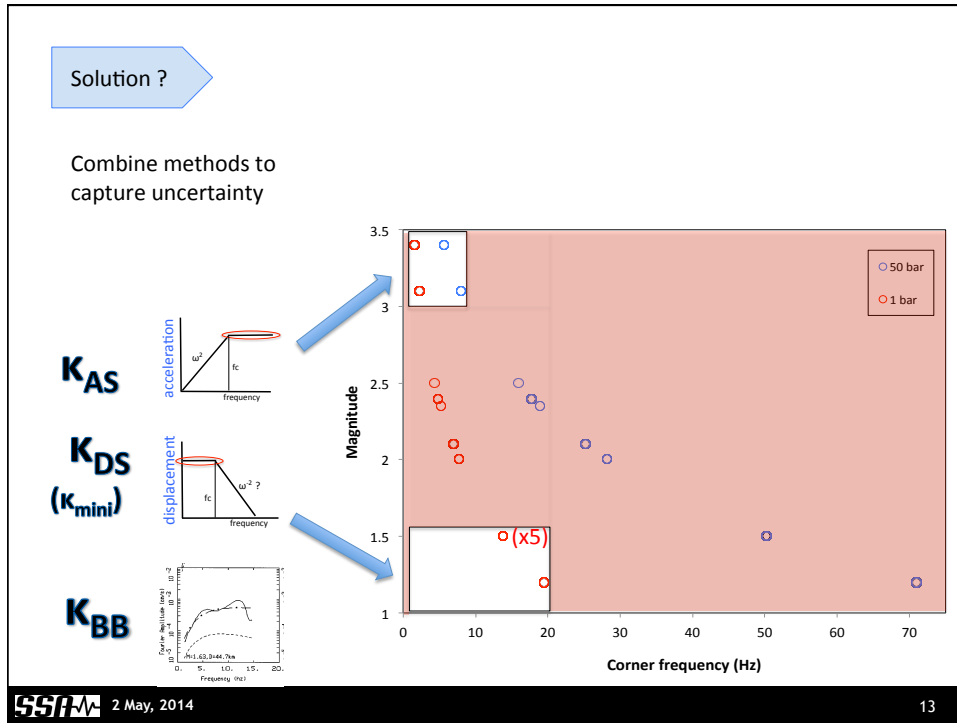
6

3





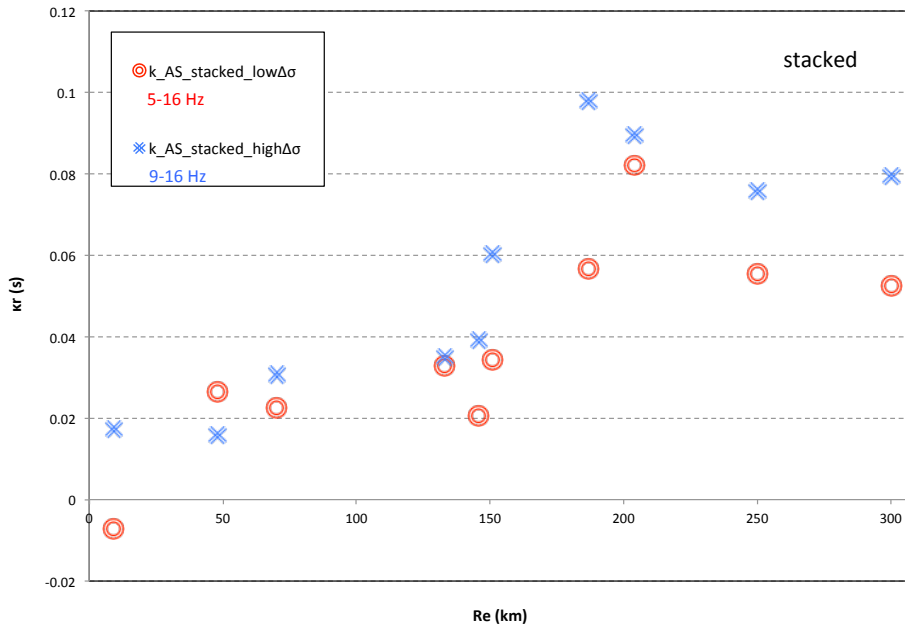
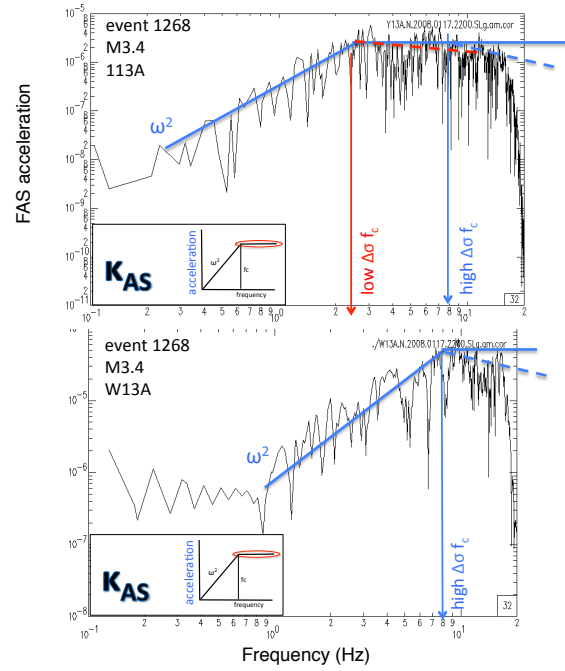


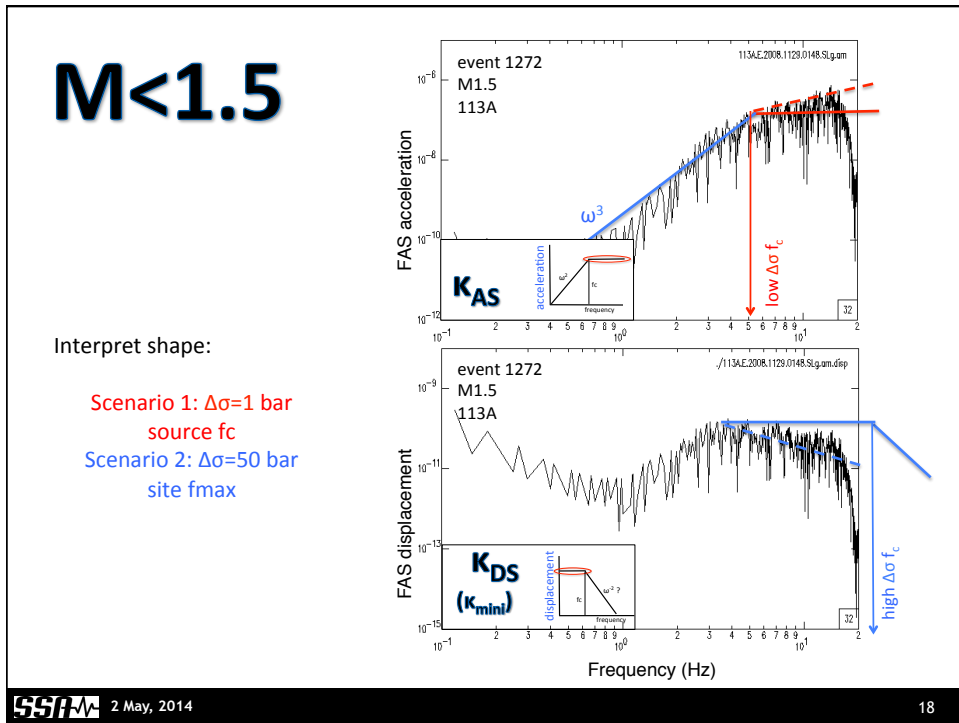
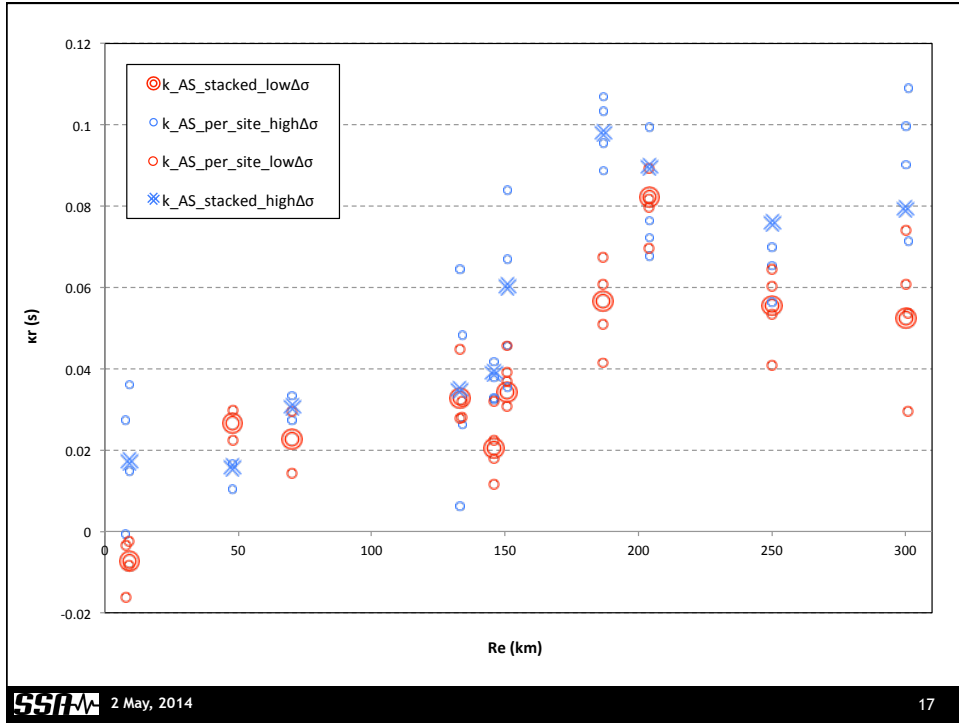


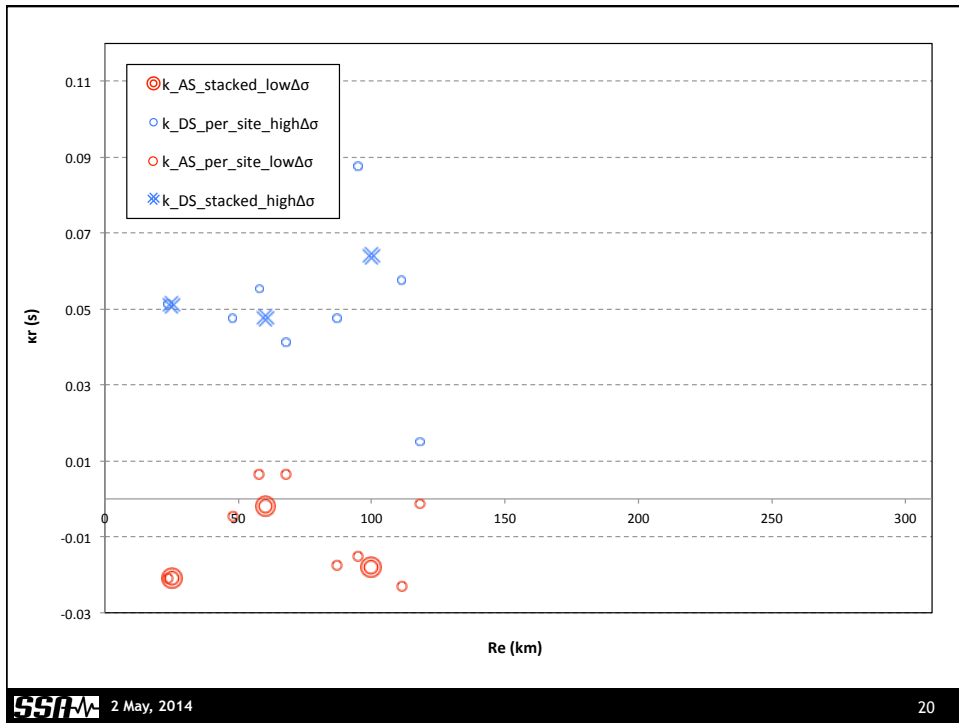
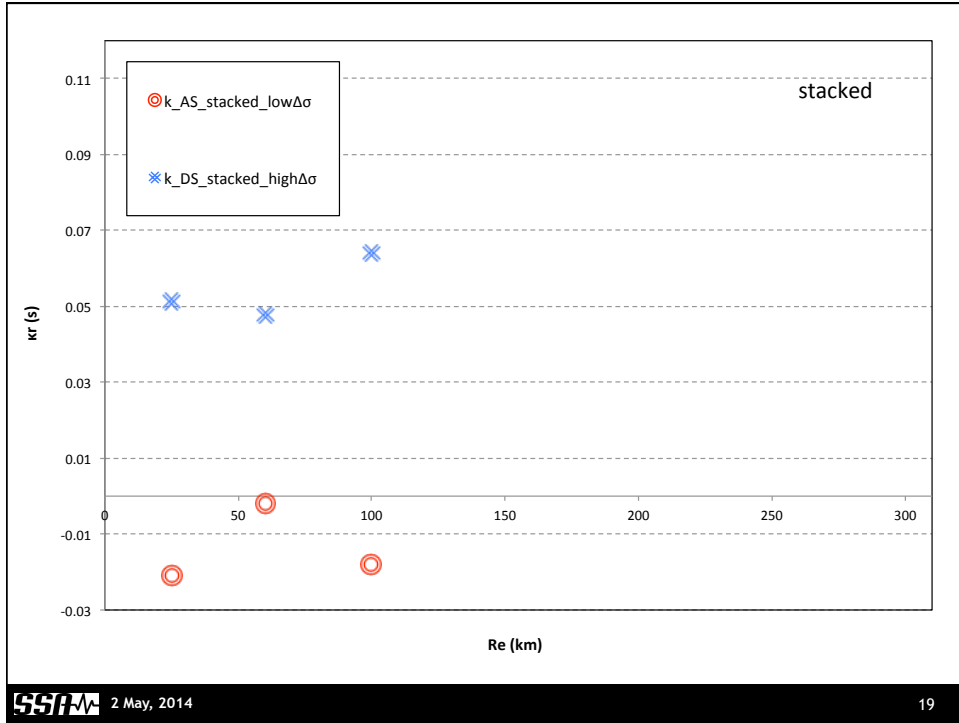
M>3

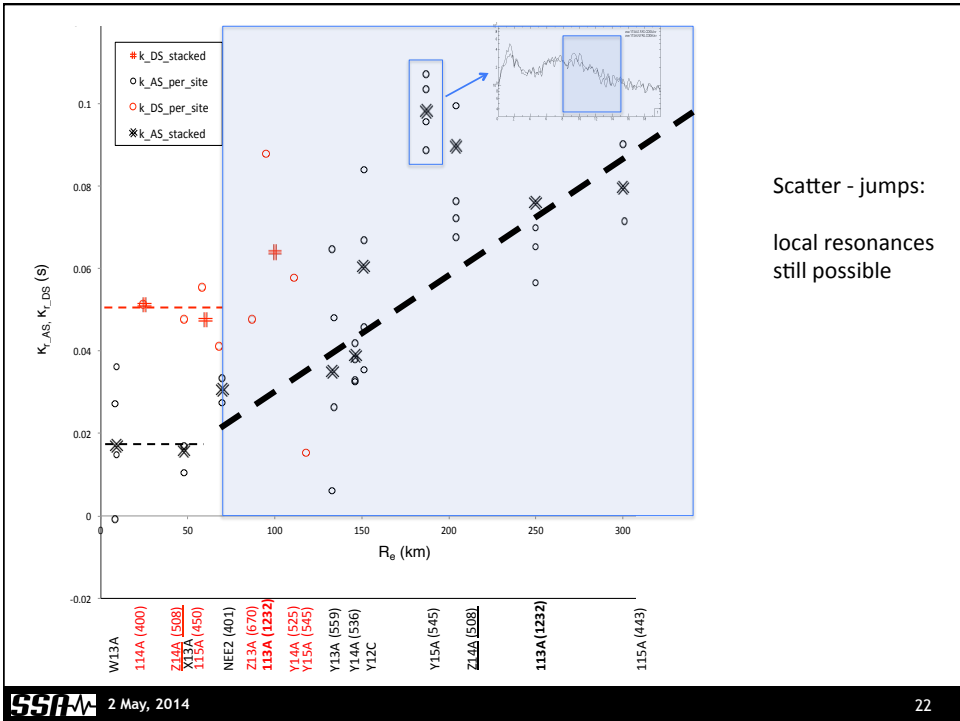
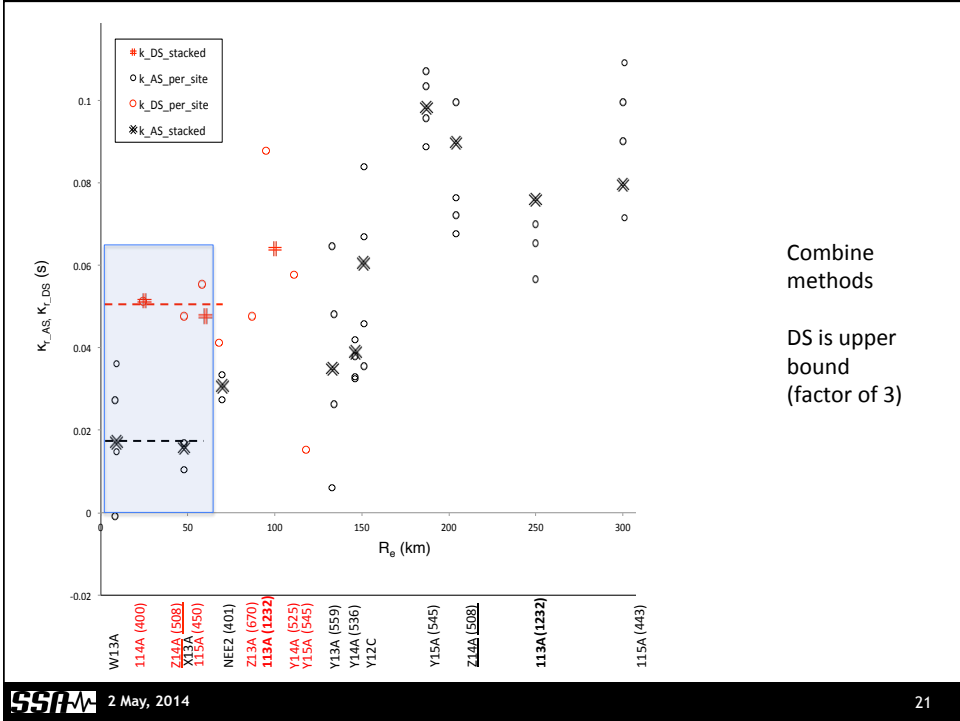
Interpret shape:

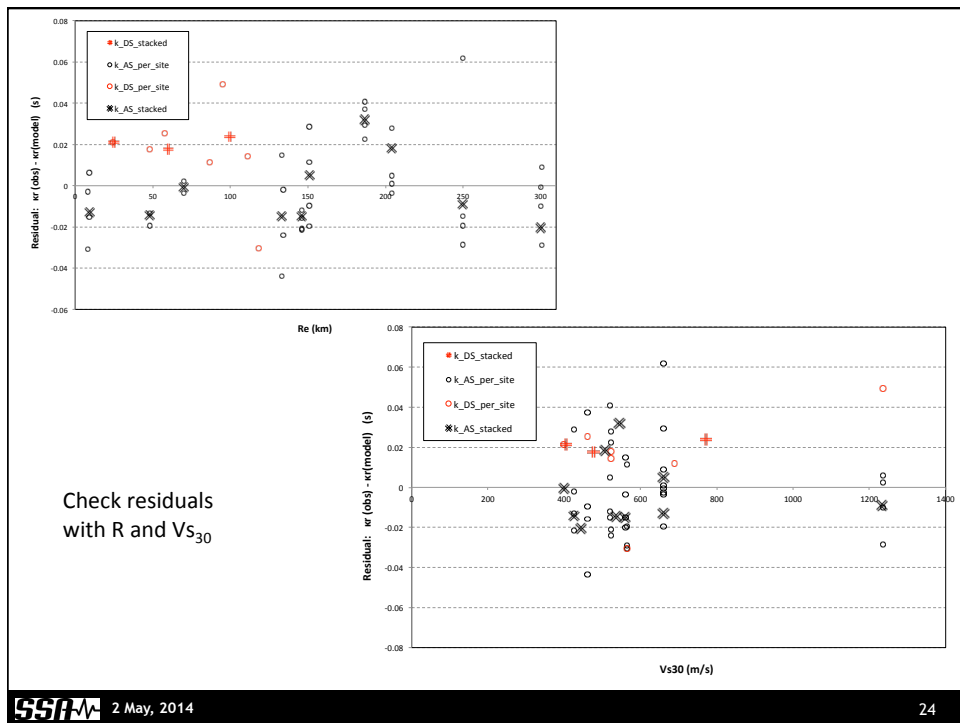
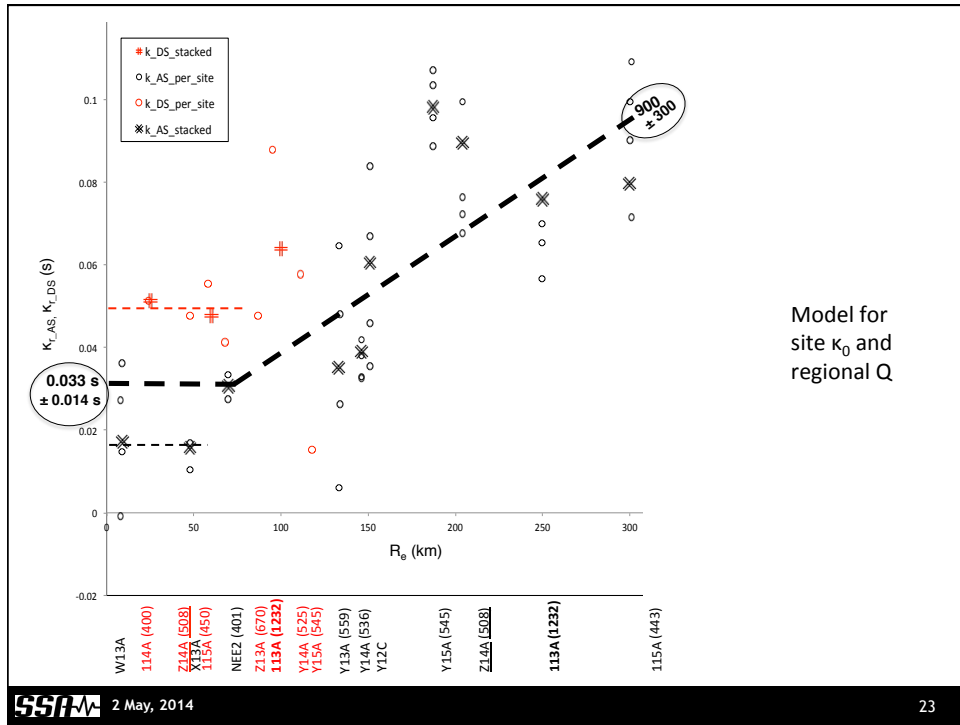
- Scenario 1: $\Delta\sigma=1$ bar
source f_c
- Scenario 2: $\Delta\sigma=50$ bar
site f_{max}

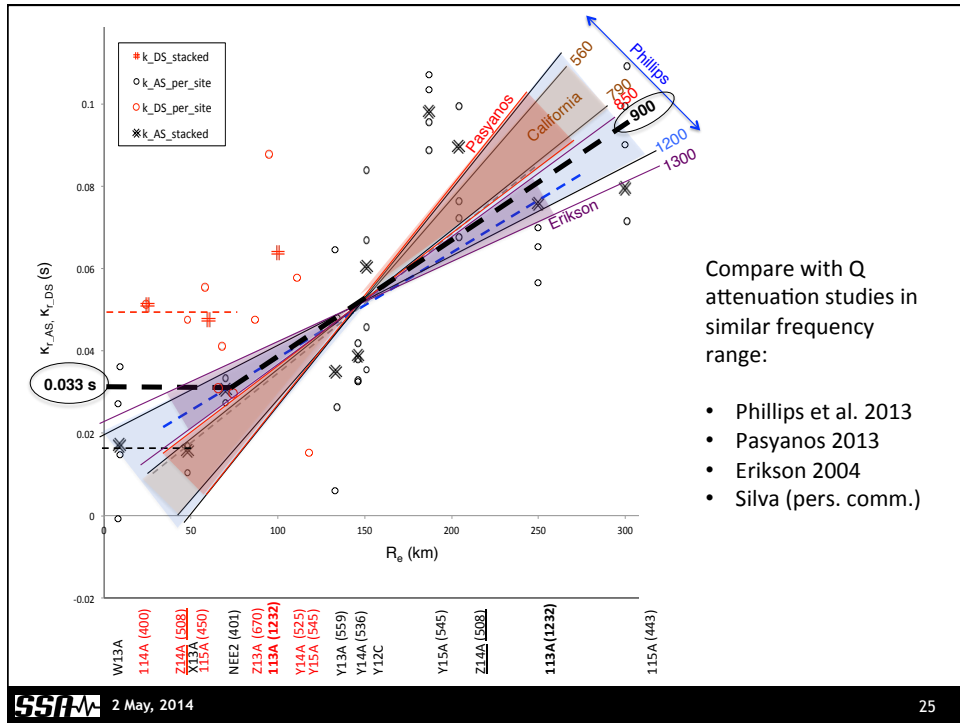












Concluding

- Many problems:
 - uncertainty in stress drop → source trade-off
 - few, distant EQs → path trade-off
 - TA sensors → very little bandwidth to resolve trade-offs
- Stacking to overcome noise + improve robustness
- DS is an upper bound
- Q compatible with independent studies
- Currently working on broadband inversion approach → getting comparable κ_0

Complaining

- TA has greatly increased data, esp. in certain low-seismicity regions
- The severe obstacles we faced will be relevant in future κ studies
- Please increase the TA sampling rate!

SSIM 2 May, 2014 26

Funding by:



References

- Anderson, J.G. (1991). A preliminary descriptive model for the distance-dependence of the spectral decay parameter in southern California, BSSA 81, 2186-2193.
- Anderson, J.G. and S.E. Hough (1984). A model for the shape of the Fourier amplitude spectrum of acceleration at high frequencies, BSSA 74, 1969-1993.
- Biasi, G.P., and K.D. Smith (2001). Site effects for seismic monitoring stations in the vicinity of Yucca Mountain, Nevada, MOL20011204.0045, a report prepared for the US DOE/University and Community College System of Nevada (UCCSN) Cooperative Agreement.
- Erickson, D., D. McNamara and H. Benz (2004). Frequency dependent Lg Q within the continental United States, BSSA 94, 1630-1643.
- Hough, S.E., and J.G. Anderson (1988). High-frequency spectra observed at Azusa, California: Implications for Q structure, BSSA 78, 692-707.
- Ktenidou O.-J., F. Cotton, N. Abrahamson, J.G. Anderson (2014). Taxonomy of kappa: a review of definitions and estimation methods targeted to applications. Seismol. Res. Letts 85(1), pp. 135-146.
- Parolai, S., and D. Bindi (2004). Influence of soil-layer properties on k evaluation, Bull. Seismol. Soc. Am. 94, 349-356.
- Pasyanos, M.E. (2013). A lithospheric attenuation model of North America, BSSA 103, p. 3321-3333.
- Phillips, W.S., K. Mayeda, L. Malagnini (2013). How to invert multi-band, regional phase amplitudes for 2-D attenuation and source parameters: Tests using the US Array, PAGEOPH, DOI:10.1007/s00024-013-0646-1
- Silva, W., R. Darragh, N. Gregor, G. Martin, N. Abrahamson, and C. Kircher (1998). Reassessment of site coefficients and near-fault factors for building code provisions, Technical Report Program Element II: 98-HQGR-1010, Pacific Engineering and Analysis, El Cerrito, USA.
- Silva, W.J. and R. Darragh (1995). Engineering characterization of earthquake strong ground motion recorded at rock sites. Palo Alto, Calif: Electric Power Research Institute, TR-102261

5. PREPARING A MAJOR DATABASE FOR MEASURING KAPPA

5.1 Selecting data and measuring κ for the NGA-West project

In May 2013, the NGA-West 2 project published a flatfile containing metadata for the records in the NGA-West2 database, along with response spectra based on corrected acceleration time histories. These data are important for the creation or updating of current ground motion prediction models. In future, however, it is possible that such models may incorporate additional parameters. Fourier spectra may allow a better fit to the data and κ_0 values (the site-specific high-frequency attenuation factor) to better describe high-frequency ground response. We describe the project of expanding the NGA-West2 database to include this new information. The process includes the windowing the time series and computation of Fourier amplitude and phase spectra with a view to: 1. creating a complementary Fourier spectrum flatfile for a suite of different time windows, and 2. enriching the metadata with values of κ_0 , along with its epistemic uncertainty for the seismic stations. This effort has set as its priority to characterize stations on stiff soil and soft rock ($V_{s30} > 600$ m/s). For these sites the knowledge of κ_0 is particularly critical in view of updating existing ground motion prediction models to better capture high-frequency site response and also of adjusting them to other regions with different κ_0 conditions.

First, we process the data in the NGA-West2 flatfile to create time windows S waves and other wave packages. Then we compute Fourier amplitude and phase spectra for each of these windows, as well as for the entire accelerograms for which response spectra had previously been computed. These will be used to create a Fourier spectrum flatfile to complement the response spectrum flatfile. This flatfile will eventually be released to the public and it can be used for of GMPEs based on Fourier spectra. Second, the metadata of the NGA-West2 flatfile will be enhanced with estimates of site-specific κ_0 values for each station, along with their respective uncertainty. The epistemic uncertainty depends among other factors on the method of estimation. We plan to estimate κ using two different approaches, a high-frequency approach and a broadband approach, to capture the range of possible values. This will later allow developers to estimate residuals for current GMPEs vs. κ_0 values and update the models accordingly if that is necessary.

This chapter reports the work shown in publication C2, and is currently being expanded within publication R1, also drawing from A5 (see Annex). More results will be reported in the final deliverable when the work is finalised.



Tenth U.S. National Conference on Earthquake Engineering
Frontiers of Earthquake Engineering
July 21-25, 2014
Anchorage, Alaska

FOURIER SPECTRA AND KAPPA₀ (κ_0) ESTIMATES FOR ROCK STATIONS IN THE NGA-WEST2 PROJECT

O.-J. Ktenidou^{1,2}, T. Kishida¹, R. Darragh³, W. Silva³ and N.
Abrahamson⁴

ABSTRACT

In May 2013, the NGA-West 2 project published a flatfile containing metadata for the records in the NGA-West2 database, along with response spectra based on corrected acceleration time histories. These data are important for the creation or updating of current ground motion prediction models. In future, however, it is possible that such models may incorporate additional parameters. Fourier spectra may allow a better fit to the data and κ_0 values (the site-specific high-frequency attenuation factor of [1] (Anderson and Hough, 1984) to better describe high-frequency ground response. This paper describes the project of expanding the NGA-West2 database to include this new information. The process includes the windowing the time series and computation of Fourier amplitude and phase spectra with a view to: 1. creating a complementary Fourier spectrum flatfile for a suite of different time windows, and 2. enriching the metadata with values of κ_0 , along with its epistemic uncertainty for the seismic stations. This effort has set as its priority to characterize stations on stiff soil and soft rock ($V_{s30} > 600$ m/s). For these sites the knowledge of κ_0 is particularly critical in view of updating existing ground motion prediction models to better capture high-frequency site response and also of adjusting them to other regions with different κ_0 conditions.

¹Postdoc researcher, Pacific Earthquake Engineering Research Center, UC Berkeley, CA 94720

²ISTerre, Universite Grenoble 1, CNRS, Grenoble, F-38041

³Pacific Engineering & Analysis, El Cerrito, CA 94530

⁴Department of Civil and Environmental Engineering, UC Berkeley, CA 94720



Tenth U.S. National Conference on Earthquake Engineering
Frontiers of Earthquake Engineering
July 21-25, 2014
Anchorage, Alaska

Fourier spectra and κ_0 (κ_0) estimates for rock stations in the NGA-West2 project

O.-J. Ktenidou^{1,2}, T. Kishida¹, R. Darragh³, W. Silva³ and N. Abrahamson⁴

ABSTRACT

In May 2013, the NGA-West 2 project published a flatfile containing metadata for the records in the NGA-West2 database, along with response spectra based on corrected acceleration time histories. These data are important for the creation or updating of current ground motion prediction models. In future, however, it is possible that such models may incorporate additional parameters. Fourier spectra may allow a better fit to the data and κ_0 values (the site-specific high-frequency attenuation factor of [1] (Anderson and Hough, 1984) to better describe high-frequency ground response. This paper describes the project of expanding the NGA-West2 database to include this new information. The process includes the windowing the time series and computation of Fourier amplitude and phase spectra with a view to: 1. creating a complementary Fourier spectrum flatfile for a suite of different time windows, and 2. enriching the metadata with values of κ_0 , along with its epistemic uncertainty for the seismic stations. This effort has set as its priority to characterize stations on stiff soil and soft rock ($V_{S30} > 600$ m/s). For these sites the knowledge of κ_0 is particularly critical in view of updating existing ground motion prediction models to better capture high-frequency site response and also of adjusting them to other regions with different κ_0 conditions.

Introduction

The NGA-West2 project recently published a flatfile with over 21,000 records from over 4,000 sites (<http://peer.berkeley.edu/ngawest2>, [2]). In the coming years, this dataset will be used in Earthquake Engineering and Engineering Seismology as one of the richest and most rigorously documented global crustal datasets. It has been used to update the existing NGA ground motion prediction equations (GMPEs) and will most probably be used soon in the formulation of new models. GMPEs predict ground motion using variables to model aspects of the source, path and site effects. For most current GMPEs, the main site response predictor variable is the time-averaged shear-wave velocity over the upper 30 meters of the site profile (V_{S30}), often coupled with an index of the depth to bedrock. Though these factors describe ground motion at low

¹Postdoc researcher, Pacific Earthquake Engineering Research Center, UC Berkeley, CA 94720

² ISTERre, Universite Grenoble 1, CNRS, Grenoble, F-38041

³ Pacific Engineering & Analysis, El Cerrito, CA 94530

⁴ Department of Civil and Environmental Engineering, UC Berkeley, CA 94720

frequencies well, it has been shown recently that they are inadequate in the high frequency range, where site attenuation may in some cases constitute the dominant factor; such are the cases of hard rock, and when high-frequency rock motion is paramount to the design of critical facilities. The parameter typically used to account for high-frequency attenuation is κ , which is the S-wave spectral decay parameter introduced by [1] and [3]. κ comprises a distance-dependent and a site-specific (zero-distance) component. The latter, termed κ_0 , is used in the site-specific adjustment of GMPEs, e.g. from rock to hard rock conditions, and in the simulation of ground motion. κ_0 is expected to be the next predictor variable to be added to GMPEs.

Furthermore, most current GMPEs use pseudo acceleration (PSA) response spectra to fit observed data to their functional forms. It is possible that high-frequency ground motion could be better represented by Fourier spectra rather than response spectra, and hence there is an emerging trend for some new GMPEs to be incorporate FAS. Hence there will be a need for databases that provide Fourier spectra. The inclusion of FAS adds additional signal processing requirements. Response spectra are computed using the entire accelerogram, since the structural response to the entire shaking duration is important. Fourier spectra are computed for specific types of waves. Hence, to create a Fourier spectrum database, the recorded accelerogram must first be windowed e.g. into P, S, coda waves, etc., before the spectrum calculations can be made.

In this paper we present a project that undertakes to address these emerging needs:

- First, we process the data in the NGA-West2 flatfile to create time windows for noise, P, S, and coda waves. Then we compute Fourier amplitude and phase spectra for each of these windows, as well as for the entire accelerograms for which response spectra had previously been computed. These will be used to create a Fourier spectrum flatfile to complement the response spectrum flatfile. This flatfile will eventually be released to the public and it can be used for of GMPEs based on Fourier spectra.
- Second, the metadata of the NGA-West2 flatfile will be enhanced with estimates of site-specific κ_0 values for each station, along with their respective uncertainty. The epistemic uncertainty depends among other factors on the method of estimation [4]. We plan to estimate κ using two different approaches, a high-frequency approach and a broadband approach, to capture the range of possible values. This will later allow developers to estimate residuals for current GMPEs vs. κ_0 values and update the models accordingly if that is necessary.

Dataset

Rock and stiff soil sites (with $V_{S30} > 600$ m/s) at distances shorter than 50-100 km are the first priority in Fourier spectra calculation and kappa estimation. Site condition and distance criteria have a significant impact on the size of the dataset. Tables 1 and 2 show the number of records and sites for the global set and per region, including the following regions: Western North America (WNA), Japan, Taiwan, China, New Zealand, and Europe and the Middle East (Europe). Because κ has a distance-dependent component which is possibly dependent on the regional geological structure and properties such as damping (Q) and shear wave velocity (V_s) of rock, it is imperative to regionalize datasets before attempting to interpret κ estimates per site. In Figure 1 we show an example of how the available data decreases when we apply V_{S30} and distance criteria. We show California, which we have chosen as a sub-region within WNA, the best-populated region in the dataset.

Table 1. The number of stations in the NGA-West2 database according to distance and site condition (V_{S30}) criteria in different regions worldwide.

V_{S30} (m/s)	R_{jb} (km)	Global	WNA	Japan	Taiwan	China	NZ	Europe
all	all	4000	1710	1233	496	273	139	240
all	150	3035	1596	648	488	1320	74	213
all	50	1962	1324	219	227	25	42	152
500	all	1069	398	365	159	46	44	94
500	150	847	370	209	155	21	15	87
500	50	515	289	72	74	9	4	67
600	all	542	231	184	75	21	23	29
600	150	425	210	103	74	8	7	28
600	50	265	168	38	30	3	3	24

Table 2. The number of records in the NGA-West2 database according to distance and site condition criteria in different regions worldwide.

V_{S30} (m/s)	R_{jb} (km)	Global	WNA	Japan	Taiwan	China	NZ	Europe
all	all	21262	15472	1946	2013	1326	223	450
all	150	15495	11484	841	1983	740	116	410
all	50	6057	4772	244	554	169	65	296
500	all	7392	5817	567	647	184	68	169
500	150	5156	3965	265	633	127	23	160
500	50	1654	1219	76	197	41	6	116
600	all	4720	4044	285	276	59	39	54
600	150	3175	2689	130	266	36	11	52
600	50	949	777	40	76	12	4	42

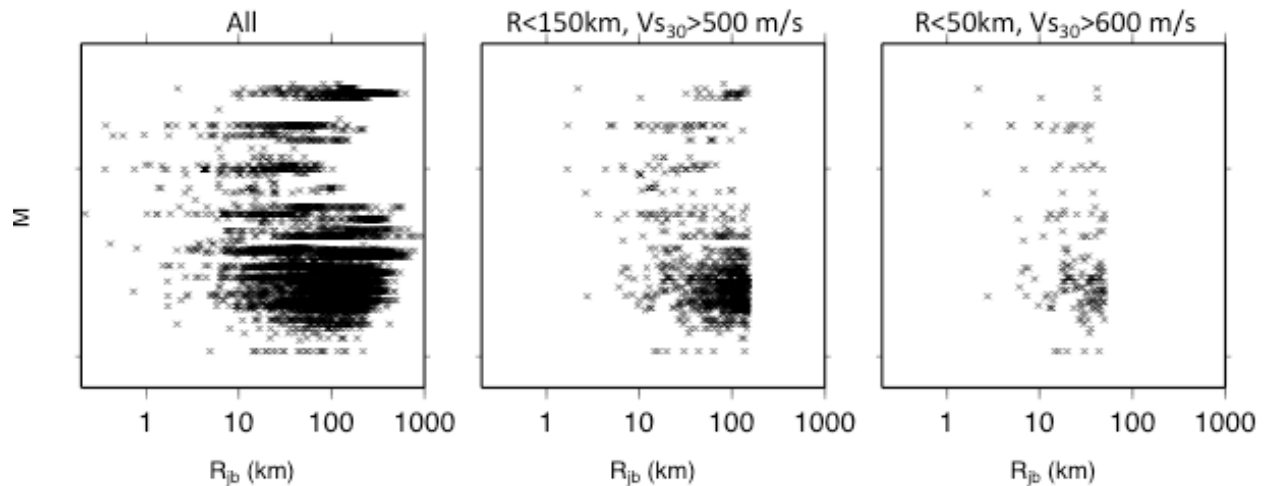


Figure 1. The magnitude-distance distribution of the data available in California depending on distance and V_{S30} criteria: a. all data, b. $V_{S30}>500$ m/s and $R_{jb}<150$ km, c. $V_{S30}>600$ m/s and $R_{jb}<50$ km.

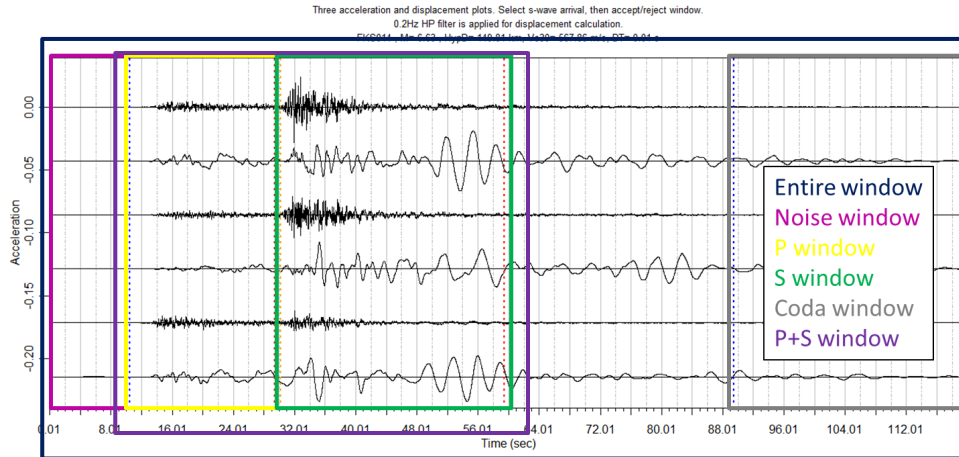


Figure 2. Choosing different time windows for an example acceleration time history.

Time series windowing

A semi-automated procedure was developed, requiring only the picking of P and S-wave arrivals and the flagging of events that would require further inspection [5]. The processing starts with the time-aligned, instrument-corrected, tapered and filtered acceleration time series. Six different time windows are selected (Figure 2): the entire record, the pre-event noise, P-wave, S-wave P and S waves, and coda waves. Not all time windows are available for all records: only the entire recording and S-wave windows are always available. The main processing steps are described below:

1. The analyst inspects the time histories and rejects late S-triggers, since the FAS of the S-wave window is considered necessary for κ estimation.
2. The analyst picks the P-wave onset. If that occurs very early in the record (e.g., if it less than 10 s long), a flag indicates possible inadequate noise window length. A flag also exists to indicate late P-triggering (and total absence of noise time window). The noise window is useful for computing the signal-to-noise ratio (SNR) and judging the signal quality of other windows by comparison. If flagged as unavailable or inadequate, the user may substitute the coda or P wave window, if desired
3. S-wave arrival is computed automatically using the analyst's P picks and the known hypocentral distance (the theoretical Δt_{P-S} is computed assuming a crustal P and S velocity values). The analyst corrects the S arrival pick if necessary from an examination of the three component acceleration and displacement time histories (Figure 2). For large discrepancies between manual and theoretical Δt_{P-S} value (more than 30%), a flag indicates possible late P trigger.
4. Based on the S arrival pick, the end of the S window is computed automatically based on the estimated duration of shaking. The duration consists of rupture duration (depending on magnitude and stress drop, assuming the point source stochastic model of [6] and propagation duration (depending on distance and Q structure along the path). Both these components have been calibrated based on data from different regions and checked on a variety of magnitudes and distances in order to define an envelope that does not greatly overestimate the overall duration.

The values used are shown in Table 3 and an example of source duration envelope is shown in Figure 3.

5. The beginning and the end of the coda window are also automatically chosen. The coda window is anchored to the end of the record and its beginning is set to either the theoretical coda onset (twice the S-wave travel time, according to the definition of [7] the end of the S wave time window. Thus we can provide as many coda windows as possible, and their quality can be judged by a flag indicating whether the theoretical onset rule is observed or not. There is also a flag if the coda window (D_c) is too short (if it less than 10 s or includes more than 30% tapered duration) or if it does not exist. Finally, the analyst can flag any problems such as aftershocks or noise in windows.

6. Flagged records are reviewed and rejected or reprocessed.

7. The flatfile is updated with all flag values (see Table 4 for an overview of all flags).

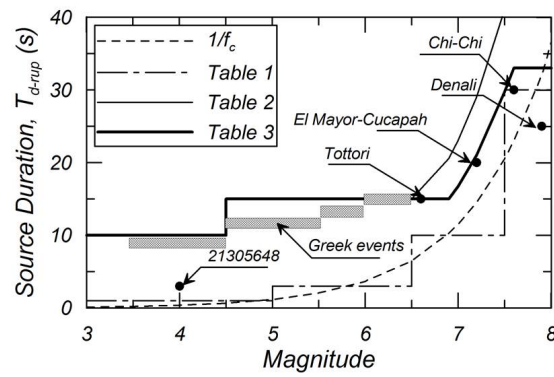


Figure 3. Example of calibration of source duration with data.

Table 3. S-wave duration versus moment magnitude and hypocentral distance (R_h).

Moment magnitude (M_w)	Source and propagation duration (s)
$M < 4.5$	$10 + 0.1R_h$
$4.5 \leq M < 6.9$	$15 + 0.1R_h$
$6.9 \leq M < 7.6$	$1.4/f_c + 0.1R_h$ ¹⁾
$7.6 \leq M < 7.9$	$33 + 0.1R_h$

1) f_c is the corner frequency of the Fourier spectra [8].

Table 4. Calibrated S-wave duration versus moment magnitude and hypocentral distance (R_h).

Name	Type	Result
Late S	User	Rejection (after confirmation)
Late P	Auto (criterion: $\Delta t_{S-P} \geq 30\% \cdot R_h/8$)	Review
Short noise window	Auto (criterion: $t_p \leq 10$ s)	Review
Short coda window	Auto (criteria: $D_c \leq 10$ s or $D_c \leq 0.17t_{end}$)	Review
Coda onset prior to theoretical	Auto (criterion: $t_c \leq t_{theo}$)	- (for info only)
Coda contaminated by S / Aftershock in any window	User	Review

Fourier spectra calculations

An automated procedure was created by [5], including the following steps:

1. Before calculation of the Fourier spectra, the various windowed time histories are processed in the time domain for DC (mean offset) removal.
2. Cosine tapers are then applied to the beginning and end of each corrected window (0.5 s at the start and end time for noise, P, S, coda windows). The entire time history is already usually tapered with the standard tapers of 1% and 5% at beginning and end, respectively. Records with the P-wave onset near the start of the time history have shorter tapers.
3. A series of zeros is added to the end of records in order to achieve a common duration (D_{tot}) for all windows in the dataset and hence a common frequency step ($df=1/D_{tot}$) in the resulting Fourier spectra. This is convenient for users for two reasons. First, a common df for the different time windows of a record will facilitate the computation of SNR, which is a standard check of data quality. Second, a common df between records facilitates statistical manipulations of many records at chosen frequency values, without the need to interpolate. For 91% of the dataset the common df is 0.000763 Hz. Limited special cases of df are dealt with separately through interpolation.
4. Fourier spectra are computed for all time windows. Results are provided in terms of Fourier amplitude spectra (FAS) and Fourier phase spectra (FPS) as well as real and imaginary parts (Figure 4 shows an example of FAS for all the different time windows).
5. The flatfile is updated with the df , the sampling rate (dt) and the number of points per time history.

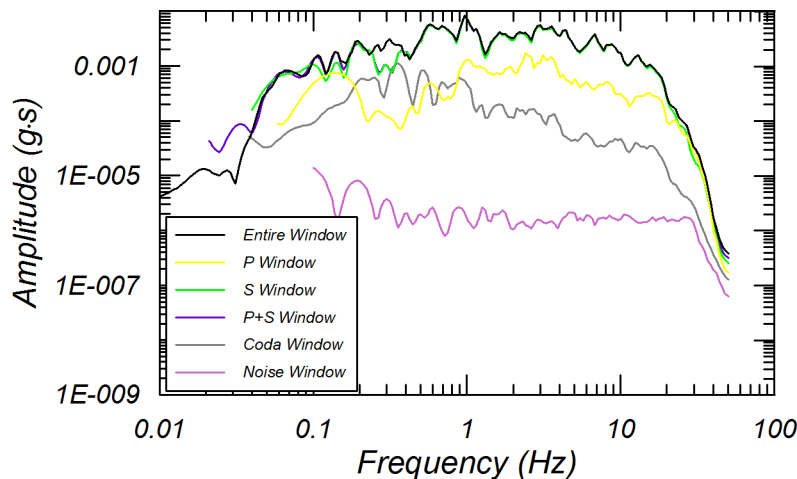


Figure 4. Example of FAS for the suite of time windows shown in Figure 2.

κ calculations

Estimation approaches

There are several approaches to estimate κ , and they can be roughly divided into two categories: ‘high-frequency’ and ‘broadband’ approaches [4]. We estimate κ_0 in two ways, using a method

from each category:

1. Following the classic definition of [1], and following recommendations from [9], κ for a particular record at epicentral distance R (denoted as κ_{r_AS}) can be directly measured in log-linear space on the high-frequency part of the FAS of the S-waves, between frequencies f_1 and f_2 (see Figure 6). Since a component of horizontal wave propagation, affected by Q , is present in these measurements (let us denote that κ_{Re}), an extrapolation to zero epicentral distance (assuming frequency-independent Q) should be made to derive the site-specific component, $\kappa_{0_AS} = \kappa_{r_AS} - \kappa_{Re}$. This approach is used for relatively large event magnitudes, as f_1 must exceed the corner frequency (f_c) to avoid any trade-off with the source.
2. Following a broadband approach such as [10] or [11], the entire frequency range of the FAS can be inverted to separate source, path and site effects. The estimate utilizes an estimate of a site amplification function, a full frequency-dependent Q model, to estimate the stress parameter and κ_{0_BB} .

By computing κ_0 at the NGA sites using both approaches we achieve two goals. First, we get an estimate of epistemic uncertainty between the methods. Second, we can then study the residuals of current GMPEs with respect to the computed κ_0 values and decide if these models need to be updated to include κ_0 as an independent variable, and which of the two approaches for κ_0 estimation is most appropriate.

Frequency range considerations and limitations

We consider the effect of certain factors on our usable frequency range, namely filtering and instrument response, SNR, magnitude and stress drop before estimating κ .

Filtering, instrument response, SNR

These three factors apply to both estimation approaches. The maximum frequency is the Nyquist frequency and it depends on the sampling rate. Even though FAS are computed up to each record's Nyquist frequency, this does not mean that they are usable over the entire range. We query the flatfile for the high-pass frequency (HP) and low-pass frequency (LP) values for each horizontal component which depends on the filtering performed on the traces. This filter takes into account noise removal and anti-alias filtering. For the Lowest Usable Frequency (LUF) we normally increase the maximum of the two horizontal component HP values by 25% and for the Highest Usable Frequency (HUF) we decrease the minimum LP value by 25% [12]. These frequencies are shown in Figure 5. κ computations are only made within the usable frequency range, and in most cases we also use a SNR criterion of 3. The SNR can be estimated with respect to a coda window if the noise window is unavailable or inadequate.

Magnitude and stress drop

These two factors apply to the high-frequency approach, where the source effects need to be separated from the site and path effects that κ is assumed to represent. Given that f_1 should be chosen above f_c , we estimate f_c . This we do based on magnitude and stress drop, assuming the point source stochastic model of [6]. The magnitude is usually well known, as the metadata of the NGA-West2 flatfile are well verified. Most of the uncertainty then lies in estimate of the

stress drop, particularly for small events. For this reason we estimate a possible range of stress drop values and choose the frequency range for κ measurement accordingly. This helps capture epistemic uncertainty in the calculation. An example of the upper and lower usable frequencies of the data (LUF, HUF) and the overall available frequency range (DF=HUF-LUF) are shown in Figures 5(a) and (b), respectively, for the California region, considering only data within 50 km with $V_{S30} > 600$ m/s. The blue lines indicate possible ranges of f_c . It is obvious that for magnitudes below 4.5 this issue cannot be ignored. Figures 5(c) and (d) show usable frequency ranges for all V_{S30} values. For DF values below 20 Hz the f_c problem should be considered, while data with greater DFs can be readily used in the estimate.

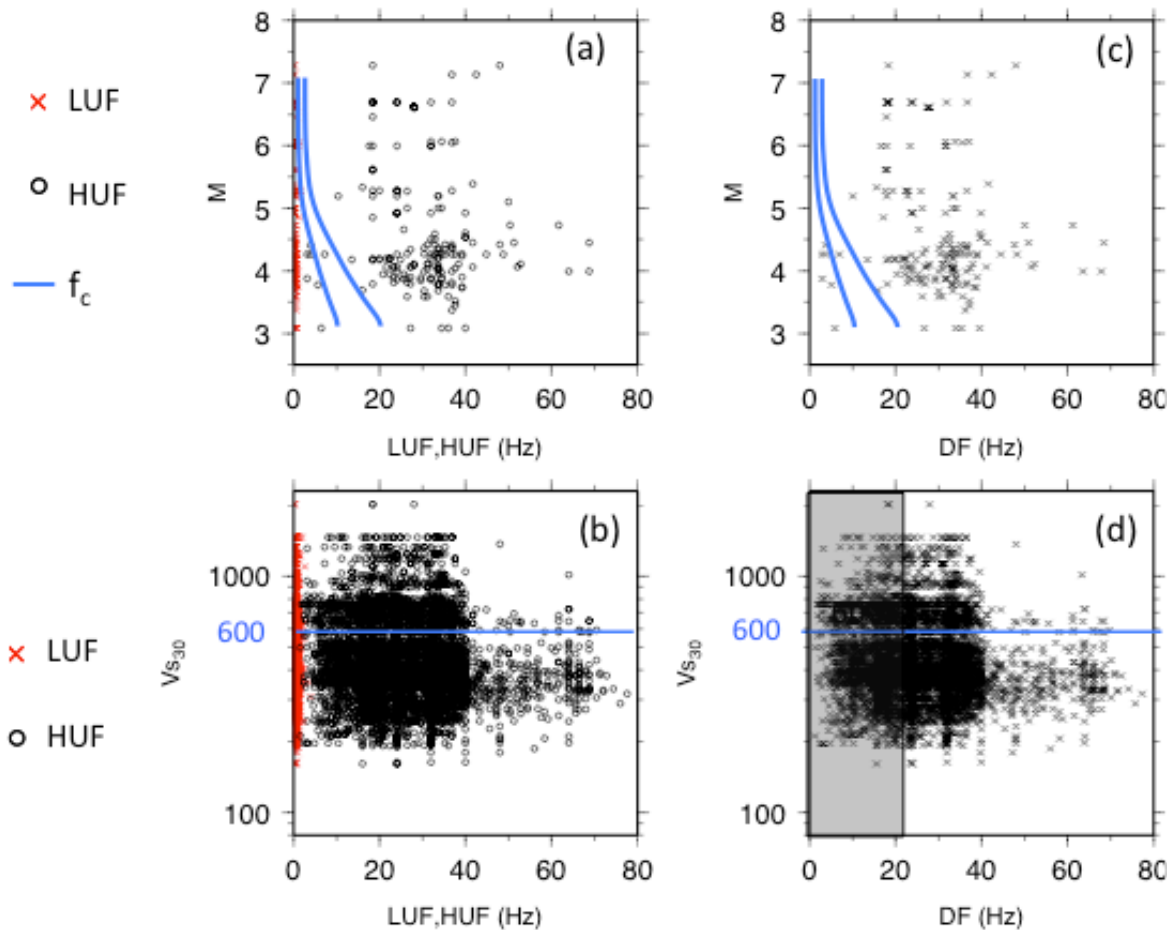


Figure 5. Distribution of data from the California region considering possible corner frequencies (f_c) and usable frequency ranges of the data.

Example of κ calculation and correlation to site conditions

In Figure 6 we show an example of the measurement of κ at three sites (PSA, 29P, and LCN) with very different soil conditions, which recorded the same event (Landers, M7.3, 6/28/1992) at similar epicentral distances (42, 44 and 44km) but different rupture distances (36, 41, and 2 km). They are described as NEHRP class D, C and B respectively and have V_{S30} values of 312, 635

and 1370 m/s. We compute κ_{r_AS} are 32, 24 and 18 ms respectively. The distances are small enough to assume that the path attenuation (κ_{Re}) is small and any differences in path attenuation between the three stations are probably negligible (so $\kappa_{r_AS} \approx \kappa_{0_AS}$). LCN contains a long-period forward directivity pulse but in the frequency range of 6-36 Hz that should not affect κ estimation. Hence the computed κ_{r_AS} values should reflect mainly the site differences.

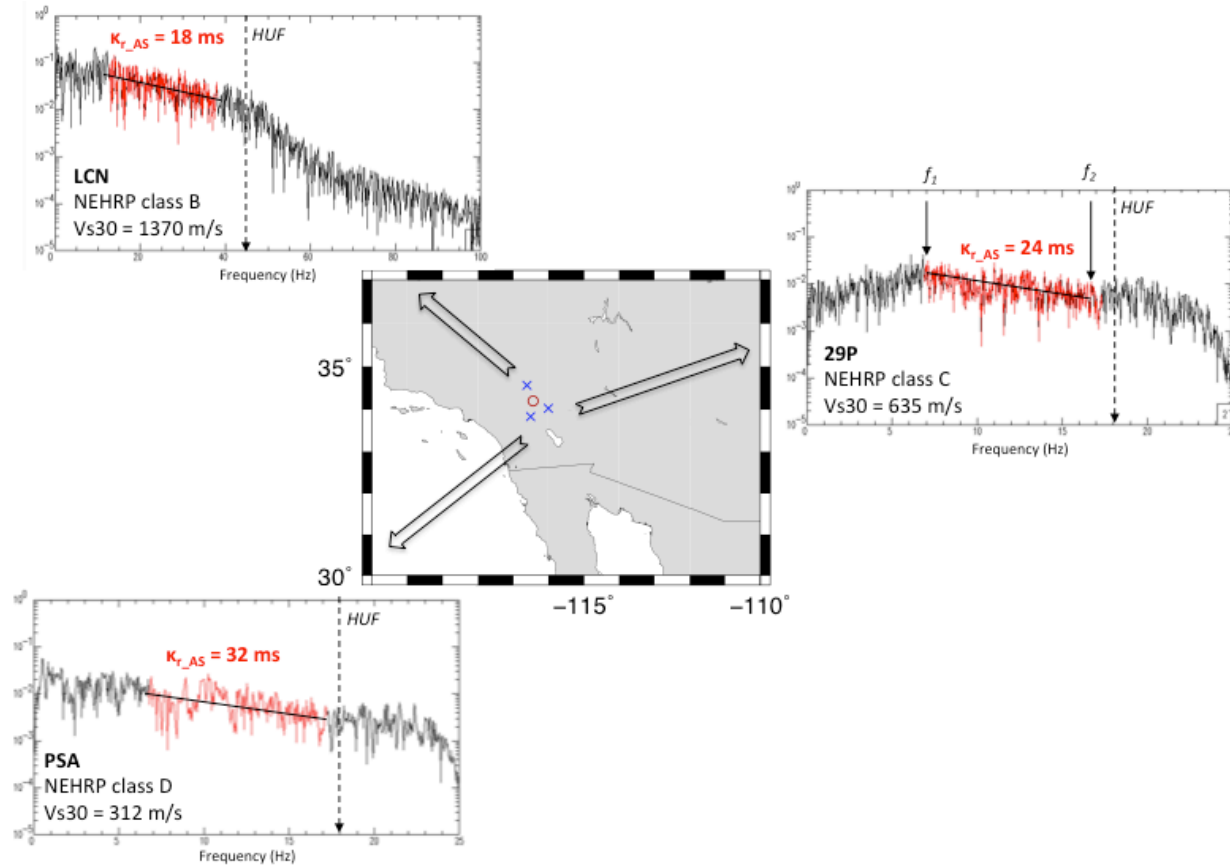


Figure 6. Example of κ_{r_AS} measurements at three sites that recorded the same event at similar epicentral distances. Black lines: FAS. red lines: linear decay of FAS at high frequencies (below HUF). Frequencies f_1 , f_2 are also shown.

Conclusions

This paper describes the process of expanding the existing NGA-West2 response spectra flatfile with Fourier spectra and station κ_0 values. We describe the windowing of the time series and the computation of Fourier amplitude and phase spectra in order to: 1. create a complementary Fourier spectrum flatfile for a suite of different time windows, and 2. enrich the metadata with values of κ_0 , the site-specific high-frequency attenuation factor [1], and its epistemic uncertainty for the seismic stations. The priority is to characterize hard sites ($V_{S30} > 600$ m/s), for which κ_0 is particularly critical for updating existing ground motion prediction models to better capture high-frequency site response and also to adjust them to other regions with different κ_0 conditions.

Acknowledgments

This study was sponsored by the Pacific Earthquake Engineering Research Center (PEER) and funded by the California Earthquake Authority, California Department of Transportation, and the Pacific Gas & Electric Company. OJK is also funded by the French SIGMA project. Any opinions, findings, and conclusions or recommendations expressed in this material are those of the authors and do not necessarily reflect those of the sponsoring agencies. Discussions with the experts of the NGA-West 2 project are gratefully acknowledged. Signal processing benefited from SAC [13] (<http://www.iris.edu/software/sac>) and some plots were made with GMT [14] (<http://gmt.soest.hawaii.edu>).

References

1. Anderson, J.G. and S.E. Hough (1984). A model for the shape of the fourier amplitude spectrum of acceleration at high frequencies, *Bull. Seism. Soc. Am.* **74**: 1969-1993.
2. Ancheta, T. D., Darragh, R. B., Stewart, J. P., Seyhan, E., Silva, W. J., Chiou, B. S.J., Wooddell, K. E., Graves, R. W., Kottke, A. R., Boore, D. M., Kishida, T. Donahue, J. L. (2013). PEER NGA-West2 Database, Pacific Earthquake Engineering Research Center, PEER Report 2013/03.
3. Hough, S.E., J.G. Anderson, J. Brune, F. Vernon, J. Berger, J. Fletcher, L. Haar, T. Hanks, and L. Baker (1988). Attenuation near Anza, California, *Bull. Seism. Soc. Am.* **78**: 672-691.
4. Ktenidou O.-J., F. Cotton, N. Abrahamson, J.G. Anderson (2014). 'Taxonomy of κ (kappa): a review of definitions and estimation methods targeted to applications'. *Seismol. Res. Letts* **85**: 135-146
5. Kishida, T., Ktenidou, O. J., Darragh, B., and Silva, W. J. (2013). Data processing for Fourier amplitude spectra (FAS) estimation from NGA-West2 processed accelerations. Database, Pacific Earthquake Engineering Research Center, PEER report (under review).
6. Boore, D. M. (1983). Stochastic simulation of high-frequency ground motions based on seismological models of the radiated spectra, *Bull. Seism. Soc. Am.* **73**: 1865-1894.
7. Aki, K. (1969). Analysis of the seismic coda of local earthquakes as scattered waves, *J. Geophys. Res.* **74**: 615-631.
8. Brune, J.N. (1970). Tectonic stress and the spectra of seismic shear waves from earthquakes, *J. Geophys. Res.* **75**: 4997-5002.
9. Ktenidou, O.-J., C. Gelis, and F. Bonilla (2013). A study on the variability of kappa in a borehole, Implications on the computation method used, *Bull. Seismol. Soc. Am.* **103**: 1048-1068.
10. Humphrey, J.R., Jr. and J.G. Anderson (1992). Shear wave attenuation and site response in Guerrero, Mexico, *Bull. Seism. Soc. Am.* **81**: 1622-1645.
11. Silva, W.J. (1997). Characteristics of vertical strong ground motions for applications to engineering design. Proc. of the FHWA/NCEER Workshop on the National Representation of Seismic Ground Motion for New and Existing Highway Facilities, I.M. Friedland, M.S Power and R.L. Mayes eds., Technical Report NCEER-97-0010.
12. Abrahamson N.A. Silva W.J. (1997). Empirical response spectral attenuation relations for shallow crustal earthquakes, *Seismol. Res. Lett.* **68**: 94-127.
13. Goldstein, P., D. Dodge, M. Firpo, and L. Minner (2003). SAC2000: Signal processing and analysis tools for seismologists and engineers, The IASPEI International Handbook of Earthquake and Engineering Seismology, W.H.K. Lee, H. Kanamori, P.C. Jennings, C. Kisslinger (Editors), Academic Press, London.
14. Wessel, P., and W. H. F. Smith (1998). New, improved version of the Generic Mapping Tools Released, *EOS Trans. AGU* **79**: 579.

5.2 Selecting data and measuring κ for the NGA-East project

The procedure for NGA-East builds on that described in the previous section for NGA-West2. An important difference compared to that dataset is the low seismicity setting and the larger uncertainty in stress drop values. This project is underway. In what follows we provide a brief summary with the main considerations behind the data selection and κ estimation for this dataset.

This chapter summarises the main considerations from the work currently underway in publication R3, Chapter 6: 'Site metadata: kappa' (see Annex). More results will be reported in the final deliverable when the work is finalised.

Summary

We use three approaches for measuring κ for NGA-East. Following the nomenclature proposed by Ktenidou et al. (2014), these will be referred to as the acceleration spectrum approach (AS), the displacement spectrum approach (DS), and the broadband approach (BB). The first is applied in a frequency range above the source corner frequency (f_c), the second below it, and the third one over the entire usable frequency range. These approaches were introduced respectively in Anderson and Hough (1984), Biasi and Smith (2001), and Silva et al. (1997). Table 5.1 outlines the approaches based on certain common features, such as the principle behind the approach and the frequency range over which κ is computed. AS and DS, generally start with individual measurements of κ_r (i.e., observations on individual spectra at distance r), which must then be combined, interpreted, and extrapolated to zero distance to obtain an estimate of κ_0 for the site. BB, yields directly the κ_0 (i.e., the site-specific, zero-distance κ derived from many observations), after having corrected for path attenuation and crustal amplification.

Table 5.1. Approaches used for estimating κ (adapted from Ktenidou et al., 2014).

Notation	Principle	Main references	Measurement / computation	Freq. range
κ_{AS}	High-frequency decay of the S-wave Fourier spectrum	Anderson and Hough (1984), Hough and Anderson (1988)	Direct measurement on the S-wave Fourier acceleration spectrum above f_c , where it is theoretically flat	Above f_c
κ_{DS}	Small magnitudes (strong trade-off with source)	Biasi and Smith (2001)	Direct measurement on low-frequency part of the Fourier displacement spectrum (much below f_c) where it is theoretically flat	Below f_c
κ_{BB}	Inversion of the entire frequency band of the spectrum	Anderson and Humphrey (1991), Humphrey and Anderson (1992), Silva et al. (1997)	Broadband inversion of the entire spectrum for source, path and site terms (usually for moment, f_c and κ_0)	Entire band

f_c : source corner frequency

In order to use the band-limited approaches AS and DS, an estimate of the source corner frequency must be made, so as to work either below it or above it. This in turn is dependent on the event magnitude, which is well constrained in the database, and the event stress drop, which is usually unknown. Published stress drop values in Central-Eastern United States (CENA) vary greatly, even within a single region, making it a difficult task to assign a single value to any region. On the other hand, each record in the database is attributed a lowest and highest usable frequency, which are typically dependent on the noise level and anti-alias filter. Data can only be used in a meaningful way between these two values. When applying either the AS or DS approach, we must check whether the source f_c lies within the usable bandwidth of the record, and whether there is an adequate overlap between the usable frequency range and the frequency range in which we should be measuring κ . Given the numerous small-magnitude events and the relatively high stress drops in the region, there are many records for which there is no such overlap, or if there is, it is inadequate. Given the large volume of records in the database, it is important to first scan the flatfile based on these parameters, and create subsets for which each of the approaches (AS and DS) may be used.

For the band-limited approaches AS and DS, we follow three steps:

1. Choosing the frequency band

This choice is affected by several considerations, such as the possible range of source corner frequencies, the highest and lowest usable frequency in the data, the signal-to-noise ratio of the record, and the adequacy of the available bandwidth after accounting for these considerations. These are considered as objective criteria for the selection of the records and the necessary bandwidth to be used.

2. Performing individual measurements

For each record, we compute κ for the average horizontal spectrum (vector sum) and for the vertical one. For each individual spectrum, we compute κ following considerations such as: the smoothing of the spectrum, use of moving windows across the chosen bandwidth, amplification effects due to local resonance patterns of crustal amplification, and the contribution of regional attenuation (Q).

3. Interpretation of individual values and creation of site-specific κ_0

To interpret the measured values, account for regional attenuation, and work towards site-specific κ values, we need to regionalize them. The main considerations then are weighing of individual measurements based on quality criteria, binning by V_{s30} or site class, and possible binning by excitation level.

Finally, results from the band-limited approaches AS and DS are combined with results of the broadband approach to build the final models and estimate their uncertainty.

References

- Anderson and Humphrey (1991). A least squares method for objective determination of earthquake source parameters, *Seismol. Res. Lett.* 62, 201-209.
- Anderson, J.G., and Hough, S.E. (1984). A model for the shape of the Fourier amplitude spectrum of acceleration at high frequencies, *Bull. Seismol. Soc. Am.*, 74(5), 1969-1993.
- Biasi, G.P., and K.D. Smith (2001). Site effects for seismic monitoring stations in the vicinity of Yucca Mountain, Nevada, MOL20011204.0045, A report prepared for the US DOE/University and Community College System of Nevada (UCCSN) Cooperative Agreement.
- Hough, S. E., and J. G. Anderson (1988). High-frequency spectra observed at Azusa, California: Implications for Q structure, *Bull. Seismol. Soc. Am.* 78, 692–707.
- Humphrey, J.R., Jr. and J.G. Anderson (1992). Shear wave attenuation and site response in Guerrero, Mexico, *Bull. Seism. Soc. Am.* 81, 1622-1645.
- Silva, W.J., N. Abrahamson, G. Toro and C. Costantino. (1997). "Description and validation of the stochastic ground motion model." Report Submitted to Brookhaven National Laboratory, Associated Universities, Inc. Upton, New York 11973, Contract No. 770573.

6. CONCLUDING REMARKS AND FUTURE PERSPECTIVES

We have presented a state of the art on κ , classifying measurement approaches into a taxonomy targeted to applications, and discussing shortcomings of current correlations with V_{S30} . We have worked towards understanding the physics of κ better, in terms of the effects of sensor orientation, instrument and data frequency constraints, and excitation level. We have introduced a possible physical model for κ_0 that includes asymptotic regional values and scattering. We have worked on κ estimation for soft and hard rock sites in low-seismicity areas, testing its sensitivity to data selection criteria and trade-offs with Q . We have illustrated a possible strategy for addressing particularly adverse conditions combining low-magnitude events and bandlimited data. Finally, we have presented the main considerations behind database preparation, record selection, and κ estimation for two major databases, NGA-West2 and NGA-East.

Especially for low-seismicity regions, we repeat some particular considerations. The number of records at short distances may be small, and it may be necessary to complement them with regional records and interpret them jointly to estimate local attenuation κ_0 and regional Q attenuation. The typical magnitude of the earthquakes is small, so it is useful to examine alternative approaches to the traditional AS approach. One way to make use of small events is to use the DS approach and measure κ not above the source corner frequency but below it. The two methods can be used in conjunction in order to make use of as many records as possible. Depending on the stress drop in the region and its uncertainty, a range of possible corner frequency values can be estimated. Based on those, the choice of approach can be made. Records should only be used within the maximum and minimum usable frequencies, which depend on the instrument sampling rate and response, and the record filtering. If these constraints are strict (maximum frequency is low), then the estimation of κ is more challenging.

Despite the progress made, there still remains large uncertainty and a lack of consensus in the estimation of κ . More research is needed in order to understand its physics better, and to be able to estimate it more accurately in different contexts. The mechanisms behind κ and their relative contribution have not yet been quantified. This is evident in the scatter observed in correlations between κ_0 and various site parameters. The variability in these κ_0 values is larger than corresponds to the variability in observed ground motion. There may still be parameters to which κ_0 is correlated, which may explain this. There is also a need for more data from which to measure κ . High-quality, high-frequency data should be sought, and attention should be paid to sampling rates, filtering, and other factors affecting the bandwidth. Data is needed especially on hard rock, because existing κ_0 values on such sites are few and scattered. Instrumentation of rock sites and critical facility sites should be encouraged. Regional variations and possible regional minima should be further explored and constrained. Finally, the way in which κ_0 values are implemented in applications is still being advanced. GMPEs have been using up to now κ_0 values indirectly estimated from response spectra and fitting to simulations, and GMPEs using κ_0 values measured ad hoc on Fourier spectra are underway. More work is also needed on how new κ_0 values can be used in adjustments of GMPEs. One promising technique is the use of random vibration theory to make adjustments to response spectra going through the Fourier spectral domain. Ongoing and future collaborations with PEER, PG&E, and GFZ-University Potsdam and use of their databases and techniques could lead to interesting progress in at least some of these new topics.

ACKNOWLEDGEMENTS

Many thanks to my collaborator Fabrice Cotton. The close collaboration with Norm Abrahamson (PG&E and UC Berkeley) is gratefully acknowledged. Discussions within the Next Generation Attenuation (NGA) group have been very useful. Thanks are due for discussions with the experts and members of the SIGMA and PEGASOS Refinement projects, as well as staff from PE&A (El Cerrito, CA), UC Berkeley, UN Reno, ISTerre, and DPRI Kyoto. The visits to UC Berkeley were partially supported by PEER (Pacific Earthquake engineering Research Centre) on invitation by Yousef Bozorgnia. Work on the Swiss data began through the PEGASOS Refinement project. In particular, collaboration and/or interaction with the following people is acknowledged: John Anderson, Stella Arnaouti, Pierre-Yves Bard, Glenn Biasi, Dave Boore, Bob Darragh, John Douglas, Stephane Drouet, Ben Edwards, Christine Goulet, Tadahiro Kishida, Maria Lancieri, Eric Larose, Aurore Laurendeau, Roberto Paolucci, Philippe Renault, Frank Scherbaum Walt Silva, Chris Van Houtte.

ANNEX: SUMMARY OF PUBLICATION ACTIVITY DURING THE CONTRACT

Peer-reviewed journals	5 (3 published, 2 in preparation)
Full papers in peer-reviewed conferences	2
Invited lectures	2
Technical reports	3 (in preparation)
Abstracts in conferences	8

PEER-REVIEWED JOURNALS

- J1. Ktenidou O.-J., F. Cotton, N. Abrahamson, J.G. Anderson (2014). 'Taxonomy of kappa: a review of definitions and estimation methods targeted to applications'. *Seismol. Res. Letts* 85(1), pp. 135-146.
- J2. Laurendeau A., F. Cotton, O.-J. Ktenidou, L-F. Bonilla, and F. Hollender (2013). 'Rock and stiff soil site Amplification: Dependency on V_{s30} and kappa (κ_0)'. *Bull. Seismol. Soc. Am.* 103(6), pp. 3131-3148.
- J3. C. Van Houtte, O.-J. Ktenidou, T. Larkin and C. Holden (2014). 'Hard-site κ_0 (kappa) measurements for Christchurch, New Zealand, and comparison with local ground motion prediction models', *Bull. Seismol. Soc. Am.* (in press).
- J4. Ktenidou O.-J., S. Drouet, F. Cotton and N. Abrahamson (2014). 'Understanding the physics of kappa (κ): insights from EUROSEISTEST', *Geophys. J. Int.* – IN PREPARATION
- J5. Edwards B., O.-J. Ktenidou, F. Cotton, D. Fäh (2014). 'On the uncertainty of near-surface attenuation (κ_0) determination for rock sites'. – IN PREPARATION

INVITED LECTURES

- L1. Ktenidou O.-J. (2013). "Don't call it kappa! (a review of κ estimation methods)". Invited presentation for DPRI, Kyoto, Japan, July 1.
- L2. Ktenidou O.-J. (2013). 'Don't call it κ ! (& implications for κ - V_{s30} correlations)'. Invited presentation for BERSSIN, IRSN, Fotenay-aux-Roses, France, Mar. 14.

FULL PAPERS IN PEER-REVIEWED CONFERENCES

- C1. C. Van Houtte, O.-J. Ktenidou, T. Larkin, C. Holden (2013). 'Engineering application of high frequency ground motions in Christchurch. New Zealand Society for Earthquake engineering Technical Conference and AGM, Wellington, 26-28 Apr., 2013.
- C2. Ktenidou, O.-J., T. Kishida, R. Darragh, W. Silva, N. Abrahamson (2014). ' κ_0 estimates for rock stations in the NGA-West2 project'. 10th US National Conference on Earthquake engineering, Anchorage, 21-25 July, 2014 (accepted).

TECHNICAL REPORTS

- R1. Kishida, T., Ktenidou, O.-J., Darragh, R., and Silva, W. (2014). 'PEER NGA-West2 Fourier Amplitude Spectra (FAS) Database". Pacific Earthquake Engineering Research Center – IN PREPARATION
- R2. Kishida, T., Kayen, R., Ktenidou, O.-J., Watson-Lamprey, J., and Darragh, R. (2014). 'PEER Arizona Strong Motion Database'. Pacific Earthquake Engineering Research Center – IN PREPARATION
- R3. Alatik, L., T. Ancheta, Y. Bozorgnia, B. Chiou, S. Cramer, R. Darragh, C. Goulet, Y. Hashash, J. Hollenback, T. Kishida, O.-J. Ktenidou, C. Mueller, E. Seyhan, W. Silva, K. Woodell, B. Youngs (2014). 'PEER NGA-East

CONFERENCE ABSTRACTS

- A1. C. Van Houtte, O.-J. Ktenidou, T. Larkin (2013). 'Near-source kappa estimates from the Canterbury earthquake sequence, New Zealand', SSA Annual Meeting, Salt Lake City, 17-19 April, 2013 (presentation).
- A2. Ktenidou O.-J., F. Cotton, N. Abrahamson, J.G. Anderson (2013). 'Kappa needs a subscript', SSA Annual Meeting, Salt Lake City, 17-19 April, 2013 (presentation).
- A3. Ktenidou O.-J., C. Van Houtte, F. Cotton, N. Abrahamson (2013). 'Kappa₀ estimates for hard rock SED stations in Switzerland using a high-frequency approach'. AGU Fall meeting, 9-13 Dec. (poster).
- A4. Ktenidou O.-J., W. Silva, R. Darragh, N. Abrahamson, T. Kishida, F. Cotton (2014). 'Squeezing kappa out of the Transportable Array: when the going gets tough', SSA Annual Meeting, Anchorage, 30 April, 2014 (presentation).
- A5. Ancheta T., B. Chiou, R. Darragh, C. Goulet, T. Kishida, A. Kottke, O.-J. Ktenidou, W. Silva (2014). 'Demonstration of PEER Record Processing Methodology', SSA Annual Meeting, Anchorage, 30 April, 2014 (poster).
- A6. Laurendeau A., F. Cotton, O.-J. Ktenidou, L-F. Bonilla, and F. Hollender (2014). 'Rock and stiff soil site Amplification: Dependency on V_{s30} and kappa (κ_0)', SSA Annual Meeting, Anchorage, 30 April, 2014 (poster).
- A7. Ktenidou O.-J., Z. Roumelioti, N. Abrahamson, and F. Cotton. 'Decreasing ground motion uncertainty (sigma) through site monitoring and characterisation: the example of EUROSEISTEST', Second European Conference on Earthquake Engineering and Seismology, Istanbul, 24-29 August, 2014 (submitted).
- A8. Ktenidou O.-J., S. Drouet, F. Cotton, N. Abrahamson. 'On the physics of kappa: Insights from EUROSEISTEST', Second European Conference on Earthquake Engineering and Seismology, Istanbul, 24-29 August, 2014 (submitted).

Comments on the report

'KAPPA (κ): Physical understanding and estimation approaches targeted to applications

Ref SIGMA-2014-D2-112

Frank Scherbaum
University of Potsdam
Potsdam, June 3, 2014

The report presents results of research on the high-frequency band limitation of the seismic spectrum, now commonly quantified by the parameter κ (kappa). Although known to be of critical importance for the seismic response of safety-related equipment in nuclear facilities, the **empirical** determination of seismic ground motion at high oscillator frequencies has been a major challenge in the past, due to the lack of sufficient amounts of high-quality seismic records sampled at sufficiently high frequencies, a situation which is now changing rapidly.

The work done by Olga-Joan Ktenidou within the framework of the SIGMA project is a mixture of original research and literature studies. The result is an (as far as I can see) comprehensive overview of the state of methodological practice regarding the quantification of κ , a systematic investigation of the consistency of the different measurement approaches, and a discussion of the correlations of κ with other physical parameters such as $Vs30$, Q , and *depth to bedrock*. Furthermore, it covers the investigation of the influence of sensor orientation, as well as of other instrumental constraints such as the sampling rate. It provides previously undocumented evidence for the sensitivity of κ on the shaking level, which if turning out to be a general feature, could be of enormous consequences (e.g. regarding the usefulness of κ estimates from records of small magnitude earthquakes). The work also consists of a systematic investigation of data selection criteria, the trade-off with Q , and a discussion of the preparation of databases for kappa measurements.

All this is a huge amount of work of very high quality, which is also documented by the fact that it led to a number of publications and manuscripts, a number of invited lectures, a number of technical reports, and conference proceedings.

Below, I am going to offer some comments on what I took away from reading the report and what might be helpful for continuing this work in the future. This is not meant as criticism of the excellent work done, but as suggestions for the work not done yet.

First of all, from my perspective it would have been very helpful for the review but also for people using this report as a starting point for subsequent research, if the results of the work would have been presented in a different way. It would for example have been very helpful if more detailed information would have been provided on the original objectives as identified at the outset of the project against which the deliverables could have been checked. This would have been quite helpful as a starting point for the evaluation of the results.

Also, an extensive summary (less than 20 pages but comprehensive in the sense of discussing all the *take-away messages* or *deliverables*) would have been appreciated. As it was provided now, there is a lot of doubling of material, e. g. on the different estimation approaches, introductions, etc. which the reviewer has to go through which is not really helpful for judging the results and/or the quality of the work. On the other hand, I have to admit that the fact that a major part of the report consists of papers having undergone a thorough review process, has certainly added to the readability.

Secondly, despite the title „Physical understanding and estimation approaches targeted to applications“, the strength of the study in my view is clearly on the investigation of the estimation approaches. Regarding the first part of the title: „physical understanding“, I had actually expected more. From reading the report, I obtained the feeling that the authors have rediscovered „scattering“ as a mechanism for the high frequency-band limitation of the seismic spectrum as something new, because I could not find evidence that the authors are aware of huge (!) amount of literature on this topic in geophysics.

To make my point, let me just cite the first sentences of the PhD thesis „Thin horizontal layering as a stratigraphic filter in absorption estimation and seismic deconvolution“ by Mateeva (2003) done at the Colorado School of Mines (2003), which was actually the first link which showed up when I made an internet search under the term „stratigraphic filtering“:

It has long been recognized that transmission through fine layering is accompanied by apparent attenuation (loss of high frequencies and dispersion) caused by short-period multiples. Thus, attenuation measurements from transmission experiments typically overestimate the intrinsic absorption. However, in exploration seismology, one conducts reflection rather than transmission experiments (even a VSP has a reflection component). That is why, contrary to popular belief, thin layering may cause an underestimate rather than an overestimate of the intrinsic absorption. The true consequences of ignoring small-scale heterogeneities depend both on the acquisition geometry and on the procedure for absorption estimation.

These are clearly problems which need to be investigated if one wants to understand the contributions of scattering effects on high frequency-band limitation of the seismic spectrum. Therefore, in order to avoid spending work on rediscovering phenomena which may long be known in other areas (in this case exploration seismology) I would suggest to look at the classical literature on stratigraphic filtering, which has started more than 50 (!) years ago.

One of the most disturbing results of the study performed is the observed dependence of κ_0 on ground shaking level with records with large peak ground accelerations (PGA) having lower κ_0 values than records with small peak ground accelerations. If this holds true in general, this would raise enormous doubts regarding the usefulness of microearthquake records for κ estimations, as the authors of the report rightly discuss. However, it may also raise doubts, and this is not addressed in the report, regarding the appropriateness of the κ -filter model, i. e. the quantification of the high-frequency band limiting effect through a Fourier spectrum filter expressed as $\exp[-\pi \kappa f]$. The parameter κ expresses the slope of the high frequency part of the Fourier spectrum, while PGA is NOT (!) measuring the high frequency part of the Fourier spectrum, but the signal energy within the dominant frequency band of the Fourier spectrum. It has not become evident to me that the authors are aware of this relation, otherwise they may have performed different experiments. In other words, PGA will be affected by any process which affects the spectral bandwidth and let's say the average signal level within this bandwidth.

Therefore, I believe that in order to find out if the observed dependence of κ_0 values on ground shaking level is reason for concern, one has to look closely the signal properties in both Fourier- and Response spectral domain and take into account their non-linear relationship. Just looking at correlations between particular parameters may not provide answers to the crucial questions. E. g. a simple test regarding the appropriateness of the shape of the κ -filter for the dataset, which shows the dependence of κ_0 on ground shaking level, could be an investigation if a similar dependence shows up for κ_0 and spectral acceleration at oscillator frequencies below the peak of the response spectrum. This could help to address the question if there is a change in the steepness of the transition band of the high-frequency band limitation filter (which could probably be appropriately quantified through κ) or if one needs to consider a change in the filter shape as well.

If the latter would turn out to true, one could rephrase what the PI Olga-Joan Ktenidou tried to state through the title of one of the papers in this report, which unfortunately later on was modified, namely „Don't call it κ “ into „It may not be just κ “.

It may be worth to take a fresh look at the classical perspective of strong ground motion as band-limited white noise (e. g. McGuire and Hanks, 1980; Hanks and McGuire, 1980) and revisit the the properties of the high-frequency cut-off filter from the perspective of filter theory without a priori assuming the validity of a particular spectral shape.

Concluding remarks

Overall, the report documents an enormous amount of work which gives an excellent overview of the state of methodological practice regarding the quantification of κ , but also discusses the key aspects of what is currently known about $f \kappa$. For anybody interested in the problem of high-frequency band limitation of strong ground motion, this report makes an excellent resource and starting point for further research.

Since I have no specific knowledge what the original objectives of the study were, I can not really judge if the original goals of the project where met. If on the other hand the purpose of my review would be to answer the question if the project management made a wise decision to fund this project, based on the presented results I would conclude:

If this is the answer, the question must have been a good one.

References

Hanks, T. C. and McGuire, R. K. [1981], "The character of high-frequency strong ground motion", Bull. Seism. Soc. Am., 71, 6, pp. 2071-2095.

Mateeva, A. A. [2003], „Thin horizontal layering as a stratigraphic filter in absorption estimation and seismic deconvolution“, PhD thesis Colorado School of Mines.
<http://www.cwp.mines.edu/documents/cwpreports/cwp-462.pdf>

McGuire, R. K. and Hanks, T. C. [1980], "RMS accelerations and spectral amplitudes of strong ground motion during the San Fernando California earthquake", Bull. Seism. Soc. Am., 70, 5, pp. 1907-1919.

REVIEW ON BEHALF OF SIGMA PROJECT

Reference: SIGMA-2014-D2-112

Title: Kappa (k): Physical understanding and estimation approaches targeted to applications

Author: O. J. Ktenidou

Reviewer: Philippe Renault

Review date: 16.5.2014

Review Comments:

The report consists mainly of a collection of journal papers developed in the course of the contract. The content of the papers is per se appropriate from a scientific point of view and clear. As the author has worked continuously on this topic over a longer period of time, the compilation of knowledge is complete and reflects the actual state of knowledge in this specific field.

Because the report mainly consists of already published or submitted scientific papers only very few typos have been found and it is not worth to point them out, as those part of a published paper cannot be corrected any more. E.g. PDF page 68, line 17 should have the number “3” for affiliation. PDF page 85, line 490, word 13: “perhaps”, PDF page 111, last section, 4th line from the bottom: “There is significant...”.

As the report is interpreted to be a direct input to the SIGMA project, I would have expected some practical synthesis for the end user (e.g. as summary of the conclusions of the individual papers and the papers itself to be cited supporting material in an appendix.) In this context it could have been useful that the author makes some recommendations on methods or approaches to determine and use Kappa. This comment is more driven by the view of an end user that by scientific aspects.

E.g. if there is not only one clearly preferred method, but there are a few “equivalently well suited” methods, there is still the practical need to build a logic tree with those models and to attribute weights to the individual branches. Some advice or guidance on this issue would be welcome from the expert in this special field.

In the following the comments are grouped by chapter in order to put them in the appropriate context.

- Executive Summary:

The presence of an executive summary is very much appreciated. Nevertheless, it is worth to comment that a brief description of the requested task and specific output in the context of the SIGMA project could be included in the summary, in order to understand why the study was performed and how the results will be used. This might of course also be taken over from the work package leader and not necessarily from the author of the study.

- Introduction:

1st paragraph: The sentence: “This is very important for infrastructures that are built on rock and are sensitive to high frequencies, e.g. concrete dams and nuclear facilities.” is misleading. Neither concrete dams, nor the structures of NPPs are sensitive to high frequencies, but both indeed are built on rock.

- Chapter 2 State-of-the-art

The paper is a good synthesis of the current methods and approaches. It highlights the issues with the different available datasets and interpretations of kappa. A more consistent treatment of Kappa is necessary in order to have consistency when interpreting results.

- Chapter 3 Physics of Kappa

It is nice to see that also this study has underlined the fact that V_{s30} is not well correlated to K_{p0} and thus, estimates of Kappa only based on geotechnical information might imply a large range of scatter. The fact, that lower magnitudes can be used to estimate Kappa for low seismicity region is encouraging, as the lack of data complicates the problem for a partially site specific parameter like Kappa.

The first paper has only evaluated horizontal Kappa values. From a practical perspective Kappa for the vertical component is almost as important as the horizontal. Future efforts on this topic need to take both components into account, as ultimately the engineering application requires predictions for the horizontal and vertical component, using three component time histories. In the past there have been very controversial interpretations of how large the vertical Kappa is compared to the horizontal (same size, half of it or even larger). Some advice from the author on how to handle the vertical kappa would be beneficial for the project.

The standard deviation of Kappa at a specific site or region is not fully explored and this issue could be further improved. Especially with the background of multiple approaches on how to measure Kappa and its relevance for the GMPE adjustments, the decomposition of the real and hidden uncertainty is of interest for further improvement and reduction of uncertainty for this parameter.

The second paper discusses the differences in Kappa measured at the surface and at borehole level. This is especially relevant for harder rock sites and when site specific analyses have to be carried out. The findings are not completely conclusive, as there is still for some stations a larger mismatch between the two measurement points, which is not explained through combination of the seismological and geotechnical part of damping. As site specific studies often make use of a reference bedrock level and add the site amplification part afterwards, the consideration of Kappa at a lower level in the ground vs. the commonly measured one at the surface this becomes an extremely relevant issue. This issue needs further research and a consistent physical explanation before drawing conclusions for the practical application.

- Chapter 4 Low seismicity regions

The reader can follow the first contribution (chapter 4.1), even if it is already a synthesis. Nevertheless, the inclusion of the figures at the corresponding place where they are discussed would improve the readability.

The second contribution (chapter 4.2) is described in a short way in the introduction, but the following slides are very hard to understand without any comments and thus, could also be placed in an appendix. The key charts from the slides could be extracted and used to describe the main conclusion. The work on the data from the transportable array shows some practical issues when working with data with limited bandwidth, but it is not clear to the reader how the described problems and limitations are of general interest or only limited to the transportable array. It is understood that the recommendation would be to use instruments which allow for working with a higher frequency content, but it is not obvious if in Europe a similar array would be used or has similar limitations. Furthermore, there are a lot of tradeoffs (see also Chapter 5.2) which complicate the use of this data and allows for a large room of interpretation by the analyst. Thus, the point here is that it is not clear what the intent of this chapter is with respect to the SIGMA project.

- Chapter 5 Database for Kappa

The first paper describes the procedure for the development of an additional NGA-West database to characterize FAS and from that Kappa. It is not clear how this is of benefit for the SIGMA project (beside statistical evaluation of Kappa within the NGA dataset). SIGMA relies to a large extent also on the RESORCE database and new Pan-European GMPEs. From the perspective of the European context it is not clear what would be the recommendation. Probably one should do a similar evaluation of FAS and Kappa for the RESORCE database, but this is not addressed by the author. As the main issue with Kappa is to derive host-to-target correction functions, the described work should be embedded in a SIGMA specific context to highlight how Kappa from the NGA database can be used. Remark: Today, it is not clear to the reviewer if the results of this additional database will be accessible to the SIGMA project or if it will pertain to PEER.

Comments on the approach described in the second paper, dealing with the NGA-East database, can be taken analogously. Nevertheless, there is one complication which is the attribution of stress drop for the region (East) and it's correlation with all other parameters during the evaluation. This adds another dimension of uncertainty to the evaluated Kappa values, which might blur the real uncertainty of Kappa within the CEUS. For future work, this issue should be addressed or at least it should be made clear on how it is maybe affecting the end results. A positive message seen in the proposed tasks is that Kappa for the vertical component will also be evaluation, which was not seen in the chapters before.

- Conclusions

As the report mainly consists of a collection of scientific journal papers the conclusions could be the right place to provide some project specific recommendations on how to use the state-of-the-art today. As mentioned by the author of the report, the ultimate goal might be to have inputs for host-to-target corrections. Under this assumption, it would be worth to mention that there are some new approaches in the field of application of Kappa to develop host-to-target corrections which should be introduced for the sake of completeness (e.g. Bora et al. 2013).

Furthermore, there is an issue of correlation of Kappa with other parameters (like e.g. stress-drop) which is not yet fully investigated. It should also be stressed that mismatch in ground motions between a prediction and site specific/regional recording might also be attributed to other parameters like differences in Q or the underlying duration model which are not parameters of GMPEs today. Thus, Kappa should be interpreted as the free parameter in the equation to correct for

all unexplainable effects left, and not necessarily as a physical constant. This does not mean that there is no physical basis to Kappa, but only that the way some approaches are using Kappa, it is a knob that can be turned to adjust models. This interpretation might help the scientist, as well as the end users, to better understand the limitations of Kappa and the way how corrections might be derived. Thus, the conclusions should not only summarize the performed work under the contract, but underline alternative aspects and relevant limitations for application of the current work. E.g. the author has already highlighted that the method to determine Kappa and the correction method must be consistent with the way the correction will be used in the PSHA. This recommendation is made by the reviewer under the assumption that this of interest for the project specific application and that the author was aware of these expectations. If this is not the case, then the review can be limited to state that the presented information is a good and useful compilation of current state-of-the-art.

General comment with respect to interface with other WP:

The presented work is to some extent still under its way and the report is not the final deliverable (at least with respect to the last two chapters). In this context one could check for the final version of this deliverable if some more "SIGMA specific" (European) outcome could be desirable. This would allow the other work packages, which are probably supposed to make use of this information, to implement the findings and to make fewer assumptions on detailed technical aspects or decisions on preferred approaches.